Characterizing turbulence in the wake of a honeycomb using Laser Doppler Velocimetry

Bachelor End Project
Department of Applied Physics - Fluids & Flows
Feb. 2021 - June 2021
M.T.A. Giesbergen (1239507)
R-2064-SB

Supervisors:
dr. ir. J.C.H. Zeegers
ir. R.A. Dellaert

Eindhoven University of Technology
June 14, 2021

Abstract

Plastic pollution is one of many challenges humanity is facing. Often, plastic is difficult to recycle due to its composition of different types of plastic. Magnetic Density Separation (MDS) is a method that can separate plastic particles based on their density. The flow inside an MDS machine containing plastic particles, is laminated by means of a honeycomb in order to increase efficiency of the separation process. Such a honeycomb introduces flow instabilities which results in turbulent flow behaviour. In this research, the turbulence in the wake of different honeycombs is investigated using Laser Doppler Velocimetry. For a honeycomb with a large hydraulic diameter and thin cell walls, it is found that the peak in turbulence intensity shifts away from the honeycomb and its maximum decreases, for decreasing Reynolds numbers below $Re \approx 1000$. Furthermore, it is found that a significant difference in flow velocity leaving the side channels and center channel introduces Kelvin-Helmholtz instabilities at the interface, causing flow to roll up and induce extra turbulence downstream in the tunnel. Especially for honeycombs with low porosity, it is important to set initial velocities such that only minimal differences in average flow velocities occur right after the honeycomb. Finally, for identical honeycombs with different lengths it is found that turbulent behaviour and decay characteristics are affected by the length, for flow in the laminar-regime. As long as the honeycomb length covers a significant part of the hydrodynamic entrance length at the turbulent Reynolds numbers, the length of the honeycomb does not play a role. Furthermore, the transition zone from laminar to turbulent has been investigated for this honeycomb, by visualizing the development of the streamwise velocity component right behind the honeycomb as a function of time. The visuals show interaction between individual honeycomb cells continuously altering from laminar to turbulent or vice versa, which characterizes the transition phase.

Contents

1 Introduction **3**

2 Theory **5**
2.1 Reynolds number . . . 5
2.2 Rectangular duct flow . . . 6
2.3 Turbulence intensity . . . 9
2.4 Turbulence decay power law . . . 9
2.5 Kelvin-Helmholtz instability . . . 9
2.6 Wake behind a flat plate . . . 10
2.7 Pressure loss . . . 11
2.8 Moody chart . . . 11

3 Experimental setup **13**
3.1 Wind tunnel . . . 13
3.2 Honeycombs . . . 15
3.3 Laser Doppler Velocimetry . . . 16

4 Results **18**
4.1 Low Reynolds numbers . . . 18
4.2 "Equalizing" top and bottom channels . . . 30
4.3 Entrance length . . . 56

5 Conclusions **68**
5.1 Honeycomb 3 . . . 68
5.2 Honeycomb 2 and 4 . . . 68
5.3 Honeycomb 1 . . . 69

6 Discussion & proposal further research **70**
6.1 Honeycomb 3 . . . 70
6.2 Honeycomb 2 and 4 . . . 70
6.3 Honeycomb 1 . . . 70
6.4 Conveyor belt . . . 70

7 Acknowledgements **71**

Appendices **74**

A Honeycomb 3 **74**

B Honeycomb 2+4 **74**

C Honeycomb 1 **76**

1 Introduction

It is one of many challenges humanity is facing now and in the next decades: plastic pollution. Plastics are used on daily basis and it is difficult to imagine life without it. However, the mass production of plastics started only six decades ago. It is estimated that since then already 8,300,000,000,000 kg (8.3 billion metric tons) of plastic has been produced by humans [1]. That is more than twenty-five thousand Empire State buildings in weight [2]. Besides environmental damage due to production of plastic, another major issue arises by using plastics as we do today: most of the plastics become waste. It is estimated that 6.3 billion metric tons of the 8.3 billion metric tons produced plastic, ended up as waste. Only 9 percent of this waste has been recycled and around 79 percent ended up on landfills and as waste in nature. A significant fraction of the plastic waste eventually ends up in the oceans, contributing to the well known Plastic Soup. Scientists estimated that if the current trend continues, there could be more kilograms of plastic than fish in our oceans around 2050 [3].

There is not a single solution for the plastic waste problem. Big companies as well as individual consumers should change habits in order to reduce the amount of plastic ending up as waste. However, the plastic that eventually ends up as waste should be recycled more than the paltry 9 percent that is recycled these days. This is where so called Magnetic Density Separation (MDS) can play a role. Plastic waste often contains different types of plastics, which makes separating and recycling more difficult. Using Magnetic Density Separation, this problem can be solved. In MDS, it is possible to separate plastics based on density, which is correlated with the type of plastic. A schematic visualization of the MDS machine is shown in Figure 1.1.

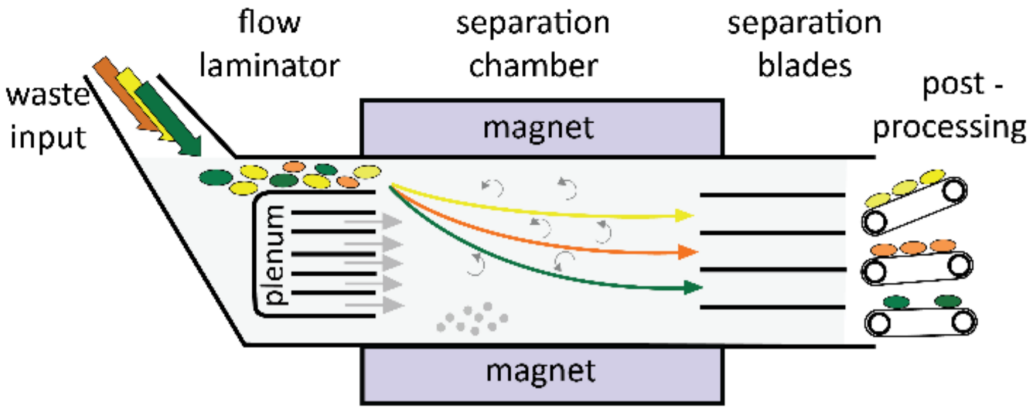

Figure 1.1: A schematic overview of the Magnetic Density Separation machine [4].

A ferrofluid enters the setup in the "waste input" zone. This fluid contains small plastic particles which differ in density. The flow is laminated by a so called honeycomb, which is placed in the center of the tunnel. The laminated flow is merged with the top and bottom channels containing the plastic waste and the flow enters the "separation chamber". In the separation chamber a density gradient in the ferrofluid is created by means of magnets placed under and above this chamber. Particles tend to float at the height where their density is equal to the density of the ferrofluid. In this way, a stream of separated particles based on density is created which enters the "separation blades" zone where the separation takes place.

This research mainly focuses on the behaviour of the flow inside the separation chamber. When flow behaves turbulent in this chamber, the plastic particles will mix and separation will fail. Therefore, it is important to investigate the effect of several parameters on the turbulence intensity in the wake of the laminator. For this research, the MDS machine is mimicked with a nitrogen flow through a tunnel. No plastic waste is added in this setup; only the fundamental behaviour of the flow in the wake of the laminator is investigated. In order to measure the behaviour of the flow, mist is added to the nitrogen flow and the behaviour is measured with a technique called Laser Doppler Velocimetry. Obtained results can be translated to the MDS machine using the universal Reynolds number.

In previous studies (Driessen [5], Vervoort [6] and Dellaert [4]), the turbulence intensity and its decay in the wake of different laminators is investigated. It is found that the intensity and rate of decay depend on variables such as individual cell size and length of the laminator, as well as initial flow velocity. Dellaert stated that *"a honeycomb with a small hydraulic diameter, thin walls and a Reynolds number of approximately 2000 inside the honeycomb results in a combination of a small maximum value and a fast decay of the turbulence intensity"*. This is confirmed by Vervoort, who found that long honeycombs with thin cell walls and Reynolds numbers above 1400 results in low turbulence intensity which decays fast. Some aspects of previous papers are the starting point for this research. Driessen stated that the low Reynolds region is interesting to investigate. Therefore, this research will start with an extension on his measurement on Honeycomb 3, especially in the low-Reynolds regime. Furthermore, measurement of Dellaert on Honeycomb 4 showed some unexpected results in turbulence intensity downstream in the tunnel. The reason for this behaviour will be investigated as well. The research will be concluded with investigation on Honeycomb 1, with a focus on the influence of the length of the honeycomb on the behaviour of the flow.

This report starts with literature research in Chapter 2 on relevant topics such as the Reynolds number, laminar and turbulent duct flow, wake behind objects and pressure loss. After that, the experimental setup and measurement method will be discussed in Chapter 3. The results of all experiments can be found in Chapter 4. The main research topics in this chapter are an extension on Driessen's measurements, the effect of the top and bottom channel on the flow and the effect of the entrance length on the flow. The results are concluded in Chapter 5. Finally, in Chapter 6 the results are discussed and proposals for future research are suggested.

2 Theory

In this section, all relevant theory for this research will be discussed. Especially the results and certain phenomena found during the experiments will be explained based on theory from this section.

2.1 Reynolds number

The Reynolds number is one of many dimensionless numbers in the field of fluid mechanics and is mainly used to calculate and predict the pattern of a flow in a certain geometry. In general, flow tends to be laminar at low Reynolds numbers and becomes turbulent at higher Reynolds numbers. Exact values for the two situations as well as the transition zone between laminar and turbulent, depend on the geometry the flow encounters. The Reynolds number is the ratio of inertial over viscous forces, where dominance of either the inertial or viscous forces determines whether the flow behaves turbulent or laminar respectively. The Reynolds number is expressed as:

$$Re = \frac{\text{Inertial forces}}{\text{Viscous forces}} = \frac{UL}{\nu} = \frac{\rho UL}{\mu}, \tag{2.1}$$

where U is characteristic velocity, L the characteristic length scale, ρ the density of the fluid, ν the kinematic viscosity of the fluid and μ the dynamic viscosity of the fluid. As mentioned, the Reynolds number is applicable to many different geometries. This research is about flow inside a rectangular tunnel and rectangular cells of a honeycomb, so in general rectangular duct flow. The exact geometry of the setup will be encountered in Chapter 3, however Equation 2.1 can already be translated to this setup. The used fluid is nitrogen thus the kinematic viscosity for this setup is constant and determined to be $\nu = 1.508 \pm 0.02 \cdot 10^{-5}$ m^2/s at $T = 291.15$ K [7], the characteristic velocity U is the average flow velocity inside the honeycomb and the characteristic length scale L is the hydraulic diameter D_h of the cells of the honeycomb. The hydraulic diameter for rectangular ducts is defined as:

$$D_\text{h} = \frac{4ab}{2(a+b)} = \frac{2ab}{a+b}, \tag{2.2}$$

where a is the width and b is the height of the duct. Another characteristic length scale for this setup is the thickness of the walls between different cells of a honeycomb. However, previous conducted research by Driessen [5] concluded that this length scale is irrelevant when $t << D_h$, which is the case for all honeycombs. Therefore, any Reynolds number in this research refers to the Reynolds number based on the hydraulic diameter and thus the Reynolds number of the flow inside the honeycomb [8].

Numerous studies were done to determine the laminar, turbulent and transition zones of flow in either square ducts or round pipes. However, there is no real consensus about the exact values of these zones. It is not only the Reynolds number that determines the state of the flow; transition from laminar to turbulent also depends on disturbances of the flow introduced by variables such as surface roughness, vibrations of the setup and fluctuations in the flow. Reynolds himself found a lower critical value of $Re = 2260$ and a upper critical value of $Re = 12,000$ at which pipe flow transits to turbulent. V.C. Patel and M.R. Head [9] concluded that for round pipe flow, first bursts of turbulence are observed at $Re \approx 2000$. These bursts increased for increasing Reynolds numbers up to $Re \approx 3000$ where a fully turbulent signal was obtained. Several other studies in

the 20th century by Binnie & Fowler, Lindgren, Leite and Wygnanski & Champagne found lower critical values in the range $1800 < Re < 2300$ [10]. This range for the lower critical value is widely accepted, however the upper critical value is difficult to determine. In theory, it is possible to maintain laminar flow at high Reynolds numbers provided that disturbances are sufficiently small. However, in practice it turns out that most pipe or duct flow is laminar up to $Re \approx 2000$, turbulent for $Re > 3000$ and transits somewhere in between those numbers. Therefore, these numbers are the guideline for this research.

2.2 Rectangular duct flow

As mentioned, the flow will encounter rectangular ducts in the setup; both the tunnel as well as the individual channels in the honeycomb are rectangular ducts. However, most literature is about circular pipe flow. The theory will be explained based on such a circular pipe flow in order to sketch what happens, since the general trend is similar for rectangular duct flow. Based on previous conducted research, this will be translated into rectangular duct flow [8].

Figure 2.1 visualizes the development of a flow entering a circular pipe. If the flow enters the pipe, it experiences friction from the wall. Assuming a no-slip condition, this means that the particles at the wall come to a complete stop. This causes particles just above the wall to experience friction, which will reduce the velocity of these particles as well. However, mass and momentum are conserved such that the velocity of the particles in the center of the channel increase, which creates a parabolic velocity profile.

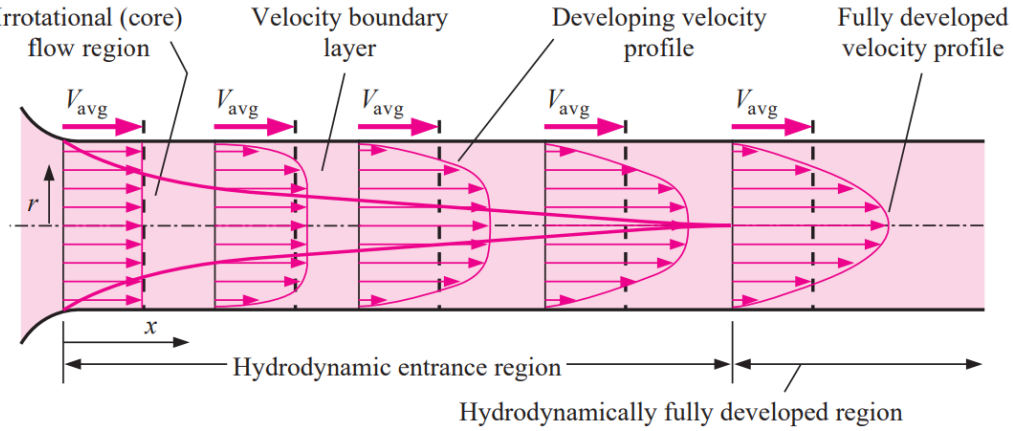

Figure 2.1: Development of a velocity profile inside a pipe [8].

Figure 2.1 shows two different regions in the radial direction. The irrotational flow region is the part of the flow that does not experience any friction from the walls and the velocity boundary layer is the part of the flow that does experience friction, which means particles are slowed down. The boundary layers start to build up radially from the wall downstream of the tunnel up to the center of the pipe where they meet. At that point, the flow is called fully developed and will not change shape anymore. The distance the flow needs to cover to be fully developed is called the hydrodynamic entrance length.

The fully developed profile can either be laminar or turbulent. As mentioned in Section 2.1, the flow is laminar below $Re \approx 2000$, turbulent for $Re > 3000$ and transits somewhere in between for most practical applications. Figure 2.2 displays the fully developed velocity profile for both laminar and turbulent flow. In the turbulent state, the velocity profile is more flattened compared to the sharply peaked profile in the laminar state.

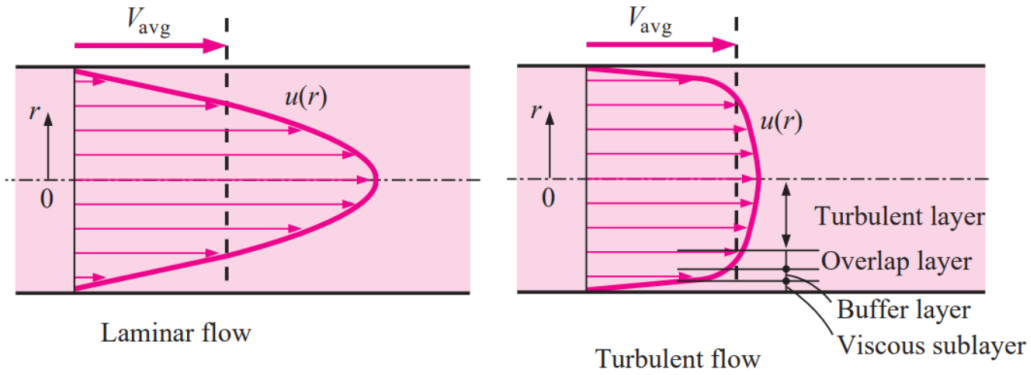

Figure 2.2: The fully developed velocity profile for laminar (left) and turbulent (right) flow [8].

2.2.1 Laminar duct flow

The left figure shows the profile for laminar pipe flow. By solving either a force balance or the Navier Stokes equation with boundary conditions of the flow, the velocity profile is given by

$$u(r) = -\frac{R^2}{4\mu}\left(\frac{dP}{dx}\right)\left(1 - \frac{r^2}{R^2}\right), \tag{2.3}$$

where R is the radius of the pipe, μ the dynamic viscosity, dP/dx the axial pressure gradient and r the radial coordinate. The average velocity for an incompressible flow in a circular pipe is

$$V_{avg} = \frac{2}{R^2}\int_0^R u(r) r dr, \tag{2.4}$$

where R is the radius. Substitution of Equation 2.3 in 2.4 and integrating yields

$$u(r) = 2V_{avg}\left(1 - \frac{r^2}{R^2}\right). \tag{2.5}$$

In the center of the tunnel, where $r = 0$, the velocity is highest. This means that for a fully developed laminar pipe flow the maximum velocity is twice the average velocity:

$$u_{max} = 2V_{avg}. \tag{2.6}$$

However, the setup in this research contains rectangular ducts, which means that the values slightly deviate due to disturbances of the flow in the corners of the tunnel. Shah and London [11] determined the ratio $U_{\text{max}}/U_{\text{average}}$ for rectangular ducts. Figure 2.3 displays a rectangular duct, where α^* is the ratio between the width and height of the duct.

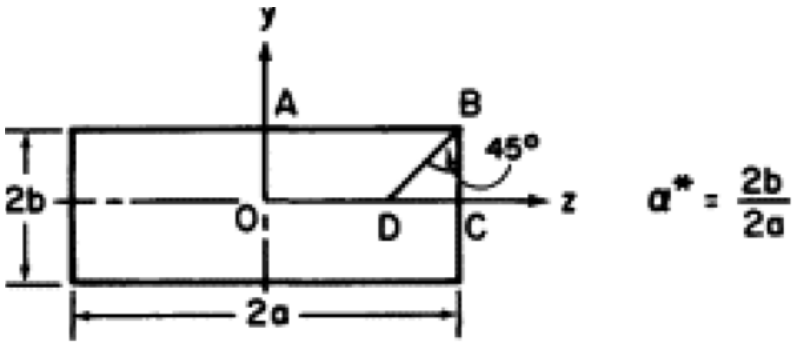

Figure 2.3: Schematic of a rectangular duct, where α^* is the ratio of the height and width of the duct [11].

It was found that for $\alpha^* = 1$, a square duct, the ratio is $U_{max}/U_{average} = 2.0962$, for $\alpha^* = 0.750$ the ratio is $U_{max}/U_{average} = 2.0774$ and for $\alpha^* = 0.500$ the ratio is determined to be $U_{max}/U_{average} = 1.9918$. The height and width of the rectangular ducts in the setup used in this research only differ a few percent. Therefore, it is expected that for a fully developed laminar rectangular duct flow the ratio $U_{max}/U_{average}$ will approximate 2.09.

2.2.2 Turbulent duct flow

The right visualization in Figure 2.2 displays a fully developed turbulent duct flow. In general, the profile of such a flow will be more flat in comparison with a parabola-like profile of a developed laminar duct flow. As can be seen in the figure, turbulent duct flow consists of four different layers. Close to the wall, viscous forces are dominant and the flow tends to be organized. In the buffer layer the flow starts to become turbulent, however viscous forces still dominate the flow. The turbulence is more significant in the overlap layer, but still not dominant. In the turbulent layer, the turbulent effects dominate over any viscous forces, which makes the flow turbulent. Characterizing the flow in all four layers is beyond the scope of this research; most relevant is the general shape of turbulent duct flow and the difference with respect to laminar duct flow [8].

2.2.3 Entrance length

Besides the flow being laminar, turbulent or in transition, the entrance length plays a major role in the velocity profile leaving a duct. As can be seen in Figure 2.1, the flow needs a certain length to become fully developed called the hydrodynamic entrance length. This length can be calculated for both laminar and turbulent flows by the following equations [12][8]:

$$L_{h,laminar} = 0.05 \cdot D_h \cdot Re \tag{2.7}$$

$$L_{h,turbulent} = 1.359 \cdot D_h \cdot Re^{\frac{1}{4}} \tag{2.8}$$

Both the Reynolds number as well as the length of the duct, determine the shape of the velocity profile leaving the duct.

2.3 Turbulence intensity

One of the important aspects of this report, is characterizing turbulence of the flow. This is done by the so called turbulence intensity [13] which is defined as

$$I = \frac{\sqrt{\frac{1}{3}\left(u_{1,RMS}^2 + u_{2,RMS}^2 + u_{3,RMS}^2\right)}}{\overline{U}_\infty}. \tag{2.9}$$

In this equation, $u_{i,RMS}$ is the root mean square for the velocity fluctuations of the velocity component in either the x-, y- or z-direction [4] and is defined as

$$u_{j,RMS} = \sqrt{\frac{1}{N}\sum_{i}^{N}(\overline{u}_j - u_j^i)^2}, \tag{2.10}$$

where $\overline{u}_j$ is the average velocity of the jth component (j=1,2,3), u_j^i is the value of the ith data point of the jth velocity component and N is the number of data points. Furthermore, $\overline{U}_\infty$ is the average velocity of the flow far downstream the tunnel and will be denoted as U_{merged}. The root mean square for velocity fluctuations will be obtained from the software during all experiments. The value of U_{merged} depends on the initial flow velocities set by the experimenter; calculations of this variable will be explained in Section 3.1.

2.4 Turbulence decay power law

In this research, the turbulence intensity obtained from a measurement will be plotted as a function of the dimensionless distance x/D_h behind the honeycomb. Apart from some exceptions, the general trend of these plots is the same: the turbulence intensity just behind the honeycomb is low and increases downstream due to mixing of the individual profiles leaving the honeycomb [4]. Once a maximum in turbulence intensity is reached, a decay follows downstream in the tunnel up to a constant value which is often in the range of the noise of the system. It is this decay that can be characterized using a extended version of the decay power from by Mohamed and LaRue [14], proposed by Thijs [13]:

$$I^2 = A\left(\frac{x}{D_\mathrm{h}} - \frac{x_0}{D_\mathrm{h}}\right)^p + N^2. \tag{2.11}$$

In this equation, A is the decay coefficient which is a scaling parameter, x_0/D_h is the virtual origin which is the position where the turbulence intensity is maximum, p is the decay exponent which indicates the rate of turbulence intensity decay and N is the noise of the system. Thijs proposed that the decay constant for the near-field, which ends at $x/D_h \approx 35$, is $p = -2$. Therefore, this will be maintained in this research.

2.5 Kelvin-Helmholtz instability

Kelvin-Helmholtz instability is the phenomenon where two uniform flows with different velocities meet which induces an instability at the interface between the two flows. The perturbations at the interface undergo growth stages which may evolve into turbulent mixing of the flow [15]. Differences in velocity occur regularly in the used setup. Behind the cell walls of the honeycomb velocities are

significantly lower than flow leaving the cells. Furthermore, velocities leaving the top/bottom channel and the center channel may differ. Both phenomena may induce a Kelvin-Helmholtz instability which contributes to turbulent mixing of the flow downstream of the honeycomb.

2.6 Wake behind a flat plate

Numerous studies are performed on both the laminar and turbulent wake behind a flat plate. Hollingdale [16] found that up to $Re = 600$ no oscillations take place in the laminar wake of a flat plate. Increasing the Reynolds number generates pseudo-oscillations behind the plate and above $Re = 1090$ well-defined oscillations of the flow are observed. The oscillations break up into isolated vortices for $Re > 1300$ which generates a so called Kármán Vortex Street; a repeating pattern of vortices. Conclusions on even higher Reynolds numbers are inaccurate due to limits of the setup. However, it was found that for higher Reynolds numbers diffusion has a significant effect and vortices disappear rapidly.

By studying the control of free-stream turbulence by honeycombs, Loehrke [17] found that turbulence induced by random velocity fluctuations is generated by the shear layer instability which occurs when flow leaves a honeycomb. In a subsequent study, Loehrke and Roadman [18] found that at low Reynolds numbers the flow tends to oscillate which is in accordance with Hollingdale.

Lastly, Ahlborn [19] performed a study in the first half of the 20^{th} century on the effect of parallel plates. Experiments were made with a towing tank where the fluid remains at rest and the plates are moving. Figure 2.4 displays the result, where the plates move from right to left. The plates have a length of 10 cm and the spacing is 2 cm. Exact numbers of flow velocity and the Reynolds number are missing, but it can be seen that vortex streets arise behind the plates. Only one plate-length of flow is visible, but it looks like the vortices disappear after a while due to diffusion of the flow. However, some vortex streets are persistent and remain present up to six diameters downstream.

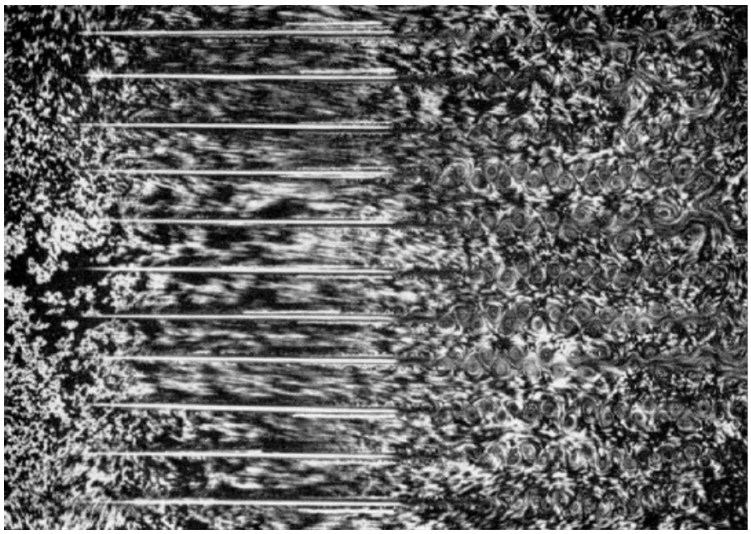

Figure 2.4: The plate system used by Ahlborn [19].

The different studies show similar results: low Reynolds number flow introduces oscillations of the flow in the wake of a flat plate. Mainly depending on the Reynolds number, these oscillations may break up into individual vortices which induces turbulence. This turbulence disappears downstream and for higher Reynolds numbers due to diffusion. As will be explained in Chapter 3, the setup in this research contains separation plates between channels. Therefore, the effect of plates on flow behaviour is important for this research, since these separation plates may induce an instability in the wake.

2.7 Pressure loss

An important, but regularly forgotten effect occurring in pipe flow is a so called pressure drop due to friction. Henry Darcy and Julius Weisbach empirically determined the following equation for pressure loss [20]:

$$\frac{\Delta p}{L} = \frac{f_D \cdot \rho \cdot v_{average}^2}{2D}. \tag{2.12}$$

In this equation, L is the length of the pipe, f_D the Darcy-Weisbach friction coefficient, $v_{average}$ the mean flow velocity in the pipe and D the hydraulic diameter. For laminar flow, Equation 2.16 can be substituted in 2.12. Eliminating Re using Equation 2.1 gives

$$\Delta p = \frac{32\mu \cdot L \cdot v_{average}}{D^2}. \tag{2.13}$$

This equation can be interpreted as the equation for pressure loss for a fully developed laminar flow inside a duct and is equal to the analytically and experimentally derived van Hagen-Poiseuille law for laminar flow through a cylindrical pipe.

2.8 Moody chart

The Moody chart is a widely accepted empirical chart in engineering which relates the Darcy-Weisbach friction factor f_D, the Reynolds number Re and the surface roughness ϵ/D for fully developed flows in circular pipes. A visualization of the chart is depicted in Figure 2.5. The chart is applicable to non-circular pipes as well, by replacing the diameter D with the hydraulic diameter D_h from Section 2.1. The most interesting variable for this research is the Darcy-Weisbach friction factor. Rewriting Equation 2.12 yields

$$f_D \equiv \frac{\Delta p}{L} \cdot \frac{2D}{\rho \cdot v_{average}^2}. \tag{2.14}$$

Combining Equation 2.3 and 2.5 gives

$$2v_{average,laminar} = \frac{D^2}{16\mu}\frac{dP}{dx}, \tag{2.15}$$

for laminar flow. Substituting this equation for average flow velocity in Equation 2.14 and rewriting in terms of the Reynolds number results in a relation where the friction coefficient is independent of the roughness of the duct walls and is inversely proportional to the Reynolds number:

$$f_{D,laminar} = \frac{64}{Re}. \tag{2.16}$$

This equation is displayed in Figure 2.5 as well in the laminar zone. Furthermore, there is a transition zone indicated by the shaded area in Figure 2.5 where the flow transits from laminar to turbulent or vice versa, or occasionally alternates between laminar and turbulent. The latter means that the friction force value alternates between laminar and turbulent as well, which affects to pressure loss over the channel [8] [21].

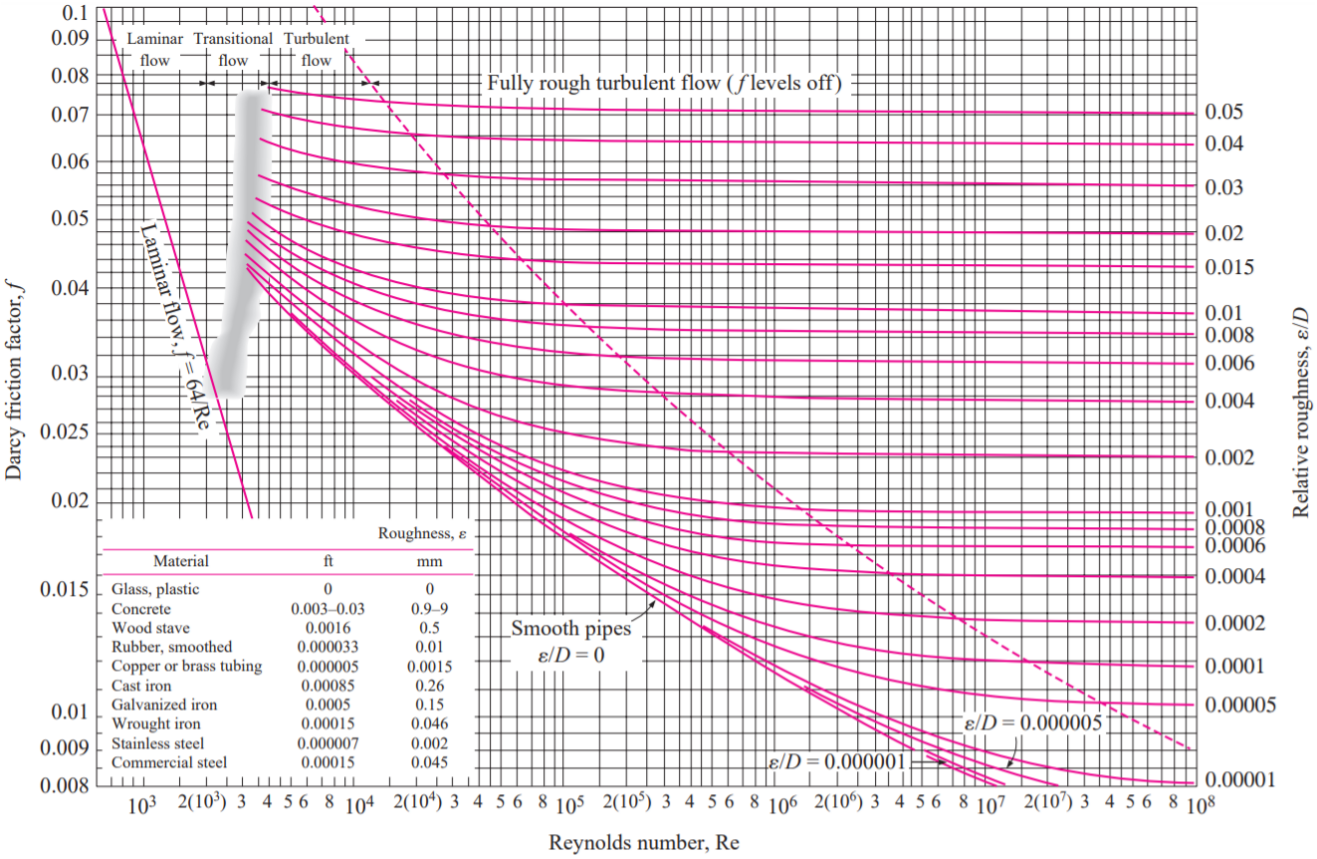

Figure 2.5: The relation between the Darcy friction factor f_D, relative surface roughness ϵ/D and the Reynolds number Re displayed in the so called Moody chart [8].

3 Experimental setup

This section contains all relevant information about the used setup for this experiment. First, the wind tunnel and its effect on flow velocity will be introduced, followed by an overview of the investigated honeycombs. Furthermore, the measurement method used to characterize the flow will be explained.

3.1 Wind tunnel

All experiments are performed with the wind tunnel depicted in Figure 3.1. The flow is from left to right and the used medium is nitrogen. The direction of the flow is labeled as the x-axis. The lateral direction and height of the tunnel are represented by the y- and z-axis respectively, as can be seen in Figure 3.2. The tunnel consists of three different parts. In Part I, there are three separated empty channels. The top and bottom channels are identical with cross sectional dimensions 70x10 mm. The center channel is the largest and has a cross sectional area of 70x50 mm. The channels are separated by two identical separation plates which are 5mm in thickness. In Part II, the three channels are still separated, however the center channel contains a honeycomb which laminates the flow. The top and bottom channels are empty channels in this research, however in the industry these channels are used to add the plastic particles to the flow. Finally, in Part III the three separate channels have merged into one channel. The point where the three separate channels merge is labeled as $x = 0$.

The top, middle and bottom channel in Part I and II all have individual inflow tubes. The flow rate of the three separate channels can be controlled independently. Pressure is build up in a pressure vessel and the nitrogen is directed into the three inlets using tubes and valves. The experimenter only sets the desired pressure and velocity using the provided software. After that, the software takes over and regulates the flow rate. In order to measure the behaviour of the flow, a particle tracer and measurement method is needed. The particle tracer in this setup is water fog. Distilled water is fed to three separate ultrasonic humidifiers; one for each channel. The three nitrogen flows pass through one humidifier each, where dense mist is added to the flow. It is assumed that these droplets of only a few micron do not affect the flow. Once enough tracer particles are present, the behaviour of the flow will be measured using Laser Doppler Velocimetry, which will be encountered in Section 3.3. The amount of water droplets added to the flow, can be regulated by the experimenter by adapting the humidity for the top/bottom and center channel in the software.

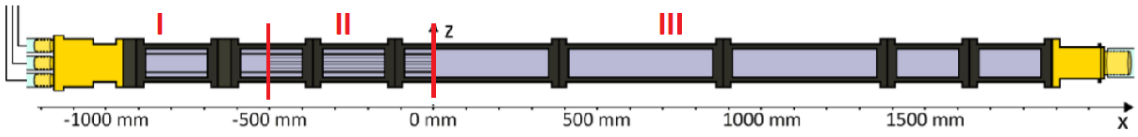

Figure 3.1: Schematic overview of the wind tunnel used for this investigation. The tunnel consists of three parts: part I with three separate ducts, part II with the same three separate ducts but a honeycomb in the middle channel and part III where the three channels are merged [4].

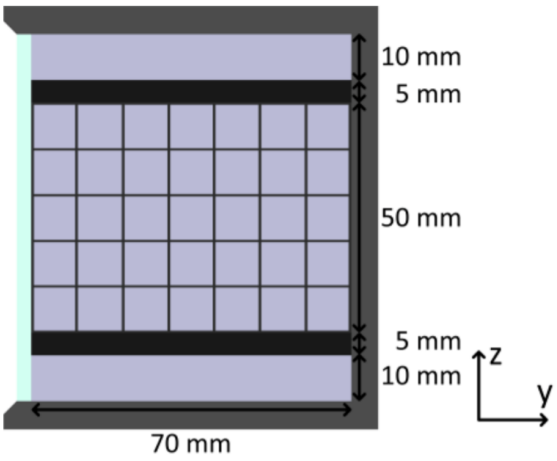

Figure 3.2: Cross sectional representation of Part II of the wind tunnel [4].

Before starting any research, it is important to understand the effect of both the tunnel and the honeycomb on the flow and its velocity. Figure 3.2 displays the cross section of the tunnel before the three channels merge. The top and bottom channel are "empty" which means that the average flow velocity leaving these channels at $x = 0$ is equal to the initial velocity set by the experimenter. The velocity for the top and bottom channel set by the experimenter will be denoted by $U_{1,top}$ and $U_{1,bottom}$ respectively. The center channel (partly) contains the honeycomb which influences the flow velocity. The initial surface of the center channel is 350 mm^2. When the flow encounters the honeycomb, the frontal surface is reduced depending on the characteristics of the honeycomb. The amount of flow passing through the center channel remains the same, while the available volume it travels through is reduced. This means that the average velocity of the flow inside the honeycomb increases. This can be proven using the equation for volumetric flow rate [8], which is defined as

$$Q = A \cdot v, \tag{3.1}$$

where Q is the volumetric flow rate, A is the surface area of the cross section and v is the velocity of the flow. The flow rate before and inside the honeycomb is equal which means that

$$A_I \cdot v_I = A_{II} \cdot v_{II}, \tag{3.2}$$

In this equation, I and II indicate the part of the tunnel as displayed in Figure 3.1. Rewriting yields

$$v_I = \Phi \cdot v_{II}, \tag{3.3}$$

where $\Phi = A_{II}/A_I$ is defined as the porosity of the honeycomb, which will be encountered in Section 3.2. Redefining the variables such that it fits in the context of this setup gives

$$U_{1,middle} = \Phi \cdot U_{1,honeycomb}. \tag{3.4}$$

Here, $U_{1,middle}$ is the initial flow velocity set by the experimenter, Φ is the porosity of the honeycomb and $U_{1,honeycomb}$ is the average flow velocity inside the honeycomb.

At $x = 0$ the top, center and bottom channel merge and the flow can be interpreted as one single flow. This introduces $U_{1,merged}$, which is the average merged flow velocity in Part III of the tunnel. Using the equation for volumetric flow rate, the equation for $U_{1,merged}$ can be derived:

$$A_{III,merged} \cdot v_{III,merged} = A_{I,top} \cdot v_{I,top} + A_{I,middle} \cdot v_{I,middle} + A_{I,bottom} \cdot v_{I,bottom}, \tag{3.5}$$

In words, this equation means that the volumetric flow rate before and after merging is unchanged. The subscripts refers to the part of the tunnel (I, II or III) and which of the three channels (top, middle or bottom). All surfaces can be calculated using Figure 3.2. $A_{I,top}$ and $A_{I,bottom}$ are equal to 700 mm^2, $A_{I,middle}$ is 3500 mm^2 and $A_{III,merged}$ is 5600 mm^2. Substituting these values in Equation 3.5 and rewriting in terms of this setup yields

$$U_{1,merged} = \frac{700U_{1,top} + 3500U_{1,middle} + 700U_{1,bottom}}{5600}. \tag{3.6}$$

With this equation, the average flow velocity in Part III of the tunnel can be calculated based on the initial velocities set by the experimenter. Previous research is often conducted with equal initial velocities in all three channels. For $U_{1,top} = U_{1,middle} = U_{1,bottom}$, Equation 3.6 reduces to

$$\frac{8}{7}U_{1,merged} = U_{1,top} = U_{1,middle} = U_{1,bottom}, \tag{3.7}$$

which is equal to the previously found relation as stated in Dellaert's paper [4].

3.2 Honeycombs

In this research, plastic honeycombs are placed in the center channel to laminate the flow. The honeycombs are 3D printed and consist of a number of identical rectangular parallel ducts, also called cells. Table 3.1 shows an overview of all investigated honeycombs and their characteristics. The table contains all relevant information for each honeycomb such as length, cell dimensions and the number of cells. The length of the honeycomb is important in order to determine whether the flow leaves the honeycomb developed. The hydraulic diameter of the cells is calculated using Equation 2.2 and the porosity Φ of a honeycomb is defined as the ratio of open area over total area. Figure 3.3 displays all investigated honeycombs.

Table 3.1: Dimensions for all used honeycombs.

Honeycomb	**Length [mm]**	**Cell height [mm]**	**Cell width [mm]**	**Cell hydraulic diameter D_h [mm]**	**Wall thickness [mm]**	**Total number of cells [-]**	**Porosity Φ [-]**
1	50	9.5	9.4	9.45	0.4	35	0.908
1*	750	9.5	9.4	9.45	0.4	35	0.908
2	240	4.15	4.15	4.15	0.22	176	0.873
3	700	15.6	15.6	15.6	0.5	12	0.892
4	500	6.05	6.30	6.17	3.2	35	0.385

Figure 3.3: From left to right Honeycomb 1, 2, 3 and 4 which are investigated in this research.

Honeycombs 1, 2, 3 and 4 can be seen in Figure 3.3 from left to right. For Honeycomb 1, two variants are investigated which differ in length. As can be seen in Table 3.1, Honeycomb 1 has a length of 50 mm and Honeycomb 1* is 750 mm. Apart from this difference in length, the honeycombs are identical. It should be noted that the lengths of the honeycombs displayed in the figure are not identical to the lengths as stated in the table, however the picture provides a good visualization of cell dimensions and number of cells for all honeycombs.

3.3 Laser Doppler Velocimetry

As mentioned in Section 3.1, mist is added to the nitrogen flow as tracer particle. Using Laser Doppler Velocimetry, the behaviour of such a water droplet can be measured and quantified. The technique is non-invasive and measures velocity at one single point in the flow with high temporal resolution and high sampling rate, using the Doppler shift of laser light. A laser beam is split into two parallel beams which pass through a lens, as can be seen in Figure 3.4. This lens focuses the beams such that they intersect at the point of interest, forming the measuring volume. The intersection of the two separate laser beams creates a fringe pattern, where the distance d_f between the fringes is known. When a particles travels through the measuring volume, light is scattered with sinusoidal varying intensity. The scattered light falls onto a photodetector, after which the data is processed to find the period Δt of the sinusoidal intensity signal. The Doppler frequency can be calculated using

$$f_d = \frac{1}{\Delta t}. \tag{3.8}$$

The velocity of the particle is then calculated as function of both the fringe spacing and Doppler frequency:

$$u = f_d \cdot d_f. \tag{3.9}$$

Since the water droplets are only a few micron, it is assumed that the measured velocity of the particle is equal to the flow velocity at that point [22].

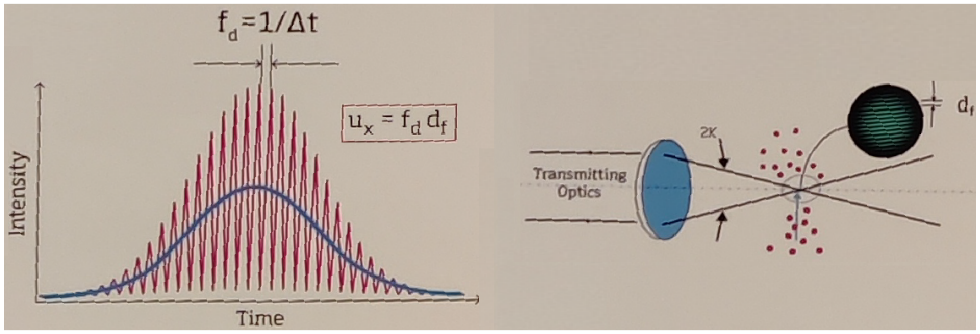

Figure 3.4: The principle behind Laser Doppler Velocimetry [22].

In order to characterize the turbulence intensity of the flow, it is necessary to measure the velocity in all three directions. To achieve this, several lasers are used in this experiment. The Spectra-Physics Stabilite 2017 Argon-ion gas laser produces two laser beams with wavelengths of 488 nm and 514.5 nm. One laser is split up horizontally and one vertically in order to measure the velocity of the flow in the x- and z-direction respectively. These laser beams are positioned perpendicular to the tunnel, as can be seen in Figure 3.5a. Figure 3.5b displays another laser under an angle with respect to the tunnel. This laser measures the particle behaviour in the y-direction. The used laser is a solid state Genesis MX 532-1000 STM diode-pumped laser which emits a single 532 nm beam. Since the laser is placed under an angle with respect to the tunnel, data from this laser should be transformed. Transformation is done by a so called transformation matrix in the software, which is fully automated. All laser beams coincide in the point of interest and with the described technique particle behaviour is measured in all three directions. So called coincidence is needed to get a valid measurement. Coincidence means that all three lasers detect a particle at the exact same time. Typical data rates for the experiments lay between 500 Hz and 15,000 Hz. A measurement at one single position is finished after either one minute of measuring or obtaining 50,000 valid counts.

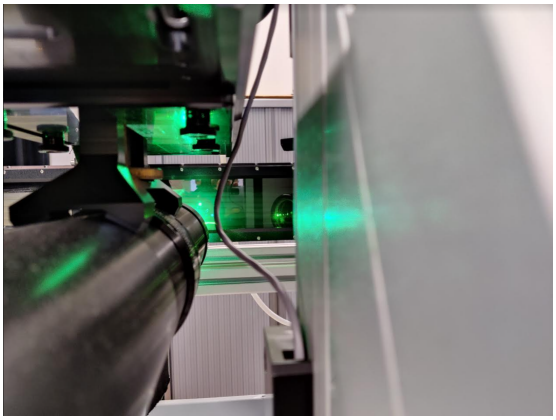

(a) Two laser beams positioned perpendicular with respect to the flow direction to characterize the flow in the x- and z-direction.

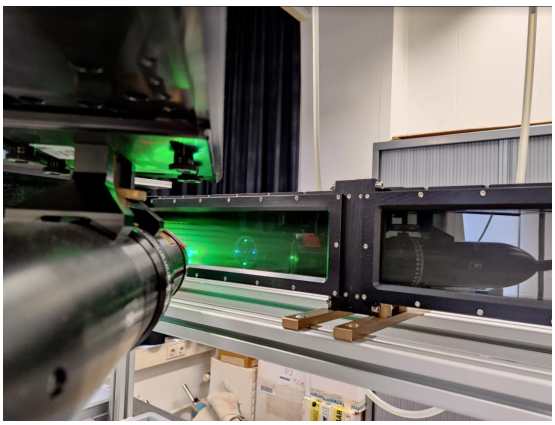

(b) Single laser beam positioned at an angle with respect to the tunnel to characterize the flow in the y-direction.

Figure 3.5: The lasers used in this experiment.

4 Results

This chapter contains the results of the performed experiments. First, some basic measurements are performed on Honeycomb 3, as an extension on the measurements of BEP student Ronald Driessen. After that, the effect of the initial velocity set on the top and bottom channel on the behaviour of the flow behind the honeycomb is investigated using Honeycomb 2 and 4. The chapter is concluded with measurements on two variants of Honeycomb 1, with the main focus on the influence of the length of the honeycomb on the behaviour of the flow.

4.1 Low Reynolds numbers

In order to get acquainted with the setup and measurement method, some basic measurements are performed on Honeycomb 3. These measurements are an extension of the measurements of BEP student Ronald Driessen [5] on this honeycomb. His research focused on a large range of Reynolds numbers starting from Re = 1160. Therefore, it is chosen to investigate a set of Reynolds numbers below Re = 1160. The 700 mm variant of Honeycomb 3 is chosen for this experiment. There are 200 mm and 900 mm variants for this honeycomb as well, however Ronald Driessen concluded that for the 200mm variant the flow will be far from developed for most Reynolds numbers due to its short length, and the 900mm variant introduced a significant inhomogeneous velocity distribution over the cells of the honeycomb due to limits of the setup .

Using Equation 2.7, it is calculated that for this 700 mm variant the flow will be fully developed and laminar up to $Re \approx 897$. Reynolds numbers ranging from $Re = 580$ up to $Re = 1160$ are investigated. Therefore, it is expected that the velocity profile for the higher Reynolds number is not fully developed. The turbulence intensity will be investigated as a function of the distance behind the honeycomb. From these turbulence intensity plots, the decay constant will be determined by applying the decay law stated in Section 2.4. Furthermore, the ratio $U_{\text{measured}}/U_{\text{merged}}$ will be investigated in order to gain knowledge on the development of the streamwise velocity component in the center of the honeycomb downstream the tunnel. Finally, the turning point for turbulence will be investigated, since it is expected that the turbulence peak will disappear for low Reynolds numbers.

4.1.1 Turbulence intensity

First, the turbulence intensity is investigated. Figure 4.1 shows the turbulence intensity as a function of the dimensionless distance behind the honeycomb for different Reynolds numbers. From this graph the following conclusions can be drawn:

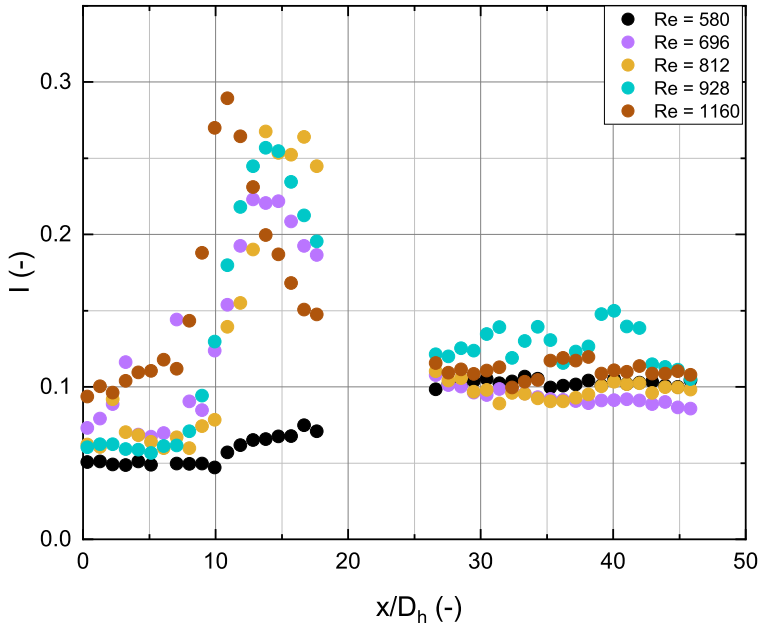

Figure 4.1: The turbulence intensity against x/D_h for different Reynolds numbers (HC3).

It is clear that the height of the turbulence intensity peak decreases for decreasing Reynolds numbers. Furthermore, the peak position for $Re = 1160$ shifts towards the honeycomb compared to lower Reynolds numbers. This is in accordance with the trend found by Driessen [5].

Despite the fact, that the results for the higher Reynolds numbers are accurate in comparison with previous research, Figure 4.1 does not provide enough information to determine the exact peak position and peak maximum of each measurement. One of the main reasons for this, is the measurement gap between $x/D_\mathrm{h} \approx 18$ and $x/D_\mathrm{h} \approx 26$ which is caused by the absence of a window between two tunnel sections. This gap makes it impossible to measure and visualize the turbulence intensity in the region where it is expected to decay. The same holds for the transition that seems to take place between $Re = 580$ and $Re = 696$. The turbulence intensity peak disappears for $Re = 580$, while for $Re = 696$ a significant peak in turbulence is visible. To accurately visualize the maximum and position of the turbulence intensity peak for all measurements, and the possible transition taking place between $Re = 580$ and $Re = 696$, two tunnel sections are swapped and all measurements are executed once again. These measurements fully cover the decay region, such that peak height and positions could be determined. Furthermore, this opens up the possibility to use the decay power law in order to determine the decay coefficients.

In addition to measuring the measurement gap, a small region before and after this gap is measured,

resulting in a measurement window ranging from $x/D_\mathrm{h} = 10$ up to $x/D_\mathrm{h} = 35$. It is assumed that converting the tunnel does not affect the flow, such that the combination of both measurements can be taken as one result in order to draw conclusions. Figure 4.2 displays the turbulence intensities as a function of distance behind the honeycomb for the converted tunnel configuration. Despite the fact that the turbulence intensities found for this swapped configuration (Figure 4.2) slightly differ from the values found before the tunnel was converted (Figure 4.1) in the region where the two measurements have overlap, the general trend of the turbulence intensity is the same.

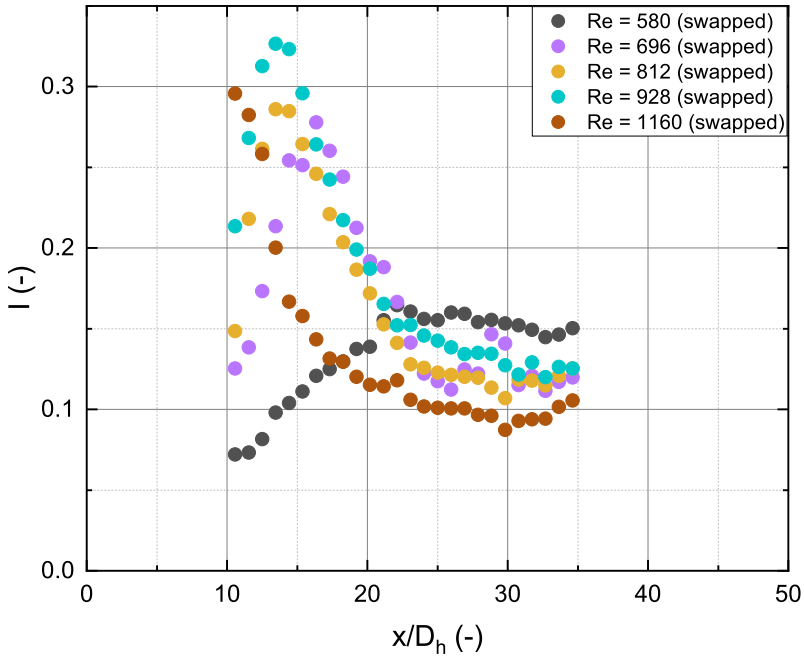

Figure 4.2: The turbulence intensity against x/D_h for different Reynolds numbers (HC3 swapped).

As mentioned, it is expected that for $Re = 580$ no clear peak of turbulence occurs. This is confirmed by Figure 4.2, as no clear peak is visible. The transition region between Re = 580 and Re = 696, where such a peak should eventually appear for a certain Reynolds numbers, is investigated in Section 4.1.6.

Furthermore, Figure 4.2 shows that for decreasing Reynolds numbers, the height of the turbulence peak decreases and the position of this peak shifts downstream of the honeycomb. The behaviour of the maximum intensity and peak position as a function of the Reynolds number will be visualized in Sections 4.1.2 and 4.1.3 respectively. All measurements, apart from Re = 1160, show the whole peak in turbulence intensity and its decay downstream the tunnel. However, by combining the results of Figures 4.1 and 4.2 it can be assumed that for $Re = 1160$ the peak is positioned at $x/D_\mathrm{h} \approx 10$ and has a maximum height of $TI \approx 0.3$, such that the first point in Figure 4.2 is the starting point for fitting. Fitting of the data to obtain the decay constants will be executed in Section 4.1.4.

4.1.2 Maximum intensity as function of Reynolds number

Figure 4.3 displays the maximum turbulence intensity as a function of the Reynolds number, combined with Driessen's data [5]. Despite the fact that Driessen found a significantly lower maximum intensity for $Re = 812$, it seems that the measurements merge well; the uptrend continues up to $Re = 928$, followed by a decay in intensity for decreasing Reynolds numbers. Lower Reynolds numbers can be investigated in the future, in order to confirm this downward trend.

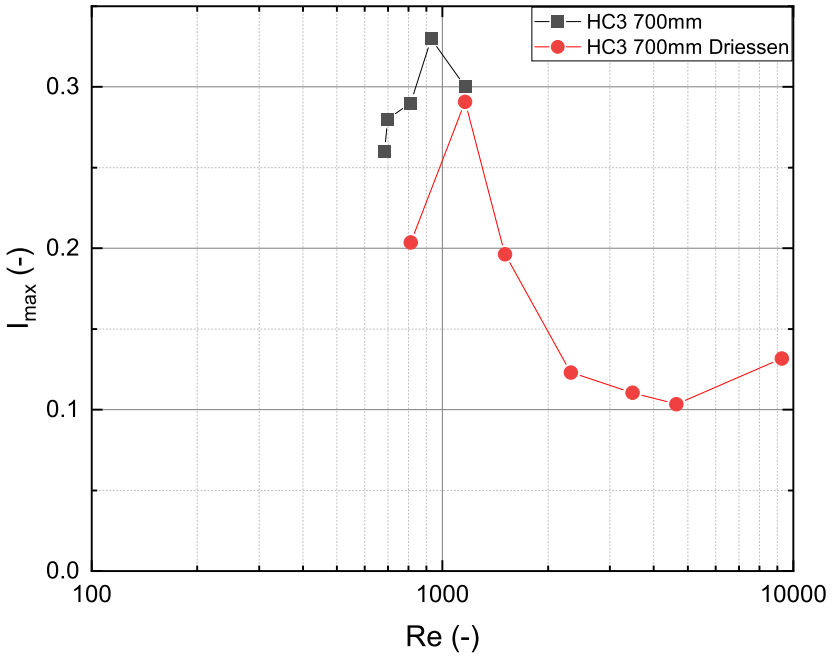

Figure 4.3: The maximum turbulence intensity against Re for different Reynolds numbers (HC3 swapped).

4.1.3 Peak position as function of Reynolds number

Figure 4.4 displays the peak position as function of the Reynolds number, again combined with Driessen's data. At $Re = 1160$ the values perfectly coincide, after which the data follows the upward trend that Driessen already found.

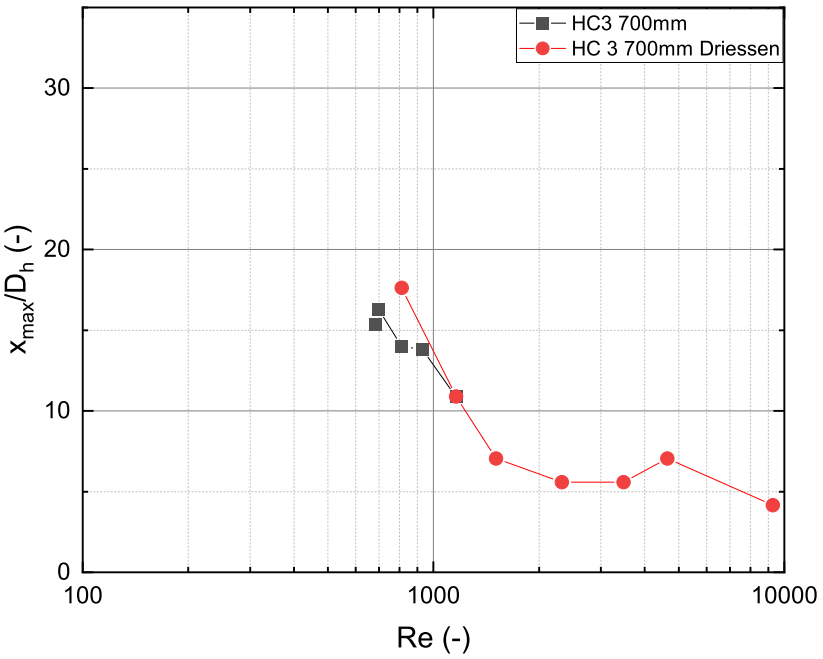

Figure 4.4: The turbulence intensity peak position against Re for different Reynolds numbers (HC3 swapped).

4.1.4 Decay characteristics

Figure 4.2 displays the turbulence intensity as a function of the distance behind the honeycomb. As mentioned in Section 2.4, these graphs typically display turbulence intensity starting low, increasing to a maximum, followed by a decay downstream. This decay can be characterized by fitting with Equation 2.11; the decay power law. Fitting of the turbulence according to this law is done by a provided Matlab script. The experimenter needs to fix the decay exponent p and choose the end point for fitting. Only the near-field is measured for this honeycomb and p is fixed at -2. To illustrate the fitting method, an example of fitting is provided where the $Re = 928$ measurement is fitted. This example resembles how a fit should be interpreted. Figure 4.5 shows the turbulence intensity as a function of position, fitted by the power law for $Re = 928$.

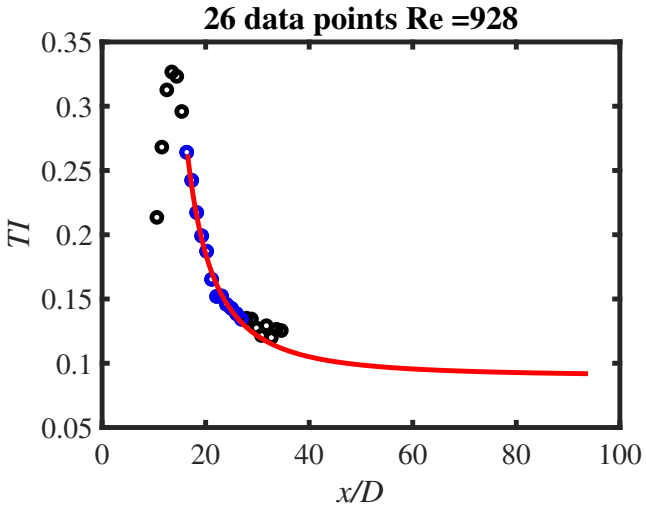

Figure 4.5: The turbulence intensity as a function of distance behind the honeycomb, fitted with the power law.

The Matlab script starts fitting one measurement point below the top of the peak and iterates a few times, where each iteration takes the point below the previous starting point. The final point should be set such that all points follow the fit. Once measurement points start to follow a trend other than the red line, these points should not be included in the fit. The fit in Figure 4.5 shows that the red line passes through all points, however solely based on this graph it is difficult to determine whether the fit is correct. Figures 4.6 and 4.7 show log-log plots, which give a more accurate indication whether the chosen points fall onto the red line.

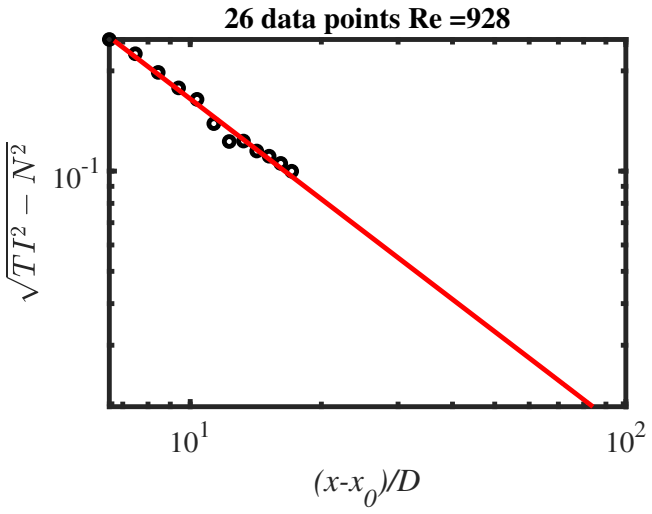

Figure 4.6: Log-log plot of the square root of the turbulence intensity squared minus the noise squared as a function of the distance behind the honeycomb, corrected with the virtual origin x_0.

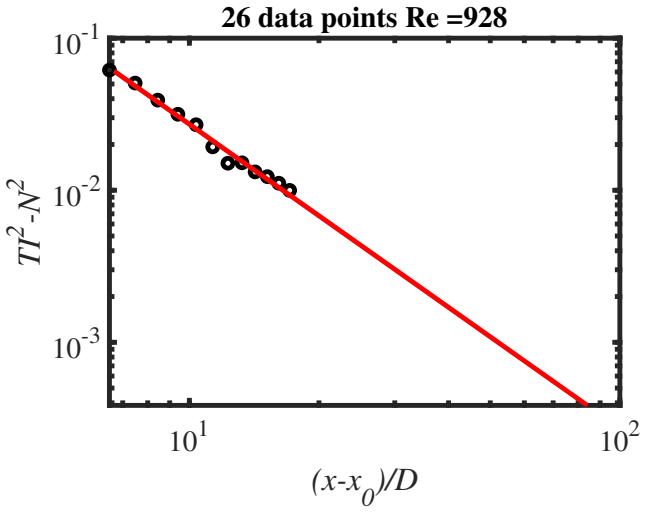

Figure 4.7: Log-log plot of the turbulence intensity squared minus the noise of the setup squared as a function of the distance behind the honeycomb, corrected with the virtual origin x_0.

Figures 4.6 and 4.7 display the log-log plot of the square root of the turbulence intensity squared minus the noise squared as a function of the dimensionless position corrected with the virtual origin and the log-log plot of the turbulence intensity squared minus the noise squared as a function of the position corrected with the virtual origin, respectively. These graphs give the experimenter insight whether measurement points deviate from the fit.

Table A.1 contains the values found by fitting the different turbulence intensities from Figure 4.2, except for $Re = 580$ since no peak appears for this Reynolds number. Figures 4.8, 4.9 and 4.10 display the data combined with the results from Dellaert [4] and Driessen [5] for this honeycomb.

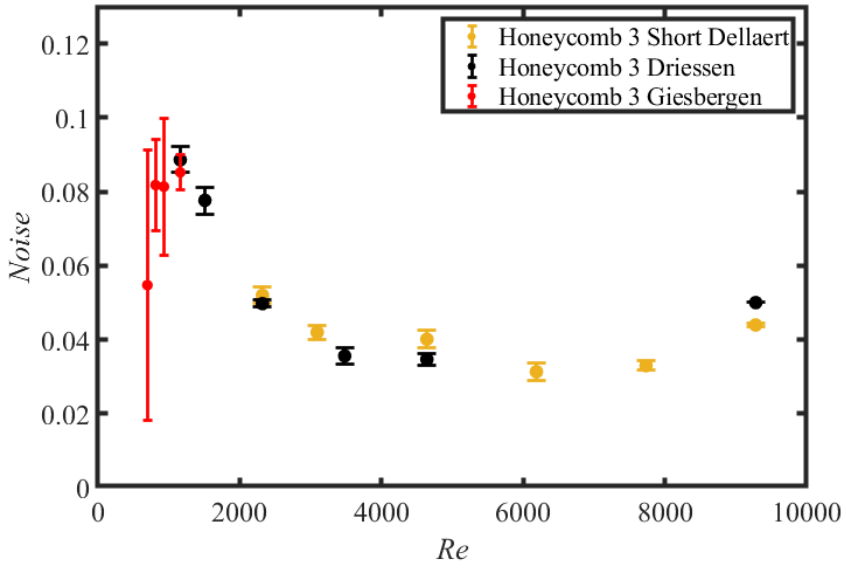

Figure 4.8: The noise N as a function of the Reynolds number, combined with results from Dellaert and Driessen (HC3).

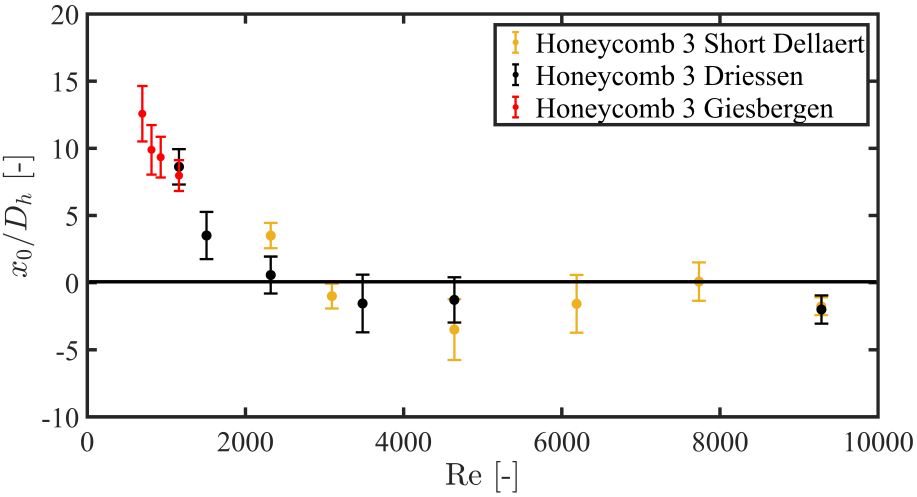

Figure 4.9: The virtual origin x_0/D_h as a function of the Reynolds number, combined with results from Dellaert and Driessen (HC3).

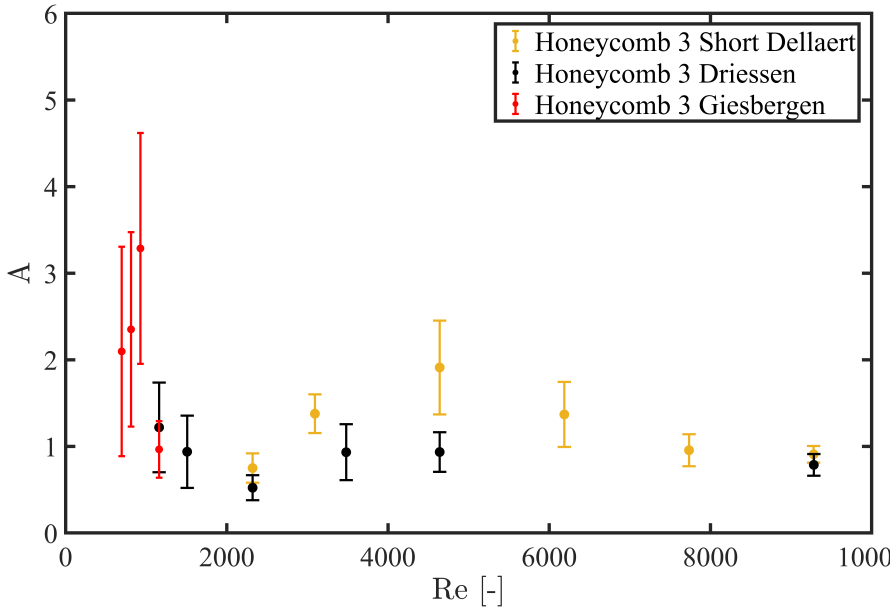

Figure 4.10: The decay coefficient A as a function of the Reynolds number, combined with results from Dellaert and Driessen (HC3).

In general, the results follow the trends found by Dellaert and Driessen. However, Figure 4.8 shows that the noise has large uncertainties compared to previous results. It is expected that this is due to the relatively low number of data points that is fitted. The virtual origin x_0/D_h up trend continues for decreasing Reynolds numbers as can be seen in Figure 4.9. This trend closely resembles Figure 4.4, although Figure 4.9 is determined via a different method and x_0 is not necessarily equal to x_{max}/D_h. For the decay coefficient A, a maximum is reached at $Re = 928$ after which the value decreases for lower Reynolds numbers. Due to the low number of data points and the fact that these were the first measurements, no hard conclusions can be drawn about the decay characteristics. However it seems that the results follow the previously found trend for all variables.

4.1.5 Velocity profile

Figure 4.11 shows the ratio of measured velocity over the merged velocity downstream the tunnel for different Reynolds numbers as a function of distance behind the honeycomb, for the set of measurements before converting the tunnel. As mentioned, the flow is laminar and fully developed up to $Re \approx 897$. This is confirmed by Figure 4.11. The starting point for $Re = 580$, $Re = 696$ and $Re = 812$ is approximately constant, which means the flow leaves the honeycomb fully developed for these Reynolds numbers. However, for $Re = 928$ and $Re = 1160$ the starting point is lower, indicating that the velocity profile is more "flat" which are signs of an undeveloped flow.

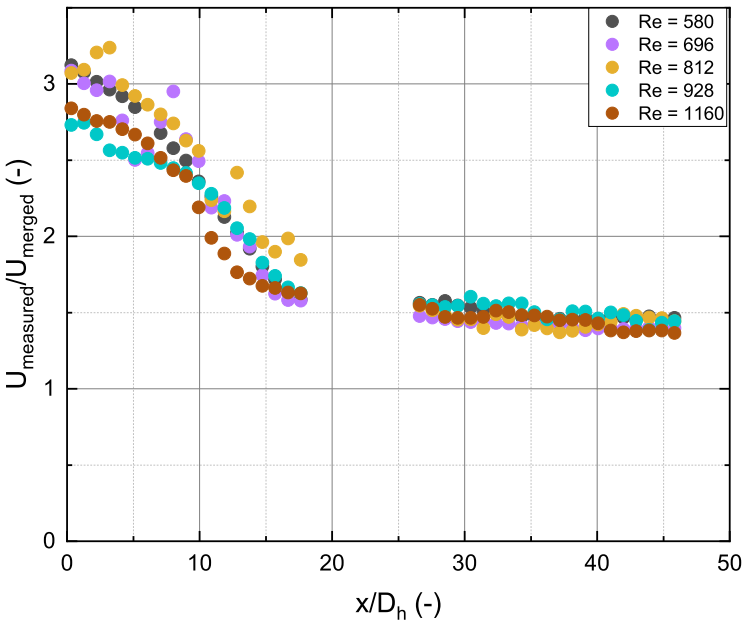

Figure 4.11: The ratio $U_{measured}/U_{merged}$ against x/D_h for different Reynolds numbers (HC3).

For all measurements in the graph above, the starting point was exactly 5mm behind the honeycomb. By extrapolating the measured average streamwise velocity component towards $x/D_{\mathrm{h}} = 0$, it can be verified whether the flow leaves the honeycomb fully developed and laminar. As stated in Section 2.2.1, the ratio $U_{\mathrm{max}}/U_{\mathrm{average}}$ is approximately equal to 2.09 for laminar square duct flow. All the measurements took place in the center of a single honeycomb cell, which means that for this setup U_{max} equals U_{measured}, where U_{measured} at x = 0 is found by extrapolation. The extrapolated data per measurement can be found in Table A.2. Furthermore, U_{average} is the average flow velocity inside the honeycomb, $U_{\mathrm{average\ HC}}$, which can be calculated using Equation 3.4. Dividing the extrapolated value of U_{measured} by this $U_{\mathrm{average\ HC}}$ gives the value of the desired ratio. The calculated values of the ratio can be found in Table A.2 for all Reynolds numbers. Figure 4.12 displays $U_{\mathrm{measured}}/U_{\mathrm{average\ HC}}$ as a function of the Reynolds numbers.

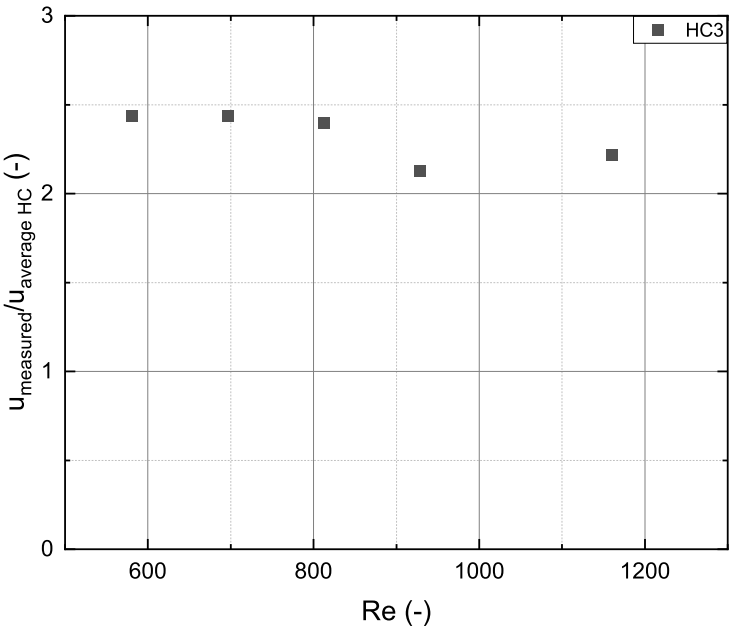

Figure 4.12: The experimentally determined values of $U_{measured}/U_{average\ HC}$ for different Reynolds numbers (HC3).

As can be seen in both Table A.2 and Figure 4.12, the calculated ratio $U_{\text{measured}}/U_{\text{average HC}}$ is slightly higher than the literature value of 2.09 for all Reynolds numbers. One possible explanation for this, is an unequal flow distribution over the individual honeycomb cells. This phenomenon was found and investigated by Ronald Driessen [5], who found that this effect is present while using the 700mm variant of Honeycomb 3. All measurements are performed behind one single cell in the center of the honeycomb. It is possible that the flow velocity in this particular cell was consistently higher due to the inhomogeneous distribution of flow, which means that the measured velocity at the top of the Poiseuille flow profile is consistently higher as well. Therefore, it is a plausible explanation that this inhomogeneity caused the higher values of $U_{\text{measured}}/U_{\text{average HC}}$.

4.1.6 Turning point turbulence

The last part of investigation on Honeycomb 3 is about the turning point of the occurrence of a turbulence peak. As can be seen in Figure 4.2, there is a major difference in turbulence intensity between $Re = 580$ and $Re = 696$. For $Re = 696$ a significant turbulence peak around $x/D_{\text{h}} \approx 16$ is present, while for $Re = 580$ the turbulence intensity does increase downstream but without the appearance of a significant peak. Determining this turning point is critical for the industrial applications. The optimal balance in turbulence intensity, its decay and flow speeds have to be found in order to make the separation process of plastic as efficient as possible. Therefore, it is interesting to determine this turning point for each honeycomb.

A detailed set of measurements is performed for Reynolds numbers between $Re = 580$ and $Re = 696$. Figure 4.13 shows the turbulence intensity as a function of x/D_{h} for this set.

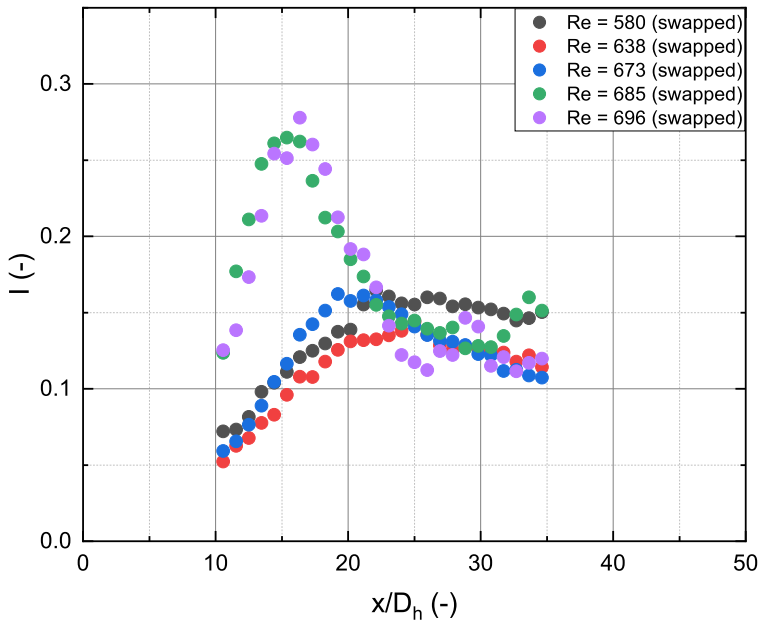

Figure 4.13: The turbulence intensity against x/D_h for Reynolds numbers between $Re = 580$ and $Re = 696$ to determine the turning point for the occurrence of a turbulence peak (HC3 swapped).

It can be seen that the turbulence intensity for $Re = 638$ and $Re = 673$ follows the same trend as $Re = 580$. The turbulence intensity gradually increases downstream, but no significant peak occurs. This is different for $Re = 685$ where a peak appears which, in approximation, is identical to the peak for $Re = 696$. It can be concluded that the transition from no peak to the appearance of a peak is not a gradual, but an instant transition which takes place at $Re \approx 679 \pm 6$. The initial velocities for all three channels were set at 0.58 m/s and 0.59 m/s for $Re = 673$ and $Re = 685$ respectively. Due to limitations of the setup/software, it is impossible to make a measurement in between these Reynolds numbers; the velocity in the software to be set by the experimenter is limited to two decimal places. To verify whether the transition is gradual or instant, an alternative setup is needed or software needs to be adapted. If it turns out that this transition is gradual, it means that this transition takes place between 0.58 - and 0.59 m/s.

4.2 "Equalizing" top and bottom channels

This section focuses on the influence of the initial velocity of the top and bottom channel on the behaviour of the flow downstream the honeycomb. For this research, two honeycombs with significant different porosity are used: Honeycomb 4 with a porosity of $\Phi = 0.385$ and Honeycomb 2 with a porosity of $\Phi = 0.873$ (see Table 3.1).

4.2.1 Honeycomb 4

In Dellaert's measurements on Honeycomb 4, two peaks appeared in the turbulence intensity plots as can be seen in Figure 4.14. The first turbulence peak is the result of the individual flow profiles out of the honeycomb which start mixing downstream resulting in turbulence [4]. However, the occurrence of the second peak is unexpected. For most of the honeycombs the effect does not occur to this extent. This subsection is mainly focused on explaining the occurrence of the second turbulence peak.

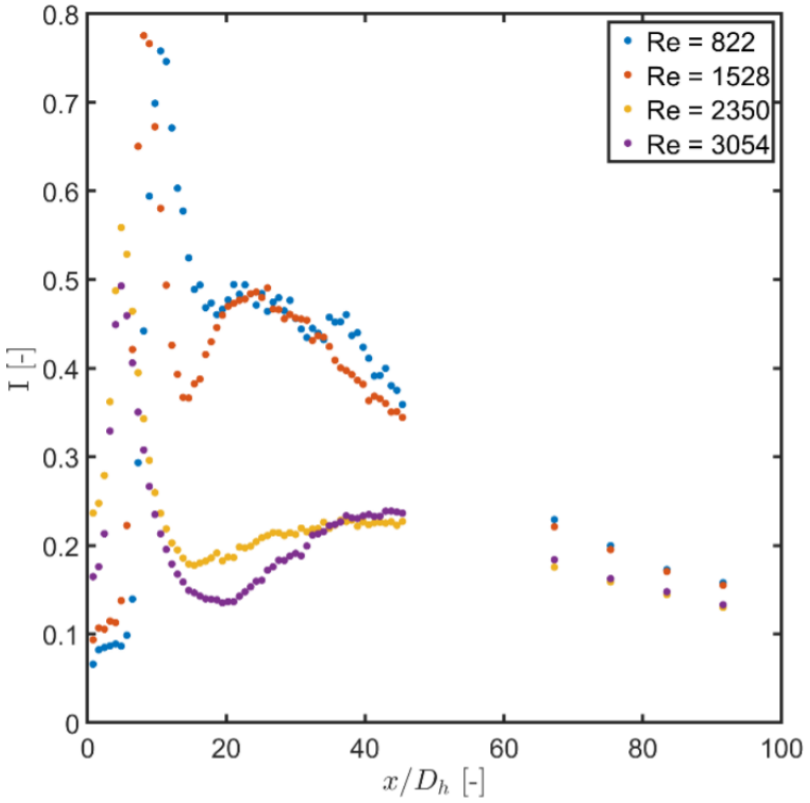

Figure 4.14: The turbulence intensity against x/D_h for different Reynolds numbers for Honeycomb 4 found by Dellaert [4].

Since Honeycomb 4 has a relatively low porosity, the average velocity of the flow leaving this honeycomb is high in comparison with the flow velocity in the top and bottom channel of the

tunnel, as can be concluded from Equation 3.4. The hypothesis is that the second turbulence peak appears due to a large difference in velocity of the flow leaving the top/bottom channel and the flow leaving the honeycomb. In the beginning, the turbulence intensity develops as expected. The large difference in velocity does not play a role in the first few diameters after the honeycomb; it is just the flow out of the honeycomb that is being measured. However, it is expected that the difference in flow velocity initiates a Kelvin-Helmholtz instability which causes the two separate flows to roll up. This roll up can induce turbulence downstream the tunnel, which results in the second turbulence peak.

In order to verify this hypothesis, the settings for the top and bottom channel are adapted in such a way that the average velocity leaving the top and bottom channel is equal to the average velocity of the flow inside the honeycomb. This cancels the relatively large difference in velocities at the point where the flow out of the top/bottom channel meets the flow leaving the honeycomb. In theory, there should be no difference in average velocity between the different flows such that no Kelvin-Helmholtz instability is initiated. Without this instability, the only turbulence occurring is the turbulence resulting from the merging process of the separate velocity profiles leaving the honeycomb and possible vortices due to the influence of flat plates as encountered in Section 2.6, eliminating the second turbulence peak and obtaining the "general" trend with one single peak.

4.2.1.1 Turbulence intensity

First of all, the turbulence intensity in the center of the honeycomb is investigated for $Re = 849$, $Re = 2334$ and $Re = 3076$. Figure 4.15 shows the results of two measurements for $Re = 849$. For both measurements, the initial velocity for the center channel is 0.8 m/s. The difference between the two situations, is in the velocities for the top and bottom channel: for one measurement the initial velocity for these channels is 0.8 m/s, whereas for the other measurement these velocities are equalized to the average velocity inside the honeycomb, which is equal to $\frac{0.8}{\phi}\,\mathrm{m/s} = 2.08\,\mathrm{m/s}$ (see Equation 3.4), where $\phi = 0.385$ is the porosity for Honeycomb 4.

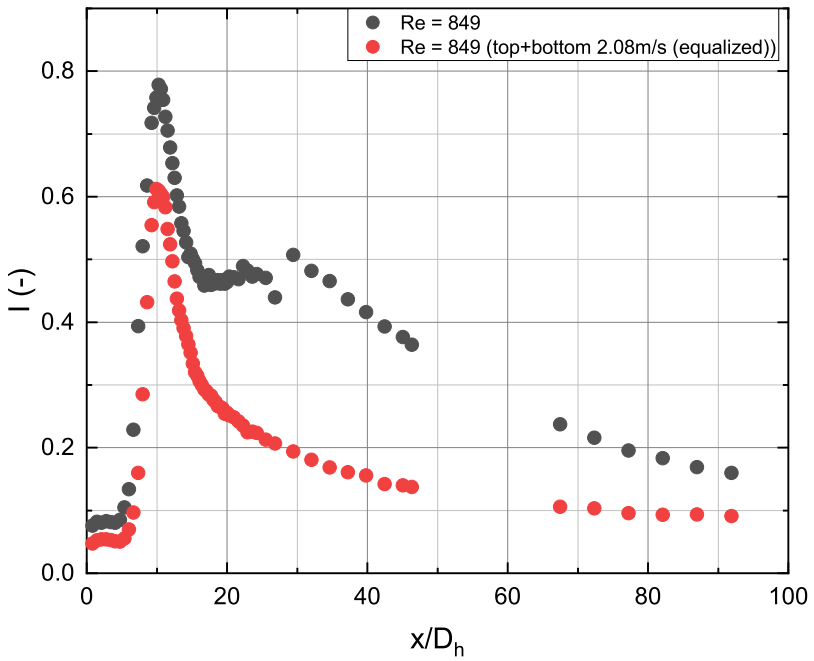

Figure 4.15: The turbulence intensity against x/D_h for different velocities in the top and bottom channel at $Re = 849$ (HC4).

When analyzing Figure 4.15, the stated hypothesis turns out to be correct: the second turbulence peak disappears when the initial velocity in the top and bottom channel is equalized to the average velocity inside the honeycomb. Furthermore, it is clear that the position of the first turbulence peak does not change; it remains at $x/D_\mathrm{h} \approx 10$.

Besides the disappearance of the second peak and lower turbulence intensity for the first peak, the turbulence intensity in general is lower when the top and bottom velocities are equalized to the average velocity of the flow inside the honeycomb. At $x/D_\mathrm{h} \approx 10$ the turbulence intensity is a factor 1.3 lower than the case where all inlet velocities are equal. This factor increases up to 2.5 at $x/D_\mathrm{h} \approx 30$ after which the relative difference in intensity decreases again downstream the tunnel.

This behaviour is also found for higher Reynolds number. Both Figures 4.16 and 4.17 show identical behaviour of the turbulence intensity as a function of distance behind the honeycomb for $Re = 2334$ and $Re = 3076$ respectively. In both cases the initial velocities of top and bottom channel are set equal to the average velocity of the flow inside the honeycomb. This results in an instant disappearance of the second turbulence peak, and a general decrease in turbulence intensity over the full measurement window.

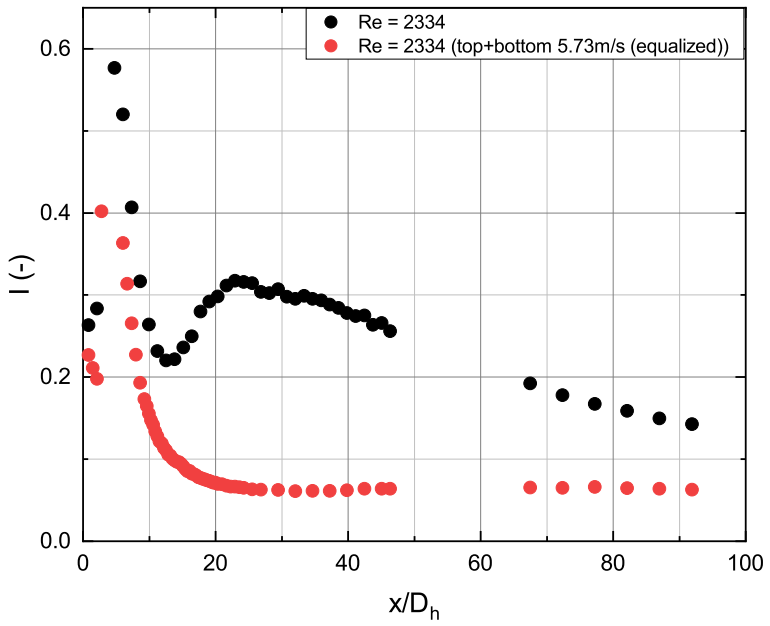

Figure 4.16: The turbulence intensity against x/D_h for different velocities in the top and bottom channel at Re = 2334 (HC4).

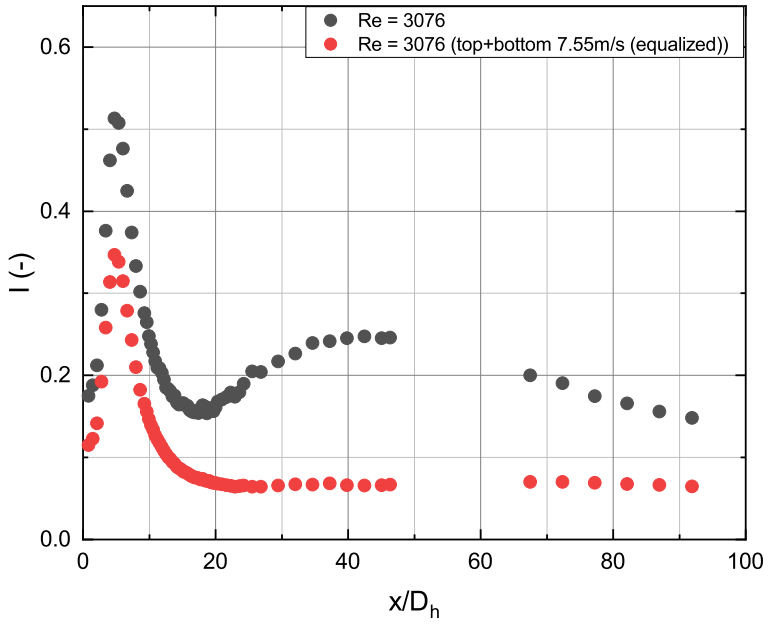

Figure 4.17: The turbulence intensity against x/D_h for different velocities in the top and bottom channel at Re = 3076 (HC4).

For Re = 1591 the research is extended: besides equalizing the initial top and bottom velocity with the average flow velocity inside the honeycomb, a whole range of top and bottom velocities is investigated. The results are displayed in Figures 4.18 and 4.19. An example concerning the way of notation in the legend is illustrated in order to prevent any misunderstandings.

Example: Figure 4.18 shows measurements for Re = 1591. This is the Reynolds number of the flow inside the honeycomb, which means that for all measurements the initial velocity of the center channel is $v_{\text{center}} = 1.50$ m/s. *"Re = 1591 (top+bottom 1.50m/s (-61.0%))"* in the legend indicates the measurement where the top and bottom velocity are set at 1.50 m/s as well. *"Re = 1591 (top+bottom 3.85m/s (equalized))"* indicates the measurement where the initial velocities for the top and bottom channel are equalized to the average flow velocity inside the honeycomb. Lastly, any percentage stated in the legend indicates how much the initial top and bottom velocities deviate from the equalized velocity: *"Re = 1591 (top+bottom 3.43m/s (-10.9%))"* means that the top and bottom velocities are set 10.9% lower than the equalized velocity of 3.85 m/s.

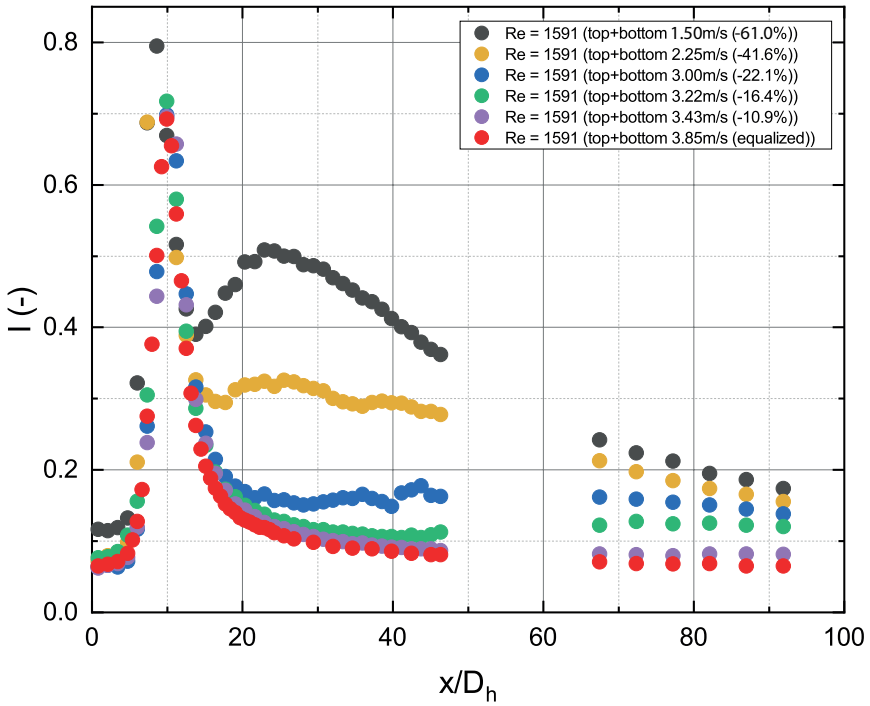

Figure 4.18: The turbulence intensity against x/D_h for different velocities in the top and bottom channel at Re = 1591 (HC4).

Figure 4.18 clearly shows the transition from a second turbulence peak at $x/D_{\text{h}} \approx 22$ to no second turbulence peak at all, by gradually increasing the top and bottom velocities. Setting the top and bottom velocity at 2.25m/s, which is approximately 41.6% lower than the average velocity inside the honeycomb, already results in a decrease of the second peak maximum from $TI \approx 0.5$ to $TI \approx 0.32$. Increasing the top and bottom velocities up to 3.85m/s, which is approximately equal to the average flow velocity inside the honeycomb, completely resolves the second turbulence

peak. Besides the disappearance of the second turbulence peak, it can be concluded that the overall turbulence intensity is generally lower for higher top and bottom velocities. Even 90 diameters away from the honeycomb, the turbulence intensity in the center of the tunnel decreases when the initial top and bottom velocity is increased.

Besides investigating the behaviour of the turbulence intensity for top and bottom velocities up to 3.85 m/s, investigation is conducted on increasing these velocities significantly above the average flow velocity inside the honeycomb. Figure 4.19 displays the results of measurement where the top and bottom velocities are increased up to 75.1% above 3.85 m/s.

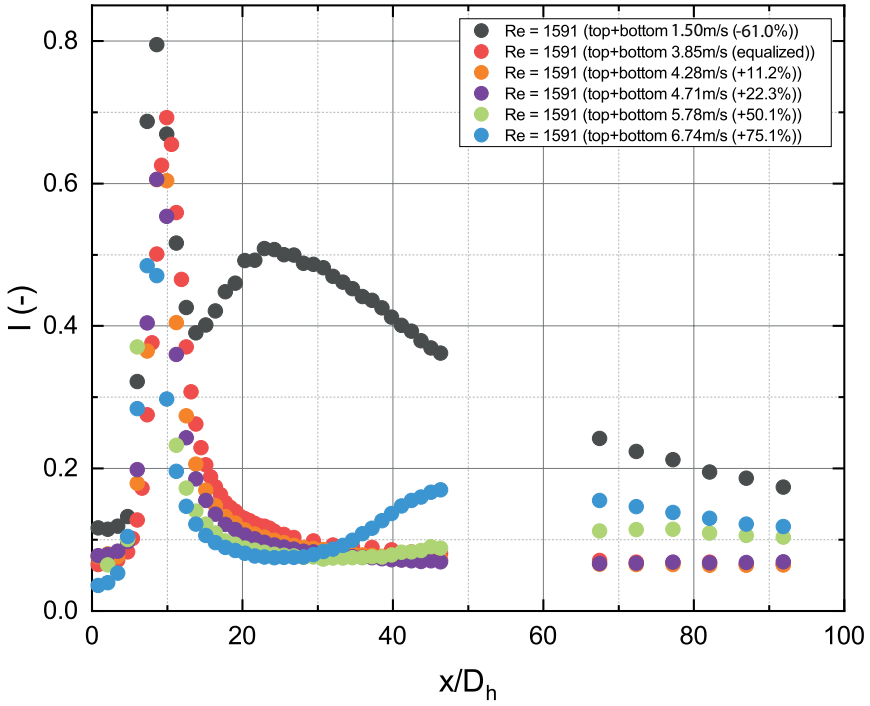

Figure 4.19: The turbulence intensity against x/D_h for different velocities in the top and bottom channel at Re = 1591 (HC4).

Figure 4.19 shows that increasing the velocity to 11.2% above 3.85 m/s results in a decrease of the height of the first turbulence intensity peak and the overall turbulence in the center of the wind tunnel. This trend continues for top and bottom velocities up to 4.71 m/s, which is 22.3% above the equalized velocity. However, increasing the top and bottom velocities to 50.1% above the equalized velocity introduces an increase in turbulence intensity starting at $x/D_\mathrm{h} \approx 30$ and results in a higher turbulence intensity further downstream. This effect is amplified when the velocities in top and bottom channel are increased to 75.1% above 3.85 m/s.

Based on Figures 4.18 and 4.19, it can be concluded that increasing the velocity of the top and bottom channel up to 22.3% above the average velocity of the flow inside the honeycomb results in the least amount of turbulence. However, it is important to emphasize, that all previous measurements

are conducted in the exact center of the honeycomb. Therefore, these results do not automatically characterize the turbulence intensity at arbitrary positions inside the tunnel. The only variable in all experiments is the initial velocity in the top and bottom channel. It is expected that this variable affects the flow across the whole cross section of the tunnel. In order to visualize this, cross sectional measurements in the z-direction are performed which will be discussed in Sections 4.2.1.3 and 4.2.1.4.

4.2.1.2 Velocity profile

It is investigated whether changing the top and bottom velocities, has a significant effect on the streamwise velocity component in the center of the tunnel. This is done by plotting $U_{\text{measured}}/U_{\text{merged}}$ as a function of the distance behind the honeycomb, for the situation where all initial velocities are the same, and for the situation where the top and bottom velocities are equalized to the average flow velocity inside the honeycomb. The results can be found in Figures 4.20 and 4.21 respectively. Note that U_{merged} changes according to Equation 3.6, when initial top and bottom velocities differ from the initial center velocity.

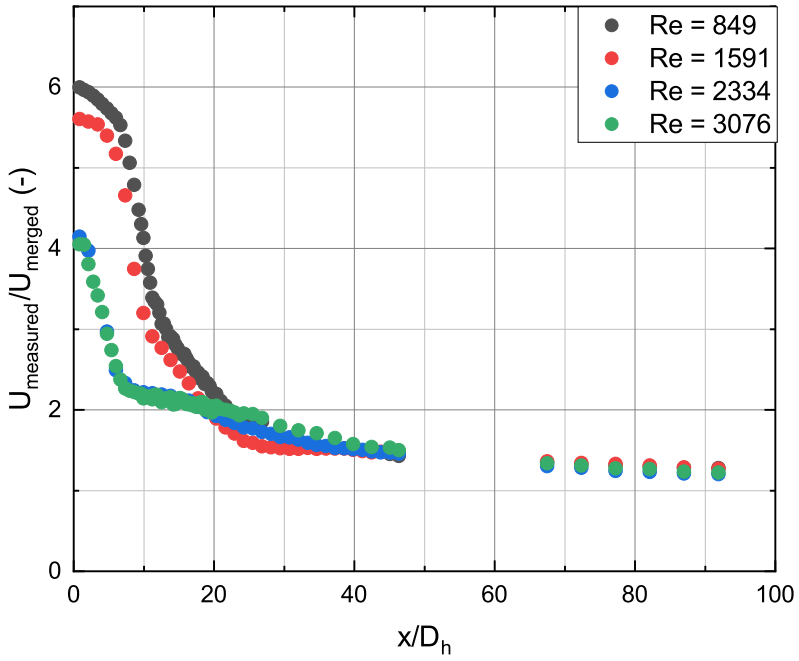

Figure 4.20: The ratio $U_{measured}/U_{merged}$ against x/D_h for different Reynolds numbers with equal initial velocity for all channels (HC4).

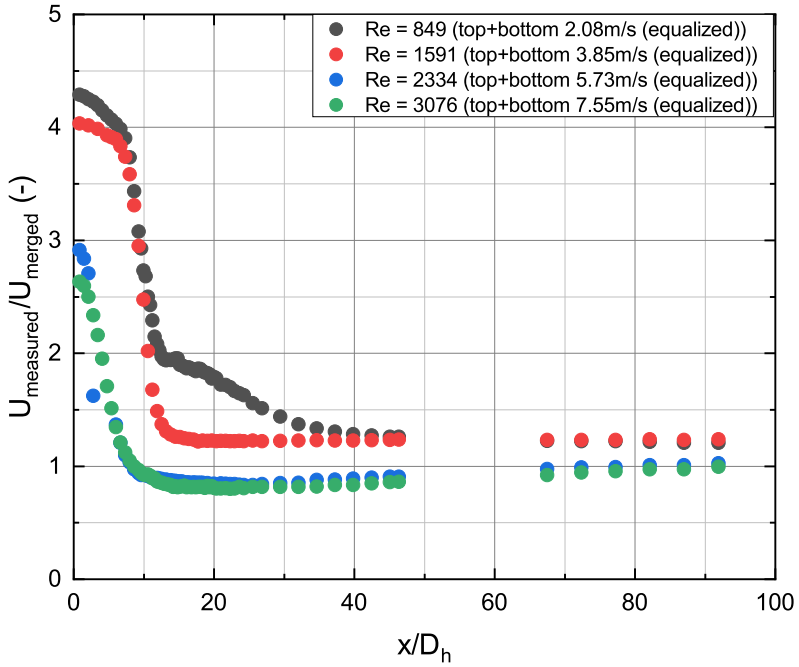

Figure 4.21: The ratio $U_{measured}/U_{merged}$ against x/D_h for different Reynolds numbers with equalized top/bottom channel velocity (HC4).

In both Figure 4.20 and 4.21, the starting points of $Re = 849$ and $Re = 1591$ are close to each other and there is a gap to the starting points of $Re = 2334$ and $Re = 3076$. The latter two have a lower velocity ratio, since the flow is turbulent. Therefore, the measured velocity in the center of a cell is lower in comparison with lower Reynolds numbers, as can be seen in Figure 2.2.

Despite similar symmetry at $x/D_\mathrm{h} = 0$, the values on the y-axis of both figures is different. This is due to the previously mentioned change in U_merged; this variable is higher in Figure 4.21 since the initial top and bottom velocities are higher (see Equation 3.6). By solely looking at U_measured provided by the raw data or factoring out U_merged, it can be concluded that the velocity profiles leaving the cells of the honeycomb are approximately equal for both cases and is independent of adapting the initial top and bottom velocities. Intuitively this makes sense because the top and bottom channels are separated from the middle channel, thus changing the top and bottom velocities has no effect on the flow inside the honeycomb.

When comparing Figures 4.20 and 4.21, it can be seen that the decay per Reynolds number is approximately the same up to $x/D_\mathrm{h} \approx 6.5$. However, further downstream in the wind tunnel the flow leaving the top and bottom channels starts to play a role in the center of the tunnel, which results in different development of the ratio $U_\mathrm{measured}/U_\mathrm{merged}$ for the equalized measurements. The ratio in Figure 4.21 decays much faster compared to Figure 4.20. Furthermore, there is a distinction between laminar Reynolds numbers ($Re = 849$ and $Re = 1591$) and turbulent Reynolds numbers ($Re = 2334$ and $Re = 3076$) in the far-field for the equalized measurements, while for the regular measurements the ratio decays towards the same value for all Reynolds numbers.

Table B.1 contains the values for $U_{\text{measured}}/U_{\text{average HC}}$, for the measurements where all initial velocities are identical and for the measurements where the top and bottom velocities are equalized to the average flow velocity inside the honeycomb. Similarly to the method of Section 4.1.5, the data is extrapolated towards $x/D_{\text{h}} = 0$ to obtain the value of the streamwise velocity component leaving the honeycomb. Figure 4.22 displays these values and the ratio $U_{\text{measured}}/U_{\text{average HC}}$ for all measurements.

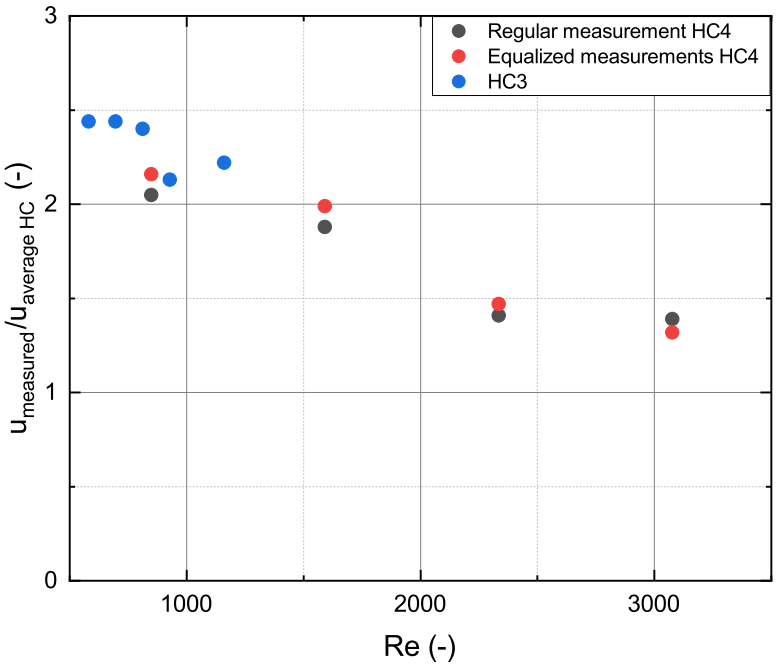

Figure 4.22: The experimentally determined values of $U_{measured}/U_{average\ HC}$ for both the regular and equalized measurements on HC4. The results of Section 4.1.5 on Honeycomb 3 are included.

From Table B.1 and Figure 4.22, it can be concluded that the ratio $U_{\text{measured}}/U_{\text{average HC}}$ slightly increases for the case where the top and bottom velocities are equalized, expect for $Re = 3076$, but they are approximately equal. It was previously found that the turbulence intensity and velocity ratio downstream in the wind tunnel develop substantially different for the equalized situation in comparison with the regular case, due to the higher initial velocity of the top and bottom channel. In order to visualize the effect of these channels on the flow, and to measure the turbulence intensity at the top and bottom of the channel, cross sectional measurements are performed for $Re = 1591$.

4.2.1.3 Height measurements for Re = 1591

The conclusion drawn in Section 4.2.1.1 that increasing the velocity of the bottom and top channels up to 22.3% above the average velocity of the flow inside the honeycomb results in the least amount of turbulence downstream the tunnel, is based on longitudinal measurements in the center of the tunnel. Height measurements on the center line of the tunnel, will tell whether this conclusion is valid at positions above or below the center of the tunnel. Furthermore, the measurements can be

used to visualize the velocity components in all three directions as a function of the height such that the experimenter gains knowledge on the development of the flow downstream the tunnel. However, visualizing the velocity profile of the flow using LDV requires to assemble many individual profiles and is preferably done using techniques such as PIV (Particle Image Velocimetry).

A typical set of measurements is performed at fixed $x/D_{\mathrm{h}} \approx 25$. As can be seen in Figure 4.18, this is the position where the second peak of turbulence intensity is located. Therefore, this is the most interesting position downstream of the honeycomb to measure. The only variable for these measurements is the initial velocity of the top and bottom channels, ranging from $v_{\mathrm{top/bottom}} = 1.5$ m/s (equal to the initial velocity in the center channel) up to $v_{\mathrm{top/bottom}} = 4.71$ m/s. The result of the measurements are shown in Figures 4.23, 4.24, 4.25 and 4.26 for the turbulence intensity, the average x- (streamwise), y- and z-velocities respectively. All these variables are displayed as a function of z-position in the tunnel. The first graph in Figures 4.24, 4.25 and 4.26, is the situation where all initial velocities are 1.5 m/s. The case where the top and bottom velocities are set equal to the average velocity of the flow inside the honeycomb, is visualized in the fourth graph in all three figures. The percentages in the legend of the remaining graphs indicates the difference of the top and bottom velocities with respect to the equalized situation.

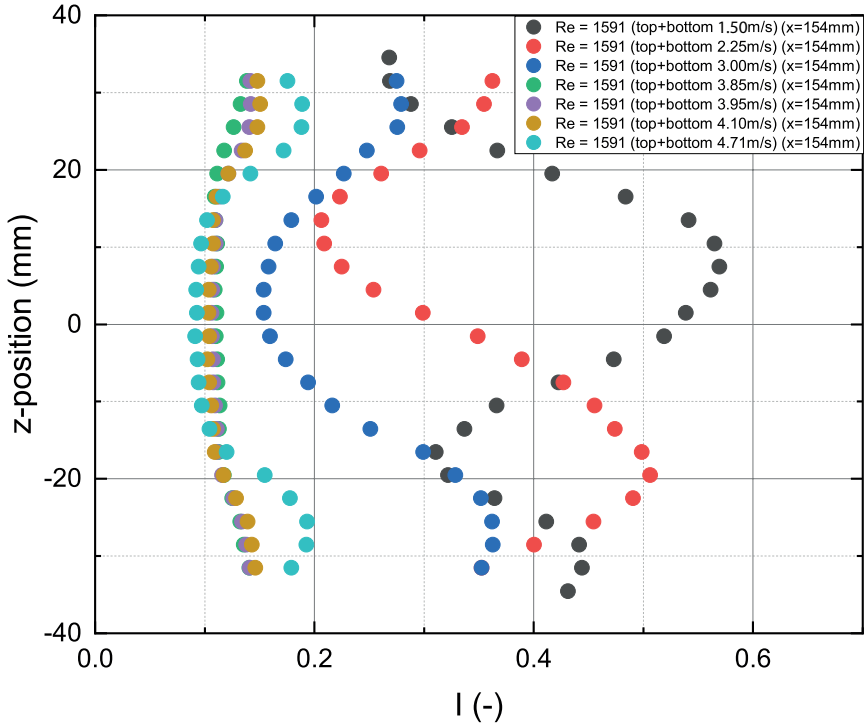

Figure 4.23: The turbulence intensity plotted as a function of the height for different top/bottom velocities, ranging from 1.5 m/s to 4.71 m/s (6).

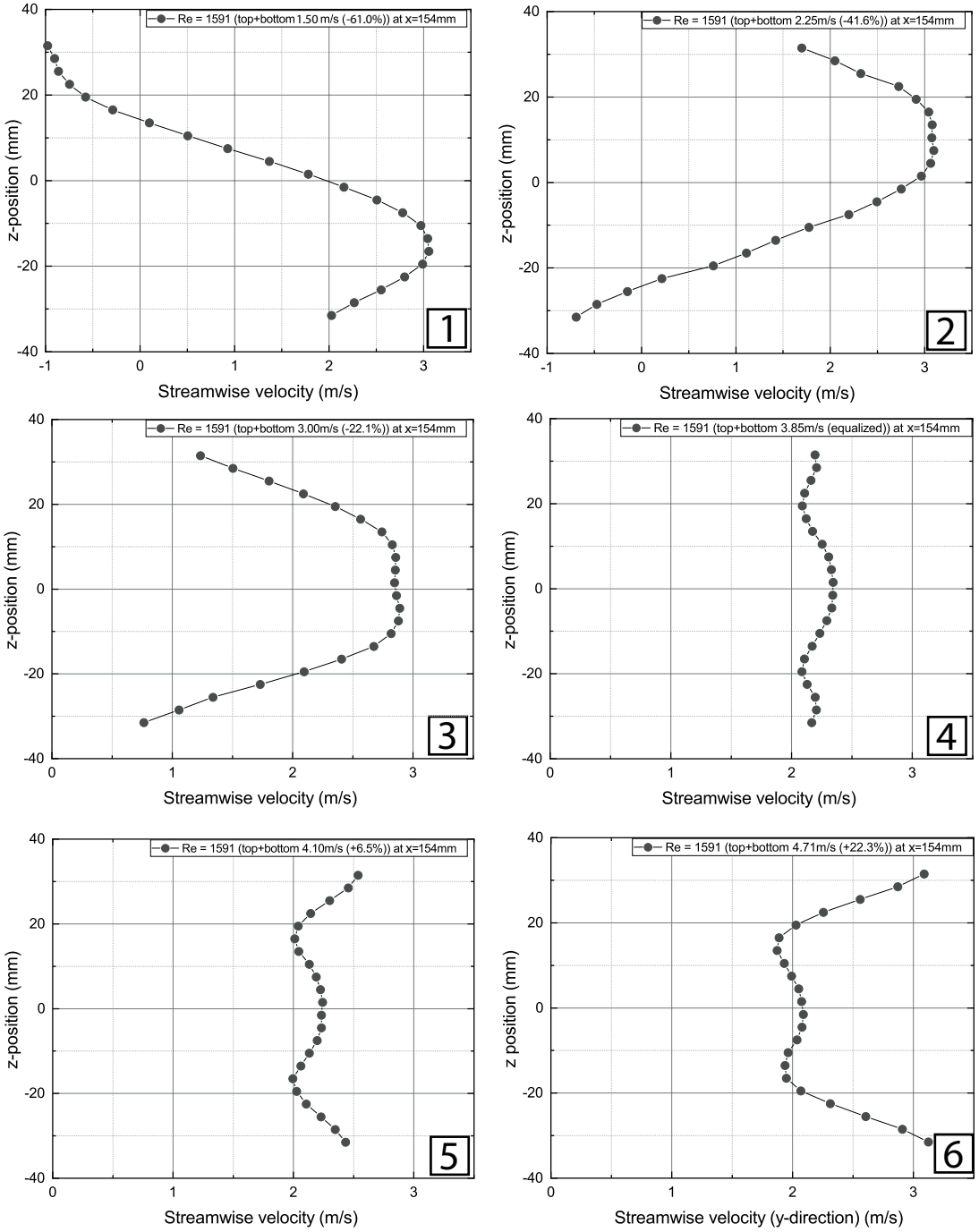

Figure 4.24: The average streamwise velocity component plotted as a function of the height at $x/D_h \approx 25$ for different top/bottom velocities, ranging from 1.5 m/s (1) to 4.71 m/s (6) (HC4).

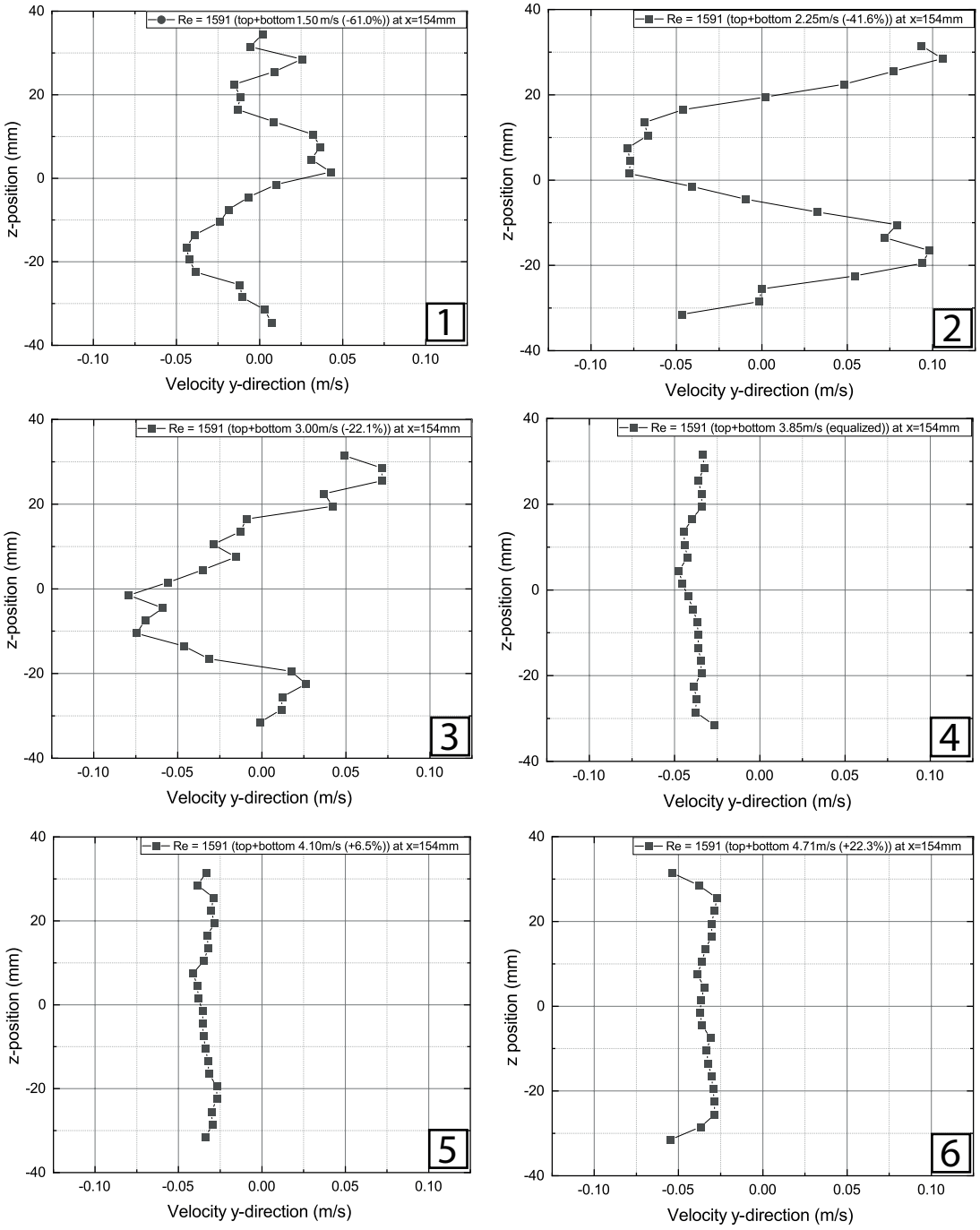

Figure 4.25: The average y-velocity component plotted as a function of the height at $x/D_h \approx 25$ for different top/bottom velocities, ranging from 1.5 m/s (1) to 4.71 m/s (6) (HC4).

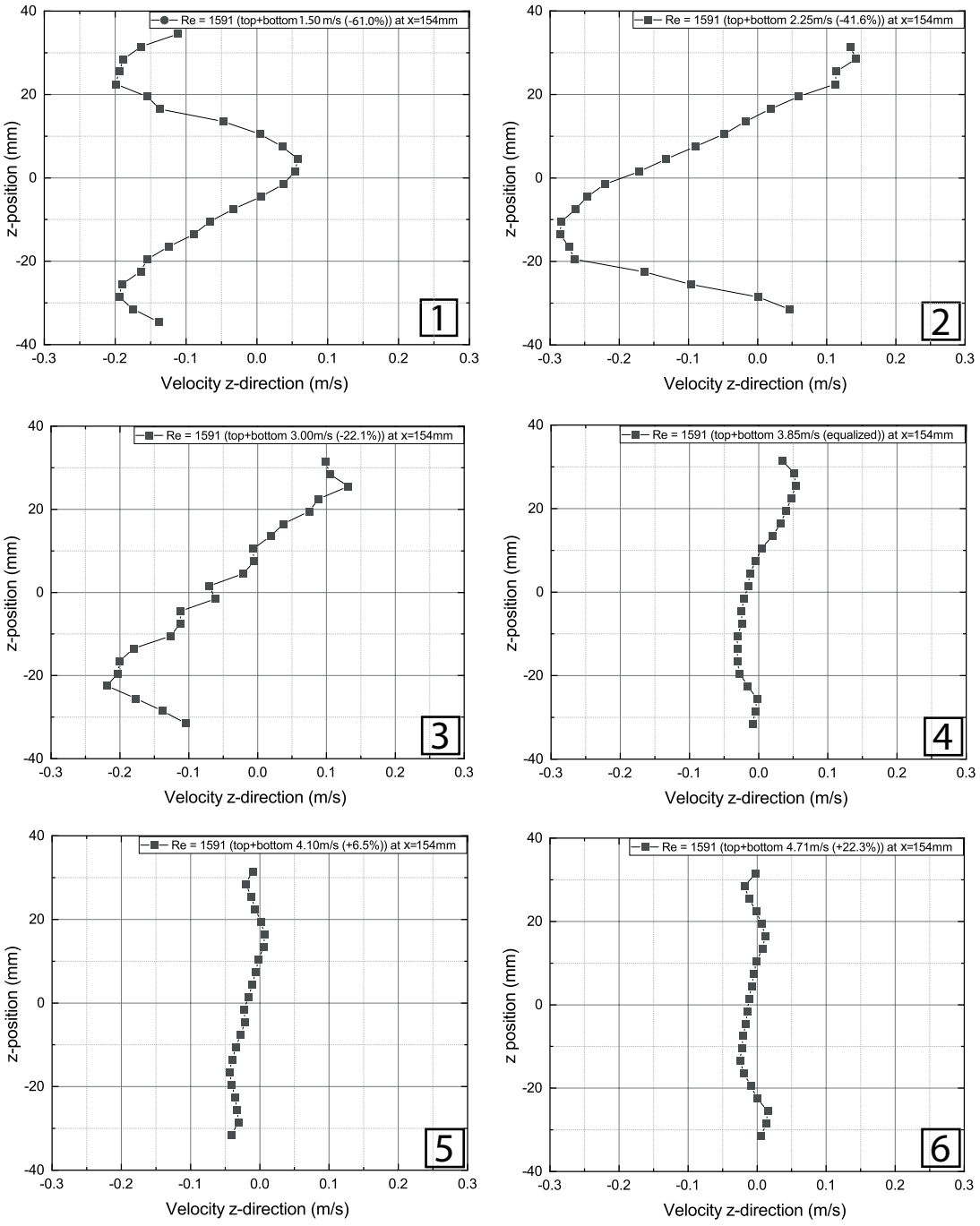

Figure 4.26: The average z-velocity component plotted as a function of the height at $x/D_h \approx 25$ for different top/bottom velocities, ranging from 1.5 m/s (1) to 4.71 m/s (6) (HC4).

The first graph in Figure 4.24, where all initial velocities are 1.5 m/s, shows a streamwise velocity profile being far from symmetric. Furthermore, the first graphs of Figures 4.25 and 4.26 show that the flow has velocity components in the y- and z-directions as well. This implies the presence of vortices in the xy- and xz-plane, which induce turbulence. This is confirmed by Figure 4.23, where it can be seen that the turbulence intensity arbitrarily fluctuates between $TI \approx 0.27$ and $TI \approx 0.58$ for "$Re = 1591\,(top + bottom\,1.50\,m/s)\,(x = 154\,mm)$". The same holds for the situation where both top and bottom velocities are set at 2.25 m/s. The second graph in Figure 4.24 resembles an anti-symmetric velocity profile for the streamwise component in this case. Furthermore, both second graphs of Figures 4.25 and 4.26 show non-zero velocity components in the y- and z-direction. This implies the presence of vortices and thus a turbulent flow, which is again confirmed by the turbulence intensity for this case in Figure 4.23.

The case where the top and bottom velocities are set at 3.00 m/s is the turning point of a less turbulent flow. The profile of the streamwise velocity component is symmetric, however there are still non-zero velocity components in the y- and z-direction. As can be seen in Figure 4.23, the flow is still turbulent, especially at the top and bottom of the tunnel. It is this measurement that confirms the importance of performing height measurements on top of the measurements in the center of the tunnel. Figure 4.18 implies that a top and bottom velocity of 3.00 m/s, drastically lowers the turbulence intensity in the tunnel. However, Figure 4.23 reveals that the turbulence intensity at the top and bottom of the tunnel is significantly higher than in the center. Drawing conclusions solely based on center measurements is not sufficient and height measurements are needed in order to confirm or decline certain conclusions.

Setting the top and bottom velocities equal to the average speed of the flow inside the honeycomb (3.85 m/s), shows an interesting result as can be seen in the fourth graph of Figure 4.24. This graph shows a relatively flat velocity profile for the streamwise component at $x/D_\mathrm{h} \approx 25$. Furthermore, both number four graphs of Figures 4.25 and 4.26 show that the velocity components in the y- and z-direction are approximately zero. This implies that the flow is significantly less turbulent for the case where the top and bottom velocities are equalized to the average flow velocity inside the honeycomb. This is confirmed by Figure 4.23; the turbulence intensity barely fluctuates and stays between $TI \approx 0.1$ and $TI \approx 0.15$ across the whole cross section.

By solely looking at Figure 4.19, one could conclude that increasing the top and bottom velocities even more has a positive effect on the turbulence intensity in the tunnel. As can be seen in Figure 4.23, this is partly true; the turbulence intensity at $z = 0$ indeed decreases for increasing top and bottom velocities. However, the graph reveals that this increase in initial top and bottom velocity results in an increase in turbulence intensity at the top and bottom of the channel. Therefore, it can be concluded that equalizing the initial top and bottom velocity with the average flow velocity inside the honeycomb, in this case 3.85 m/s, ensures the lowest average turbulence across the height of the tunnel.

4.2.1.4 Development of velocity profile for Re = 1591

In order to gain knowledge on the development of the velocity profile while moving away from the honeycomb, height measurements are performed at different distances behind the honeycomb for the situation where all channels have an initial velocity of 1.5 m/s and for the case where the top and bottom channel are equalized to the average flow velocity inside the honeycomb (3.85 m/s). The results are shown in Figure 4.27, which displays the development of the streamwise velocity component downstream of the honeycomb for both cases.

From the upper left graph in Figure 4.27, it can be concluded that the flow leaves the honeycomb symmetric. Despite the measurement gap at $x/D_{\mathrm{h}} \approx 10$ due to water droplets on the glass, the graph clearly shows five different but identical peaks, which corresponds to the number of cells in the z-direction. Therefore, it can be concluded that the anti-symmetric velocity profile which arises downstream in the tunnel, is not due to an imbalance in flow velocity inside the honeycomb, but can be fully assigned to the difference in maximum velocity between the flow leaving the top/bottom channel and the flow leaving the honeycomb. The maximum velocity leaving the honeycomb is more than three times as high as the velocity leaving the top and bottom channel. This difference in velocity across the interface where the top/bottom flow meets the flow leaving the honeycomb, induces a Kelvin-Helmholtz instability, vortices arise and the flow gets turbulent, which visually results in the anti-symmetric velocity profile and velocity components in the y- and z-direction as was concluded in Section 4.2.1.3. This is a possible explanation for the second turbulence peak arising in Figure 4.18.

When the top and bottom velocities are set at 3.85 m/s, the flow leaves the honeycomb symmetric as well, as can be seen in the bottom left of Figure 4.27. However, the maximum velocity out of the honeycomb is not even two times larger than the maximum flow velocity out of the top and bottom channel. The flow leaving the top and bottom channel is measured to be around 4 m/s. It is not possible to measure the full profile leaving these channels, since part of the laser light is blocked by the tunnel. Therefore, it may be possible that the flow leaving the top and bottom channel is even higher than the measured 4 m/s. The smaller difference in velocity between the flow leaving the three channels, induces significantly less Kelvin-Helmholtz instabilities at the interface. Almost no vortices arise, which leads to a symmetric and significantly less turbulent development of the flow, as can be seen in the -middle and bottom right graph of Figure 4.27. Combining this with the fact that the velocity components in the y- and z-direction are approximately zero as concluded in Section 4.2.1.3, makes it a plausible explanation that the disappearance of the second turbulence peak in Figure 4.18 is due to equalizing the initial velocity of the top and bottom channel with the average flow velocity inside the honeycomb.

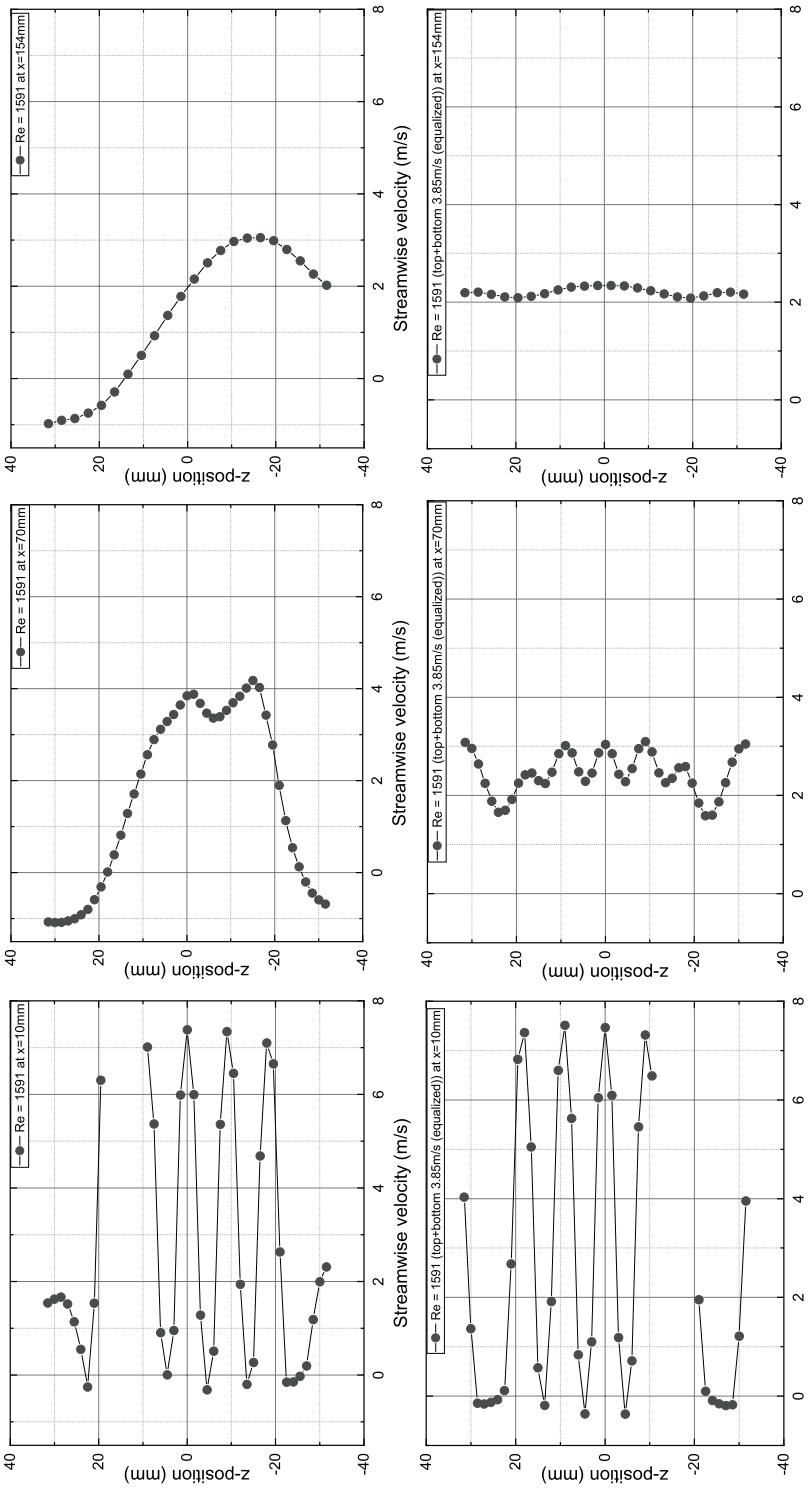

Figure 4.27: Average streamwise velocity plotted as a function of the height at three different positions behind the honeycomb; $x/D_h = 1.63$ ($x = 10$ mm), $x/D_h = 11.38$ ($x = 70$ mm), $x/D_h = 25.04$ ($x = 154$ mm) . The top three graphs display the case where all initial velocities are 1.5 m/s. The bottom three graphs display the case where the top and bottom velocities are equalized to the average flow velocity inside the honeycomb (HC4).

4.2.1.5 Turning point turbulence

The turning point for the occurrence of a turbulence peak is investigated for this honeycomb, as in done for Honeycomb 3. Since Honeycomb 4 has a relatively low porosity, it is chosen to equalize the top and bottom channel velocities to the average flow velocity inside the honeycomb for determination of the turning point. The results of the measurements can be found in Figure 4.28.

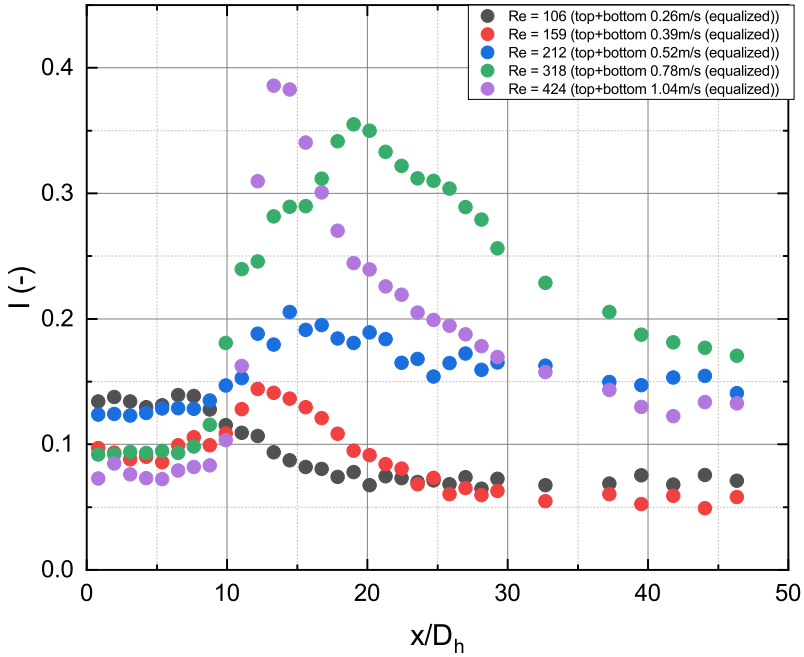

Figure 4.28: The turbulence intensity against x/D_h for low Reynolds numbers (HC4).

Figure 4.28 shows that there is a clear and gradual transition of the appearance of a significant turbulence intensity peak. For $Re = 106$, the intensity fluctuates around a constant value up to $x/D_\mathrm{h} \approx 9$, after which it decreases and becomes constant at $x/D_\mathrm{h} \approx 20$. For $Re = 159$, a small peak is appearing at $x/D_\mathrm{h} \approx 13$, followed by a decay towards the same constant value as for $Re = 106$. For $Re = 212$, the turbulence increases to a local maximum at $x/D_\mathrm{h} \approx 15$, followed by a decrease towards $TI \approx 0.15$. The very first significant peak appears for $Re = 318$, with a maximum of $TI \approx 0.35$ at $x/D_\mathrm{h} \approx 20$, followed by a decrease towards $TI \approx 0.15$ as well. The turbulence intensity peak for $Re = 424$ is higher and shifted towards the honeycomb, compared to $Re = 318$. Determination of a turning point for this honeycomb is somewhat arbitrary, since the transition seems to be gradual instead of instant as was the case for Honeycomb 3. However, the appearance of a significant peak takes place at $Re = 265 \pm 53$, which could then be noted as the turning point in appearance of a turbulence intensity peak.

4.2.1.6 Velocity profile low Reynolds numbers

Besides determination of the turbulence turning point, the measurements are used to investigate the velocity profile leaving the cells of the honeycomb for low Reynolds numbers. Figure 4.29 shows the development of the ratio $U_{\text{measured}}/U_{\text{merged}}$ as a function of the distance behind the honeycomb.

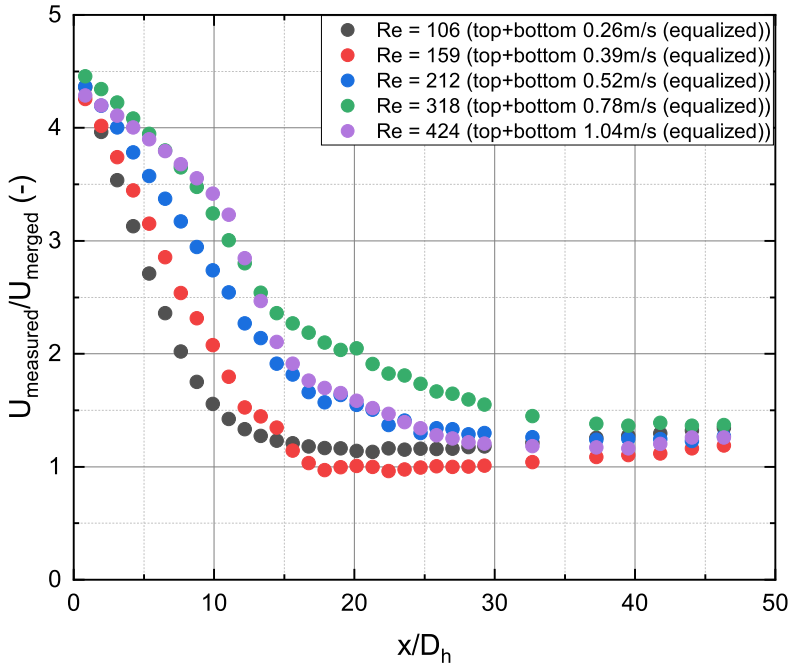

Figure 4.29: The ratio $U_{measured}/U_{merged}$ against x/D_h for low Reynolds numbers with equalized top/bottom channel velocity (HC4).

For all Reynolds numbers the zero value is approximately 4.3. Furthermore, the ratio decays to approximately 1.25 for all measurements. The only difference between the measurements is the rate of decay. For $Re = 106$, the decay rate is highest and in general the decay rate decreases for increasing Reynolds numbers.

In Section 4.2.1.2, it is found that increasing the Reynolds number results in a decrease of the ratio $U_{\text{measured}}/U_{\text{average HC}}$. Around $Re \approx 2300$, duct flow becomes turbulent. However, all Reynolds numbers in this section are well below $Re = 2300$, which means the flow is laminar. Furthermore, by applying Equation 2.7, it can be proven that for all Reynolds numbers the flow leaves the honeycomb fully developed. Therefore, it is expected that the ratio $U_{\text{measured}}/U_{\text{average HC}}$ is approximately 2.09 for all five Reynolds numbers. Table B.2 contains the extrapolated value of U_{measured} at x = 0, which is obtained by the same method as in Sections 4.1.5 and 4.2.1.2. Dividing the extrapolated value of U_{measured} by U_{merged} for each measurement, gives the desired value. The obtained ratios are displayed in Figure 4.30 (most left five values), which contains the previously found values of $U_{\text{measured}}/U_{\text{average HC}}$ for different honeycombs as well.

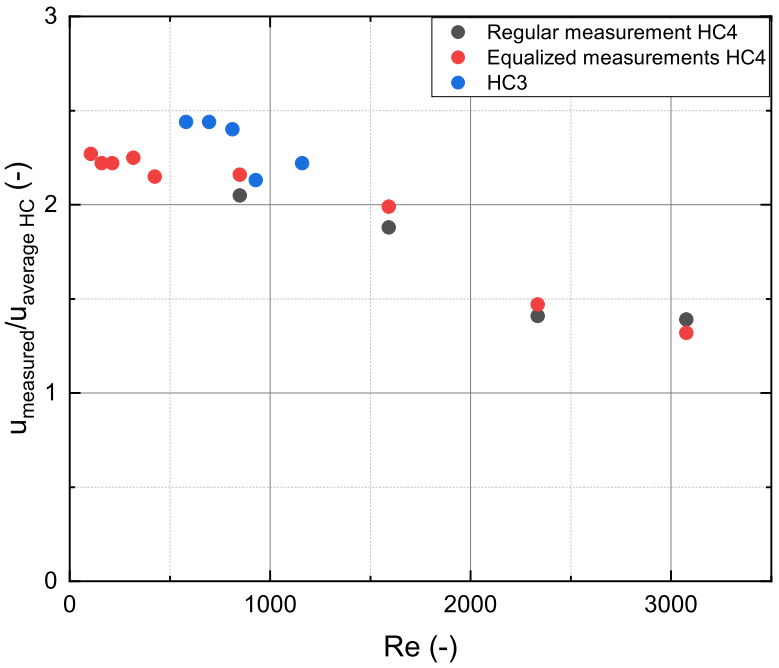

Figure 4.30: The experimentally determined values of $u_{measured}/u_{average\ HC}$ for equalized measurements at low Reynolds numbers on HC4. The results of Sections 4.1.5 and 4.2.1.2 are included as well.

From Table B.2 and Figure 4.30, it can be concluded that obtained values for $U_{\text{measured}}/U_{\text{average HC}}$ are somewhat higher than expected literature value of 2.09 for all five low Reynolds numbers. Possible explanations for this deviation are the uncertainty of the overall setup, a porosity that slightly deviates from the calculated porosity in Table 3.1 or some inhomogeneity of the flow inside the honeycomb. Further research can be conducted in order to investigate the reason of the slightly increased values of the ratio.

4.2.2 Honeycomb 2

A short research on the effect of the top and bottom channels on the flow for Honeycomb 2 was conducted, to investigate whether unbalanced flow velocity in the center and side channels leads to similar observations as for Honeycomb 4. Honeycomb 2 has a significantly higher porosity than Honeycomb 4, which means that the relative difference in velocity between the flow leaving the honeycomb and the flow leaving the top/bottom channel for identical initial velocities for all channels, is smaller for Honeycomb 2 in comparison with Honeycomb 4. In Section 4.2.1, it is concluded that this difference leads to the occurrence of a second turbulence peak. Measurements are performed at $Re = 1008$ and $Re = 1513$. By analyzing the turbulence intensity plots, conclusions can be drawn about the effect of the top and bottom channel on this honeycomb.

4.2.2.1 Turbulence intensity

Figure 4.31 shows the turbulence intensity plot for Re = 1008. Each measurement has an identical initial velocity of $v_{\text{center}} = 3.2$ m/s for the center channel, but a different initial velocity for the top and bottom channel. As can be seen in Table 3.1, the porosity of Honeycomb 2 is $\Phi = 0.873$, which means that the average flow velocity inside the honeycomb is $\frac{3.2}{0.873} \approx 3.67$ m/s (see Equation 3.4). In the figure, this is called the "*top+bottom 3.67 (equalized)*" measurement. All percentages in the legend indicate the deviation of the initial top and bottom velocity of a particular measurement with respect to the "equalized" velocity of 3.67 m/s (identical to example given in Section 4.2.1).

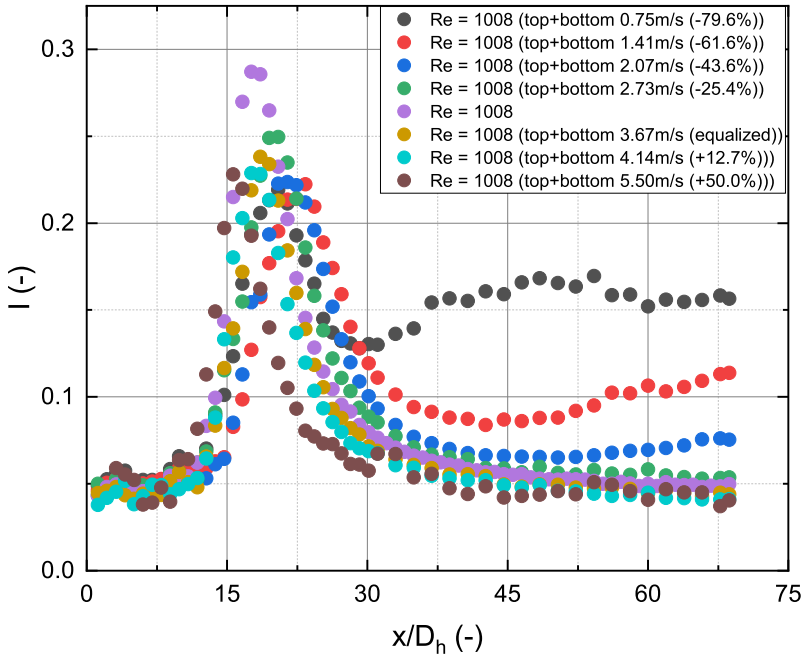

Figure 4.31: The turbulence intensity against x/D_h for different velocities in the top and bottom channel at Re = 1008 (HC2).

From Figure 4.31, it can be concluded that a second turbulence peak occurs for a large difference

in velocity between the flow leaving the honeycomb and the flow leaving the top/bottom channel. This is most prominent at $v_{\text{top/bottom}} = 0.75$ m/s. The average velocity of the flow inside and just behind the honeycomb is 3.67 m/s, which means that a relative difference of 79.6% and an absolute difference of 2.92 m/s between the flow leaving the honeycomb and the flow leaving the top/bottom channel, leads to the appearance of a second turbulence peak starting at $x/D_{\text{h}} \approx 30$. Increasing the initial velocity for the top and bottom channel up to $v_{\text{top/bottom}} = 1.41$ m/s, leads to a disappearance of a significant second turbulence peak, however it can be seen that at $x/D_{\text{h}} \approx 45$ the turbulence intensity starts to increase. Increasing the initial velocity in the top and bottom channel even more, gradually decreases the turbulence intensity far downstream the tunnel.

Figure 4.32 shows the turbulence intensity as function of distance behind the honeycomb for $Re = 1519$ (initial $v_{\text{center}} = 4.8$m/s). The number of measurements is lower in comparison with $Re = 1008$ due to limitations of the setup. A combination of high pressure in the pressure vessel and a large difference in velocity between the top/bottom channel and the center channel, resulted in large fluctuations of the flow velocity in the center channel. Despite this, the same trend as for $Re = 1008$ is found for this Reynolds number.

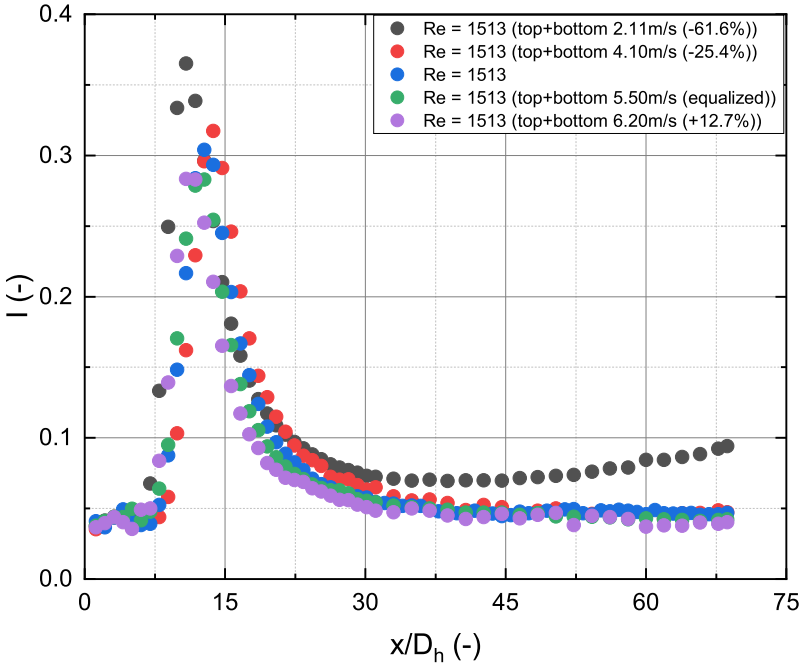

Figure 4.32: The turbulence intensity against x/D_h for different velocities in the top and bottom channel at $Re = 1513$ (HC2).

Figure 4.32 also shows that for measurements where the initial top and bottom velocity are around the equalized velocity, a gradual decrease occurs in turbulence intensity far downstream the tunnel. However a larger difference in velocities, for instances $v_{\text{top/bottom}} = 2.11$ m/s, already results in an increase of turbulence intensity at $x/D_{\text{h}} \approx 45$. It is expected that decreasing the initial top and bottom velocity even more, will result in the appearance of a significant second turbulence peak.

4.2.3 Decay characteristics

The decay characteristics for the measurements on both Honeycomb 2 and 4 can be determined using the method explained in Section 4.1.4. The decay will be characterized for two situations. First, for all Reynolds numbers where the top and bottom velocities are approximately equal to the average flow velocity inside the honeycomb for both Honeycomb 2 and 4. Secondly for all the measurements on Honeycomb 4 at $Re = 1591$. In this way, the effect of the initial top and bottom velocity on the decay characteristics can be investigated.

4.2.3.1 Equalized measurements

The measurements on Honeycomb 4 from Section 4.2.1.1 where the initial top and bottom velocity is equalized to the average flow velocity inside the honeycomb, as well as the measurements on Honeycomb 2 from Section 4.2.2.1 where the initial velocity is equal for all three channels, can be fitted with the power law in the near-field. For Honeycomb 2, it is possible to fit the far-field as well. Table B.3 in the Appendix contains all values obtained from fitting the turbulence intensity with the power law. The near-field values are plotted as a function of the Reynolds number combined with the data from Dellaert and Driessen, as can be seen in Figures 4.33, 4.34 and 4.35.

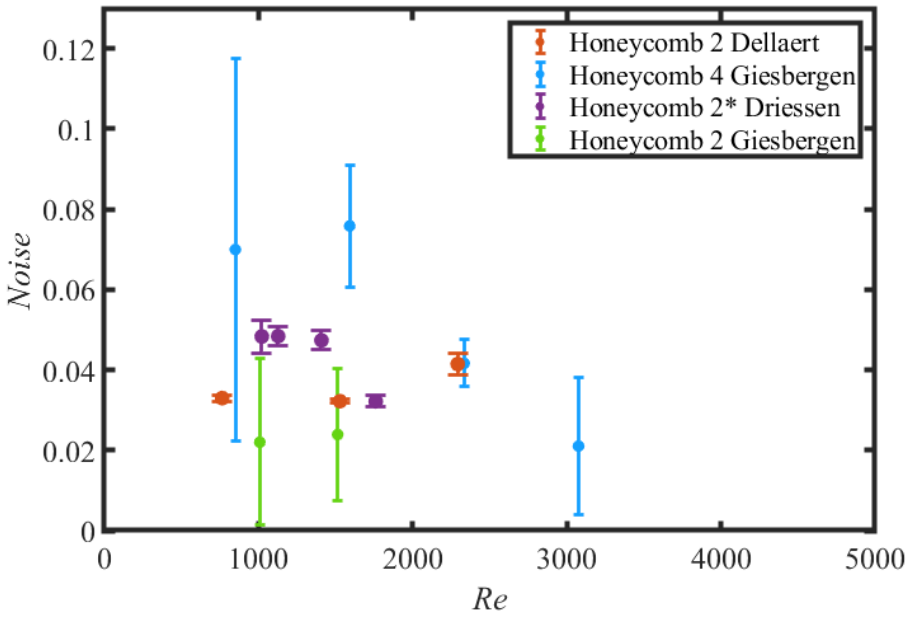

Figure 4.33: The noise N as a function of the Reynolds number, combined with results from Dellaert and Driessen (HC2+HC4).

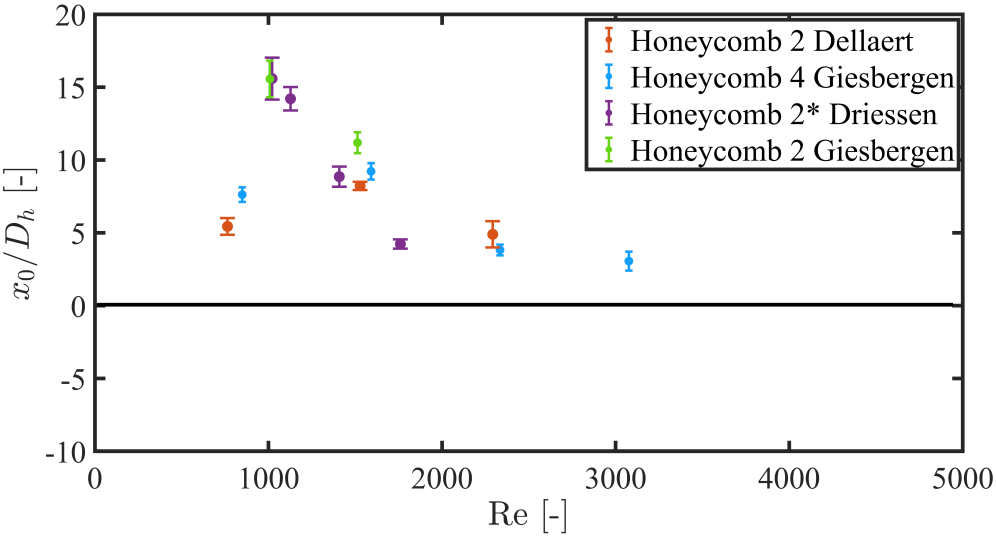

Figure 4.34: The virtual origin x_0/D_h as a function of the Reynolds number, combined with results from Dellaert and Driessen (HC2+HC4).

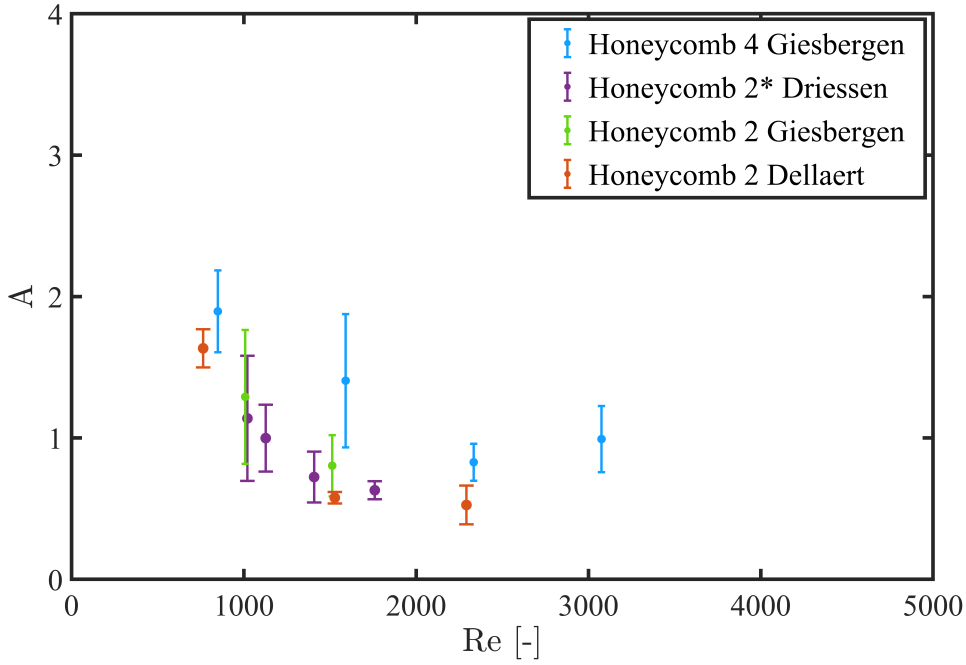

Figure 4.35: The decay coefficient A as a function of the Reynolds number, combined with results from Dellaert and Driessen (HC2+HC4).

Figure 4.33 shows the noise as a function of the Reynolds number. It is clear that the uncertainties in the found noise are substantially larger than the uncertainties found by Dellaert and Driessen, especially for Honeycomb 4. For Honeycomb 4, the initial top and bottom velocities are equalized to the average flow velocity in the honeycomb. As concluded, this leads to the disappearance of the second turbulence peak. However, this may not automatically imply that the turbulence intensity plots are suitable for fitting, resulting in the large error bars. Figures 4.34 and 4.35 show that for Honeycomb 2, the values for both the virtual origin x_0/D_h and decay coefficient A are in line with the values found by Driessen. The values found for Honeycomb 4 also follow the general trend in both graphs.

Besides fitting the turbulence decay in the near-field, it is possible to fit the decay in the far-field for Honeycomb 2 as well. The far-field starts at $x/D_h \approx 35$. Especially for honeycombs with small hydraulic diameters the far-field can be measured, since it requires less absolute distance behind the honeycomb. Far-field fits follow the same general procedure in Matlab as near-field fits. However, in the case of far-field the experimenter needs to set both the begin and end point for the fit manually, and the virtual origin x_0/D_h and noise N found during the near-field fit are fixed. Thus, the decay exponent p and decay coefficient A are the variables being determined during far-field fits. The two measurements from both Figures 4.31 and 4.32 where the initial velocity for all three channels is identical, so without any percentage indicated in the legend, are fitted. For $Re = 1008$, the noise and virtual origin are fixed at 0.022 and 15.56 respectively, and for $Re = 1518$ the noise is fixed at 0.024 and virtual origin at 11.19 (see Table B.3). This results in $p = -0.7342$ and $A = 0.032$ for $Re = 1008$, and $p = -0.25$ and $A = 0.004$ for $Re = 1518$.

It should be noted that fitting the far-field is not as accurate as the near-field. In the far field, disturbances in turbulence intensity are more common and therefore the selection of begin and end point of the fit has a significant effect on the decay constants. Fitting of the points which fit perfectly versus fitting all points in the far-field including the disturbed points, results in a different value for p and A.

4.2.3.2 Re = 1591

In Section 4.2.1.1 research is described on the effect of the top and bottom channel on the turbulence intensity for Re = 1591. By fitting these measurements with the power law, the effect of misalignment of the center honeycomb flow and side channel flow on the fit parameters is investigated. Measurements with a second turbulence peak cannot be fitted. Furthermore, measurements where the initial top/bottom velocities and center velocities differ, do not follow the general trend the power law is based on. Therefore, fitting these measurements should be done with care and conclusions based on the fit may be inaccurate. All obtained fitting values can be found in Table B.4.

Figures 4.36, 4.37 and 4.38 show the relation between the noise, virtual origin and decay coefficient with respect to the deviation of the initial top/bottom velocity relative to the equalized situation for $Re = 1591$, respectively. So the measurement at zero is the measurement where the initial top and bottom velocity are equalized to the average flow velocity inside the honeycomb. The percentages in the plot match with the percentages in the legend of Figures 4.18 and 4.19

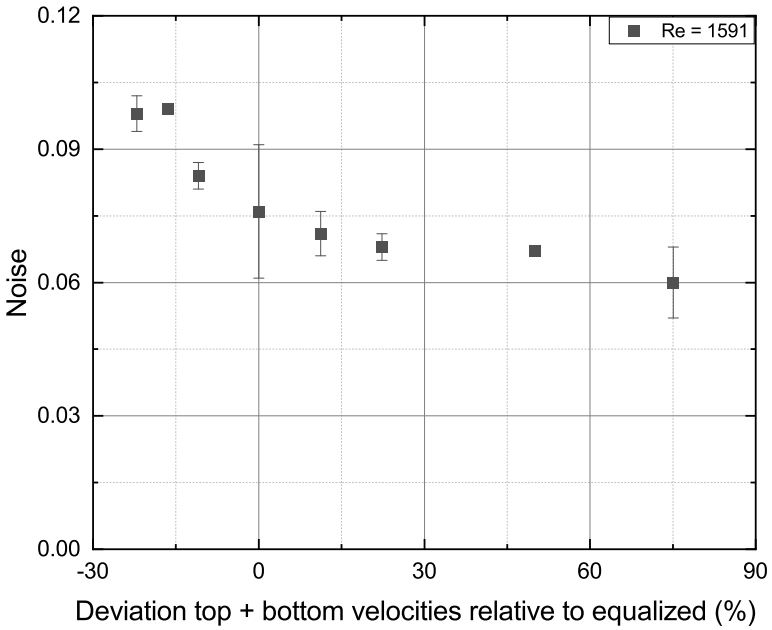

Figure 4.36: The noise N as a function of the deviation of the initial top/bottom velocities relative to the equalized situation (HC4).

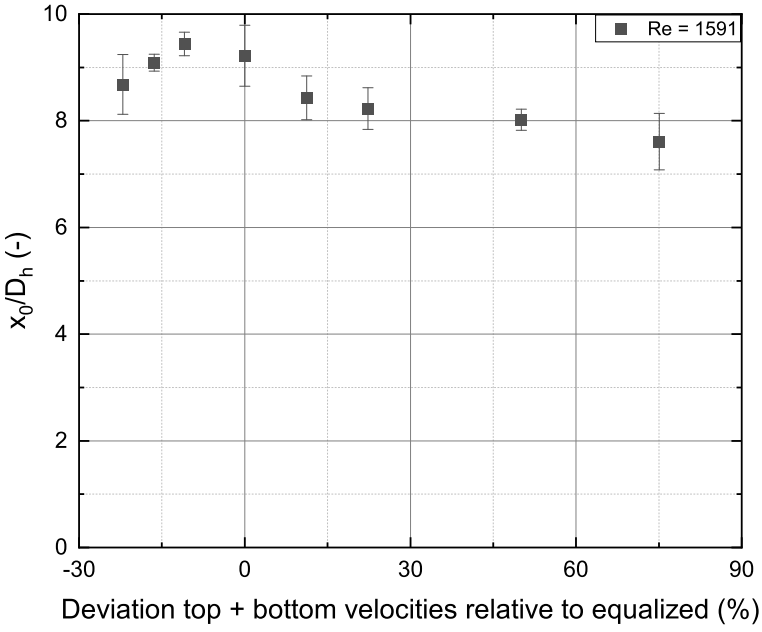

Figure 4.37: The virtual origin x_0/D_h as a function of the deviation of the initial top/bottom velocities relative to the equalized situation (HC4).

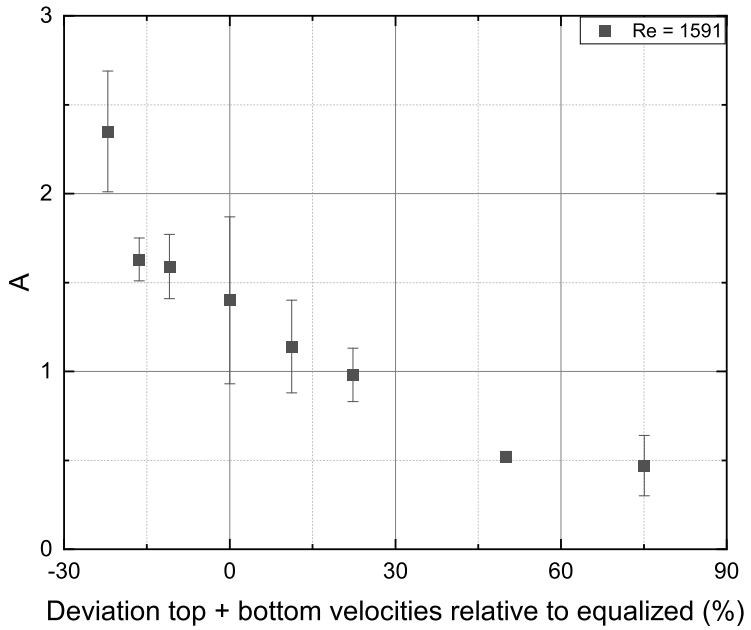

Figure 4.38: The decay coefficient A as a function of the deviation of the initial top/bottom velocities relative to the equalized situation (HC4).

These figures show some trends. Figure 4.36 shows that the noise decreases for initial top/bottom velocities above the equalized velocity and increases for initial top/bottom velocities below the equalized velocity. Furthermore Figure 4.37 shows that the virtual origin is maximum around equalized top/bottom velocities and decreases for top/bottom velocities under or above this value. Finally, the decay coefficient shows a linear relation with respect to the deviation in top/bottom velocity; the coefficient decreases for initial top/bottom velocities above the equalized case and increases for initial top/bottom velocities below the equalized velocity.

4.3 Entrance length

This section is about the influence of the length of a honeycomb on the behaviour of the flow. The investigation is conducted on Honeycomb 1 which has two variants, one with a length of 50 mm (Honeycomb 1) and one with a length of 750 mm (Honeycomb 1*) (see Table 3.1). It is expected that there is a transition from laminar to turbulent around $Re \approx 2300$. Therefore, the Reynolds numbers are chosen such that both turbulent and laminar flow are investigated, as well as the transition zone. Besides the Reynolds number, it is important to take the hydrodynamic entrance length L_h into account, in order to determine whether the flow is fully developed.

4.3.1 Honeycomb 1

4.3.1.1 Turbulence intensity

Figures 4.39, 4.40 and 4.41 show the turbulence intensity plots for both variants of Honeycomb 1 for $Re = 1035$, $Re = 1726$ and $Re = 3037$ respectively. The Reynolds numbers are chosen such that there is a laminar ($Re = 1035$) and turbulent ($Re = 3037$) flow, as well as one in between those two ($Re = 1726$).

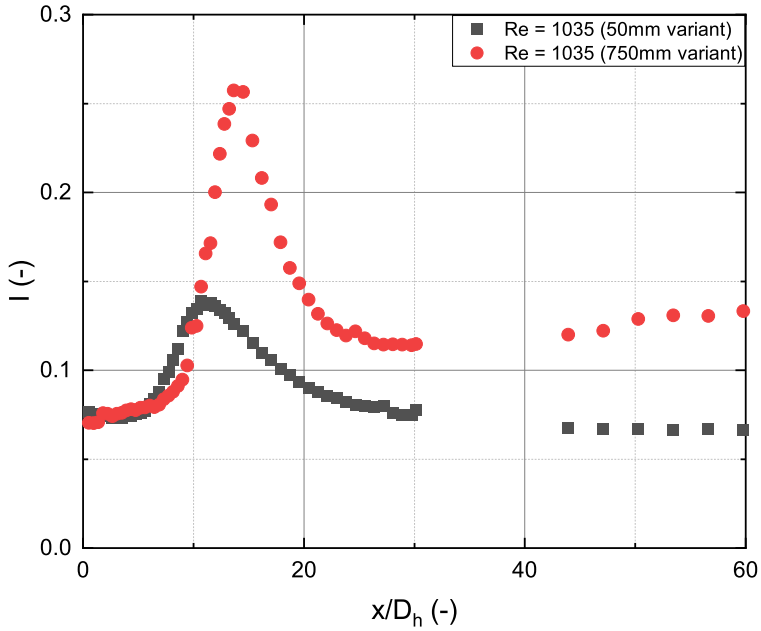

Figure 4.39: The turbulence intensity against x/D_h for $Re = 1035$ of both the 50 mm and 750 mm variant of Honeycomb 1.

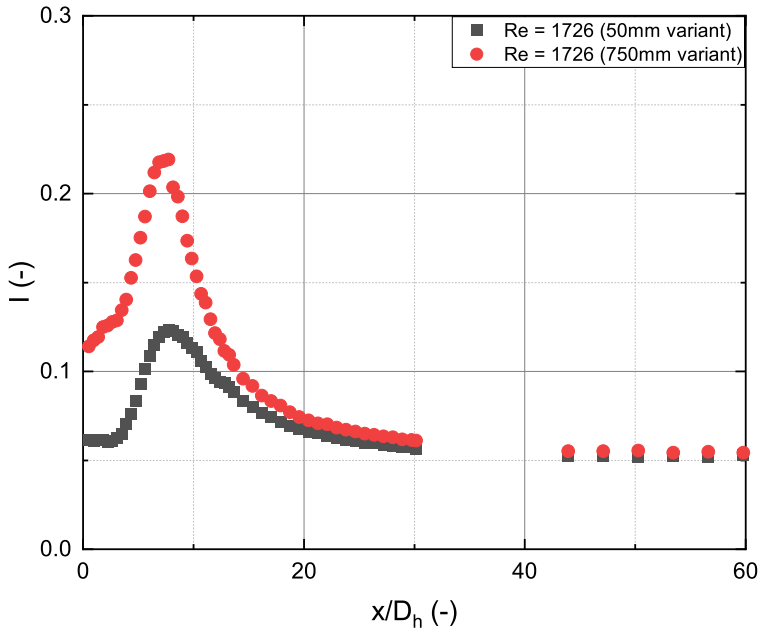

Figure 4.40: The turbulence intensity against x/D_h for $Re = 1726$ of both the 50 mm and 750 mm variant of Honeycomb 1.

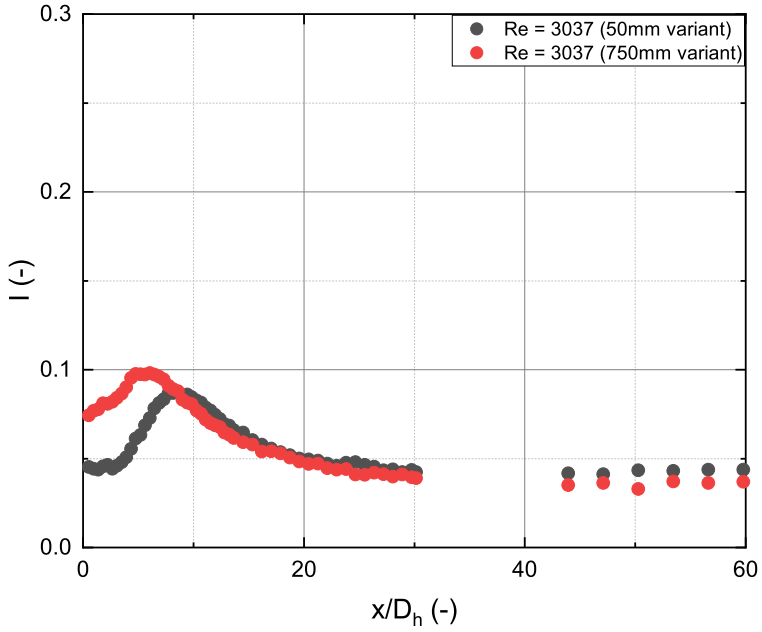

Figure 4.41: The turbulence intensity against x/D_h for $Re = 3037$ of both the 50 mm and 750 mm variant of Honeycomb 1.

The turbulence intensity plots reveal some interesting aspects about the influence of the length of the honeycomb. For $Re = 1726$ and $Re = 3037$ the turbulence intensity decays to approximately the same value in the far-field, independent of the length of the Honeycomb. It is the peak intensity that significantly changes. Especially for $Re = 1035$ and $Re = 1726$, the turbulence intensity peak drastically decreases when the honeycomb is shorter. Since the turbulence peak is induced by mixing of flows leaving separate cells of the honeycomb, it is important to investigate the influence of the length of the honeycomb on the velocity profile of the flow leaving the honeycomb, which will be done in Section 4.3.1.3. Furthermore, Figure 4.40 shows that the flow leaving the 750 mm variant of Honeycomb 1 is quite turbulent, since the turbulence intensity at $x/D_h = 0$ is approximately 12%. Since it is expected that transition from laminar to turbulent takes place at $Re \approx 2300$, it is investigated in Section 4.3.1.4 what causes the flow to be turbulent at this Reynolds number.

4.3.1.2 Decay characteristics

The power law is applied to the turbulence intensity plots of $Re = 1035$, $Re = 1726$ and $Re = 3037$ using the method as explained in Section 4.1.4. The obtained values are combined with the values Dellaert found for 500mm variant of Honeycomb 1.

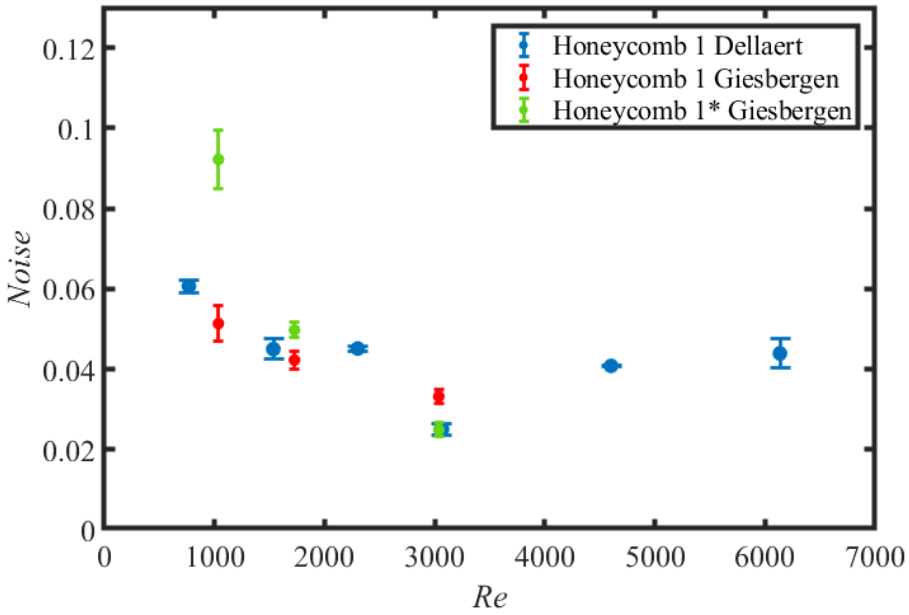

Figure 4.42: The noise N as a function of the Reynolds number, combined with results from Dellaert (HC1+HC1).*

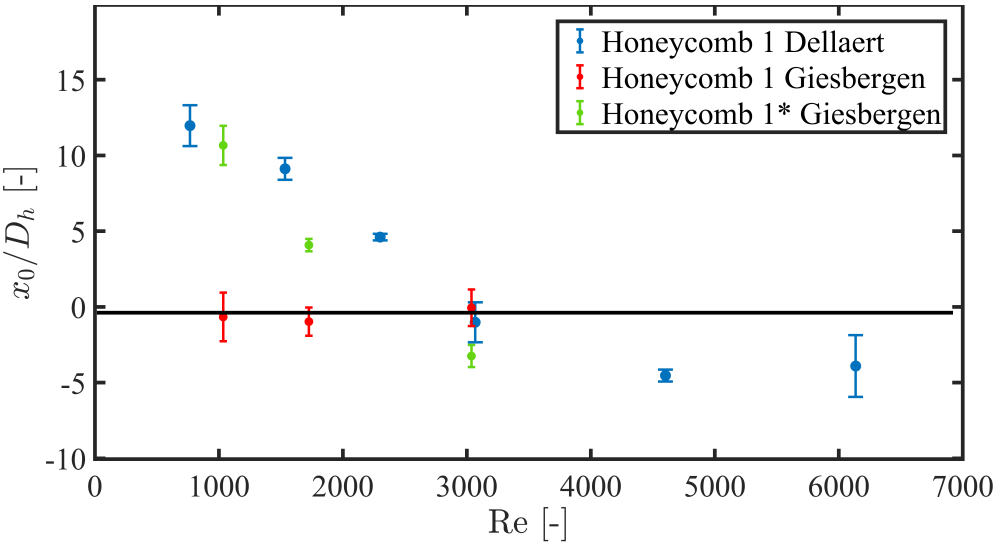

Figure 4.43: The virtual origin as a function of the Reynolds number, combined with results from Dellaert (HC1+HC1).*

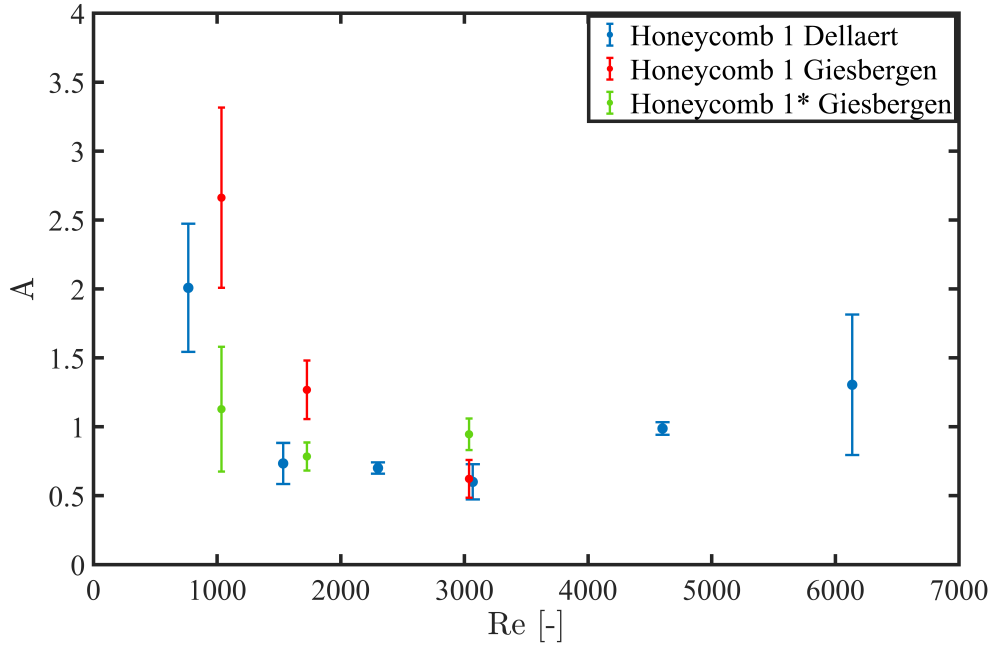

Figure 4.44: The decay coefficient A as a function of the Reynolds number, combined with results from Dellaert (HC1+HC1).*

From the graphs, a few things can be concluded. Figure 4.42 shows that the noise is independent of the length of the honeycomb. At $Re \approx 1800$ and $Re \approx 3000$, the noise is approximately equal for all three honeycombs. Only at $Re \approx 1000$ there is a significant difference between the values. The same holds for the values of the decay coefficient A depicted in Figure 4.44, which follow the same trend with respect to the Reynolds number for all three honeycomb lengths, however the values for the 50 mm variant are substantially higher for lower Reynolds numbers, compared to the longer variants. It is the virtual origin displayed in Figure 4.43, where the length of the Honeycomb starts to play a major role. At $Re \approx 3000$, the values are approximately equal for the three different lengths. However, for smaller Reynolds numbers, the values of the virtual origin for the 50 mm variant of the Honeycomb stay constant around zero, while the values obtained for the 750 mm variant follow the trend found by Dellaert.

4.3.1.3 Velocity profile

In order to investigate the velocity profiles leaving the cells of the honeycomb, the ratio $U_{\text{measured}}/U_{\text{merged}}$ is plotted as function of the distance behind the honeycomb. Figures 4.45, 4.46 and 4.47 show the velocity ratio for $Re = 1035$, $Re = 1726$ and $Re = 3037$ respectively. In all three figures, it can be seen that the velocity ratio decays towards a constant value of approximately $U_{\text{measured}}/U_{\text{merged}} \approx 1.2$, independent of the length of the honeycomb. However, it is the region just behind the honeycomb that distinguishes the 50 mm variant from the 750 mm variant for all Reynolds numbers.

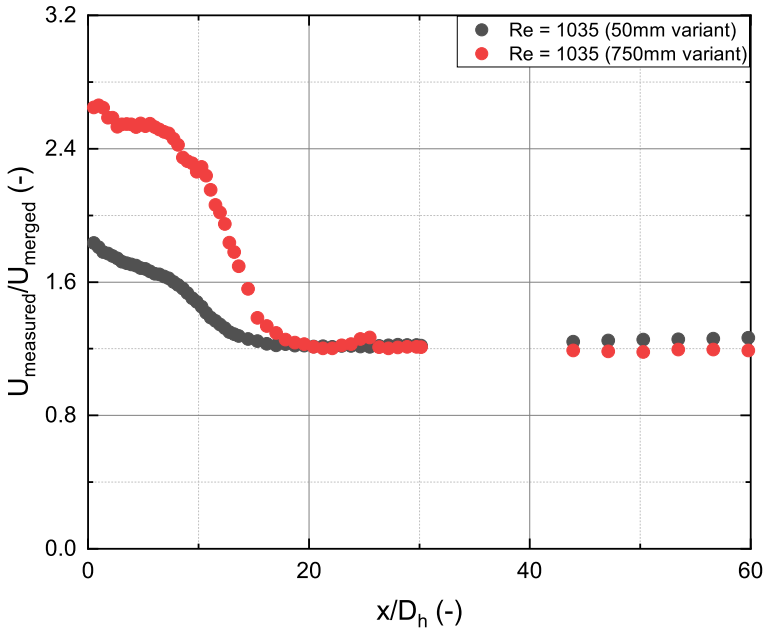

Figure 4.45: The ratio $U_{measured}/U_{merged}$ against x/D_h for the 50 mm and 750 mm variant of Honeycomb 1 at Re = 1035 (HC1).

Figure 4.45 shows that for the 50 mm variant, the ratio is significantly lower at $x/D_{\text{h}} = 0$ at Re = 1035. Here the length of the honeycomb matters. By applying Equation 2.7, it can be concluded

that for $Re = 1035$ the entrance length of the honeycomb is 489 mm in order to obtain a fully developed flow. With its 50 mm, the short variant of the honeycomb covers just over 10% of the desired length. Therefore, the flow leaving the honeycomb is not fully developed resulting in a "flat" and undeveloped velocity profile. Therefore, U_{measured} is significantly lower which is translated into a lower starting point of the velocity ratio for the 50 mm honeycomb in Figure 4.45. For the 750 mm variant it is calculated that $U_{\text{measured}}/U_{\text{average HC}} \approx 2.11$ which is in accordance with the literature value. Therefore, it can be concluded that the flow leaving the 750 mm variant of Honeycomb 1 at $Re = 1035$ is laminar and fully developed.

This result is an implicit explanation for the turbulence intensity plot as displayed in Figure 4.39. The maximum velocity of the flow leaving the 750 mm variant of the honeycomb is higher in comparison with the 50 mm version, since the flow is fully developed. Therefore, merging of the individual velocity profiles out of the longer honeycomb induces more turbulence, because the differences in velocities across the flow are much higher. For the short honeycomb, the velocity profile out of the individual honeycomb cells is more flattened which means that differences in flow velocities are reduced and merging induces less turbulence.

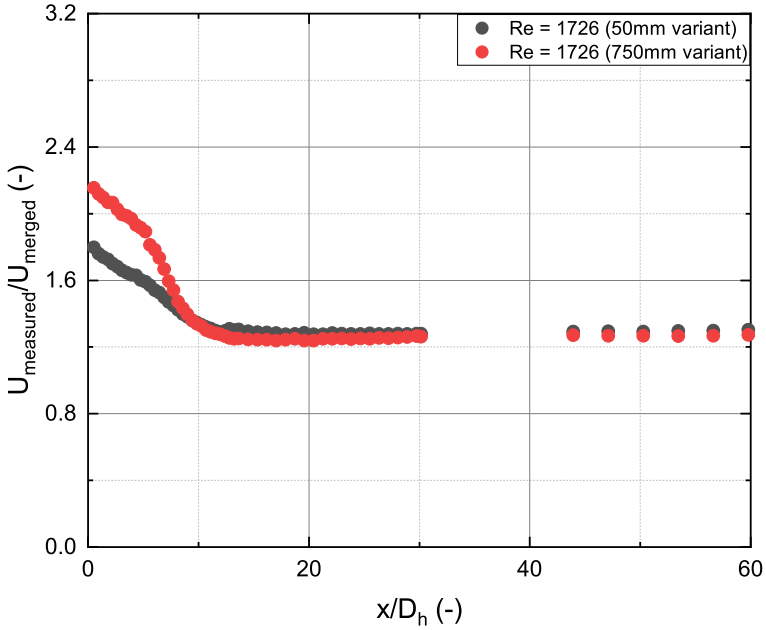

Figure 4.46: The ratio $U_{measured}/U_{merged}$ against x/D_h for the 50 mm and 750 mm variant of Honeycomb 1 at $Re = 1726$ (HC1).

Figure 4.46 displays the turbulence intensity for $Re = 1726$. It is expected that the flow at this Reynolds number is laminar. However, as mentioned in Section 4.3.1.1, the flow seems to leave the honeycomb turbulent. This is confirmed by investigating the ratio $U_{\text{measured}}/U_{\text{merged}}$. Factoring out U_{merged} and dividing by $U_{\text{average HC}}$ should return a value around 2.09. However, calculating the value returns 1.71. This means that U_{measured} is lower than expected, which may imply that the flow is turbulent instead of laminar. This will be investigated in Section 4.3.1.4. The starting

point of the velocity ratio for the 50 mm honeycomb is lower compared to the 750 mm variant for the same reason as for $Re = 1035$. The entrance length of the honeycomb for this Reynolds number is approximately 815.5 mm. The length of the short honeycomb only covers 6.1% of this distance, which means that the flow is far from developed. This means that U_{measured} is lower which results in the lower starting point.

The undeveloped flow leaving the short version of the honeycomb is the reason for the lower turbulence intensity peak in Figure 4.40. The profile is less developed which means that differences in velocity across the flow are smaller, such that significantly less turbulence is induced during merging of the individual profiles.

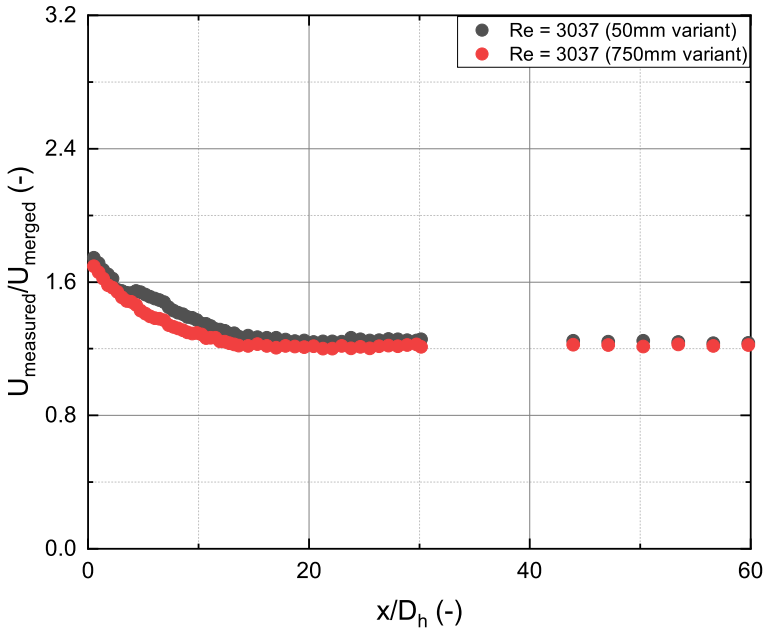

Figure 4.47: The ratio $U_{measured}/U_{merged}$ against x/D_h for the 50 mm and 750 mm variant of Honeycomb 1 at $Re = 3037$ (HC1).

For $Re = 3037$ in Figure 4.47, the two lines are almost identical. Since the flow is turbulent inside the honeycomb, the entrance length is much shorter according to Equation 2.8. This length is calculated to be 95.3 mm for $Re = 3037$, which means that the 50 mm variant of the honeycomb already covers 52.5% of this length. It turns out that 50 mm already results in a quite developed turbulent flow inside the honeycomb, since the lines are almost identical. This is the reason that the turbulence intensities from Figure 4.41 do not differ that much; the flow leaving the honeycomb is almost identical for both honeycomb lengths.

4.3.1.4 Transition around Re = 1726

As mentioned in Section 4.3.1.1, Figure 4.40 shows something odd: the turbulence intensity plot of the 750 mm version of Honeycomb 1 shows that the flow leaves the honeycomb significantly turbulent for $Re = 1726$. This phenomenon is investigated by single point measurements right behind the honeycomb.

All measurements are performed on one single cell in the center of the honeycomb. Therefore, it is plausible that there may be an inhomogeneity in the flow before the honeycomb, which causes an imbalance in flow velocity inside the honeycomb as was the case for Honeycomb 3 (see Section 4.1.5). This is investigated by performing a measurement in both the y- and z-direction at $x/D_h \approx 1.64$. By plotting the average streamwise velocity component as a function of the position, it can be verified whether the flow leaves the honeycomb homogeneous. Figure 4.48 and 4.49 displays this for the y- and z-direction respectively.

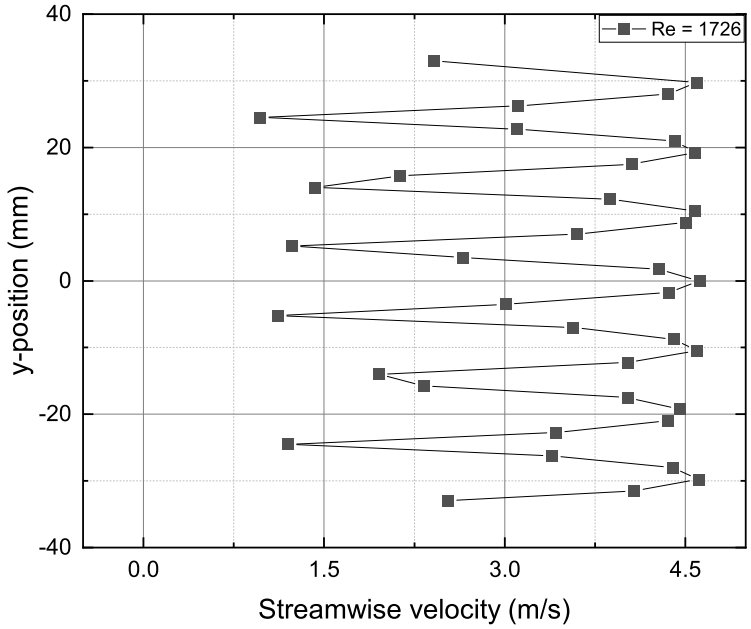

Figure 4.48: The average streamwise component plotted as a function of the y-position at Re = 1726 (HC1).*

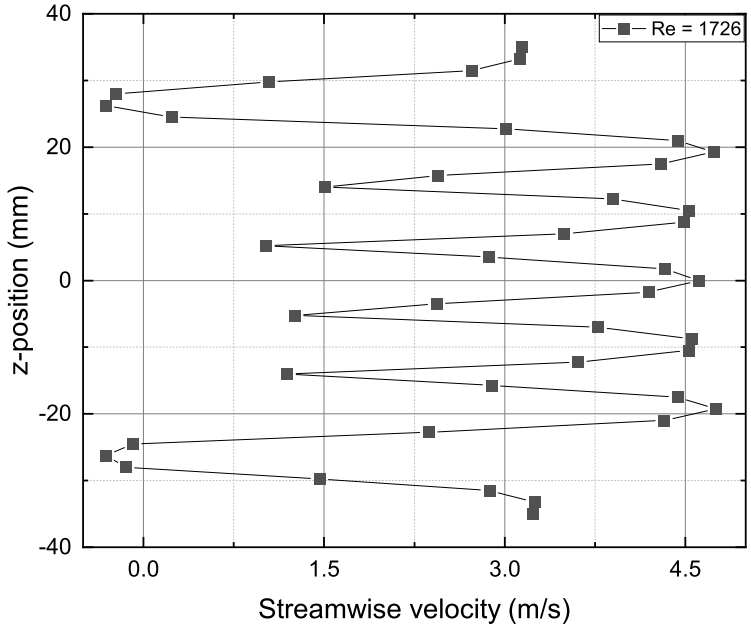

Figure 4.49: The average streamwise component plotted as a function of the height at Re = 1726 (HC1)*

From Figure 4.48 and 4.49 it can be concluded that the flow leaves the honeycomb homogenous. The velocity profile across the height and width of the tunnel is symmetric and the flows leaving the individual cells of the honeycomb are almost identical in both the y- and z-direction. No inhomogeneity is present and there must be another reason for the turbulent behaviour of the flow at $Re = 1726$.

A set of measurements in the center of the center cell just behind the honeycomb is performed for Reynolds numbers ranging from $Re = 1035$ to $Re = 2485$, in order to investigate the behaviour at $Re = 1726$. As mentioned in Section 3.3, measurements at each position take either one minute or 50,000 data points before moving on to the next position in the tunnel. It is the 50,000 data points that are used for this investigation. These data points contain the velocity in all three directions as function of time. By plotting the streamwise velocity as function of time, it can be investigated how the component develops over time at a fixed position behind the honeycomb. The behaviour and especially the outliers of the streamwise velocity component will tell whether a flow is turbulent, laminar or in transition. The results of the measurements can be found in Figure 4.50 and 4.51.

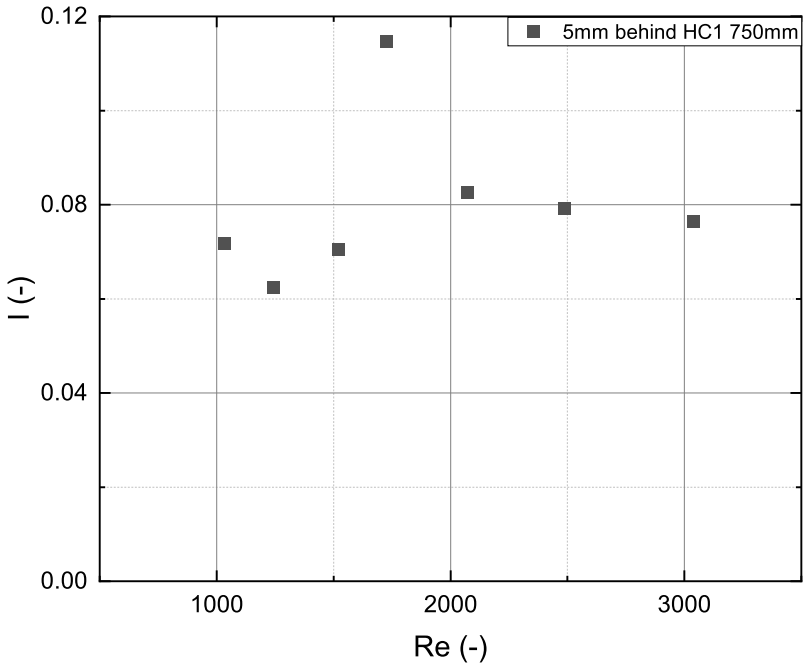

Figure 4.50: The turbulence intensity as function of the Reynolds number at 5 mm behind the center of the honeycomb (HC1).*

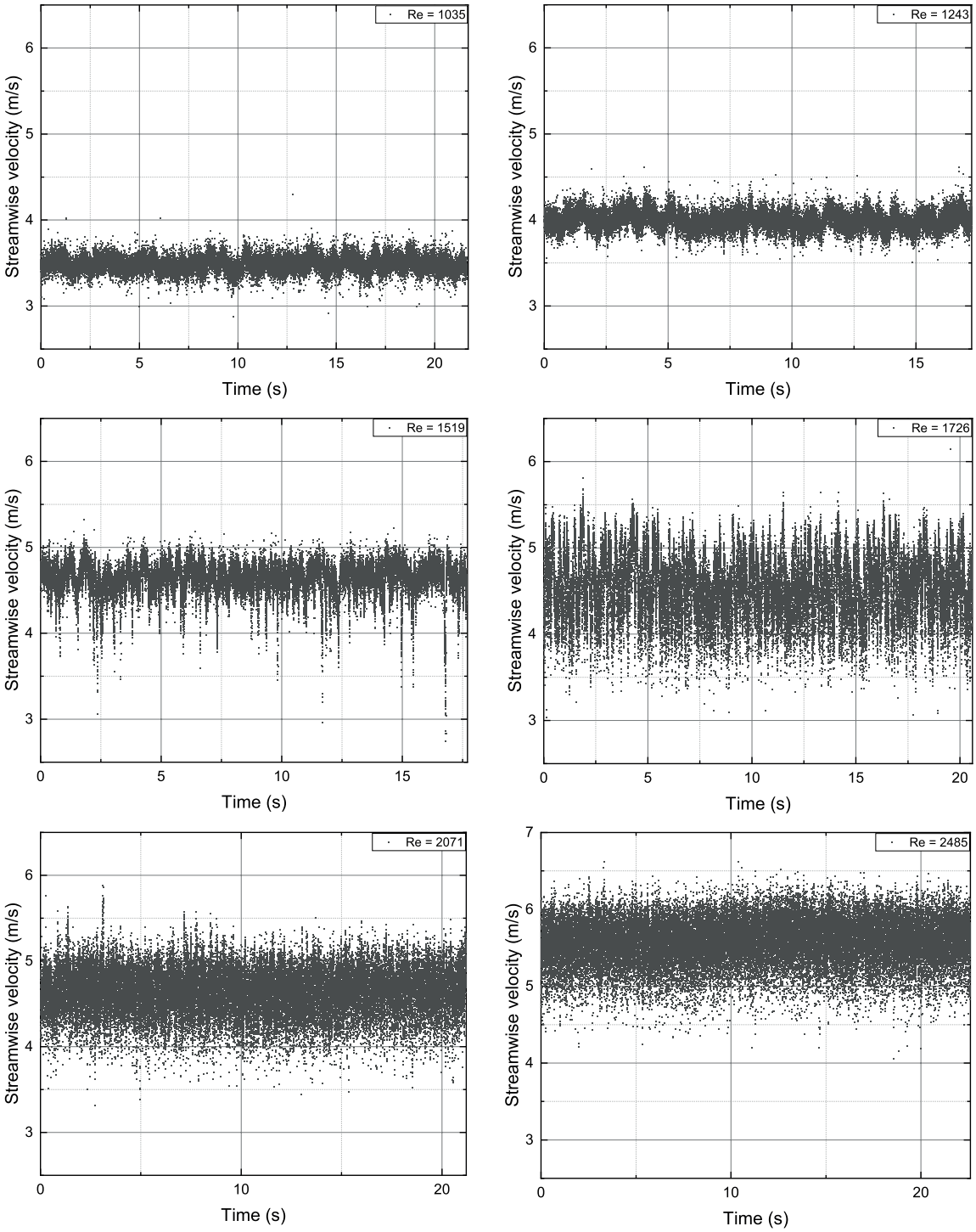

Figure 4.51: The streamwise velocity component as a function of time 5 mm behind the center of the honeycomb for different Reynolds numbers (HC1).*

Figure 4.50 shows the turbulence intensity as a function of the Reynolds number at 5 mm behind the honeycomb. This already shows the previously found trend; the turbulence intensity at $Re = 1726$ is significantly higher in comparison with other Reynolds numbers, while this Reynolds number is well below the zone at Re $\approx$ 2300 where transition from laminar to turbulent is expected.

In order to understand the flow status at $Re = 1726$, the streamwise velocity signal can be plotted as function of time which is done in Figure 4.51. Each graph displays a measurement of a certain Reynolds number in the center and at 5 mm behind the honeycomb and contains 50,000 data points. The top two graphs are measurements where the Reynolds number is such that the flow should be laminar. This is confirmed by the plots, since the streamwise velocity component is approximately constant for both measurements and has, apart from some outliers, minimal fluctuations in velocity.

This trend continues for Re = 1519, however there are some significant downward peaks in velocity and the fluctuations are larger, which indicate transition. It is difficult to prove with this setup, but the hypothesis is that the downward peaks arise from a phenomenon where flow in certain ducts transits from laminar to turbulent. This transition means a instant local increase of the Darcy-Weisbach friction factor inside the individual duct were transition takes place, as can be seen on the Moody chart displayed in Section 2.5. Assuming no other variables change, the pressure loss increases in that particular duct according to Equation 2.12. However, the pressure loss over the whole honeycomb should remain constant, which means that flow is increased in other ducts. This can lead to a cascade of transitions in the other honeycomb cells. At $Re = 1519$ this is already happening to some extend, but especially for $Re = 1726$ there is a constant interaction between laminar and turbulent ducts resulting in significant ups and downs in velocity over time. The velocity does not behave random, since a clear pattern is visible indicating the interaction between different ducts. Thus the overall flow is not turbulent yet, however the large fluctuations in velocity result in a large turbulence intensity, because the turbulence intensity is a function of the root means square of the velocity in all three directions. Almost no literature research is done on this phenomenon. Robbins [23] mentions sort of the same observations in his research on water tunnel turbulence behind a honeycomb: *"However, the low Reynolds number indicates the flow is still in transition from laminar to turbulent, based on a curve of friction factor vs Reynolds number in Shames. Apparently, only some of the cells have fully developed turbulent flow at this low-flow velocity"*. The hypothesis seems plausible, however proving it using LDV is difficult, since investigation on the flow inside the honeycomb is impossible.

The bottom two graphs reveal the pattern of a turbulent flow; there is no clear trend visible and velocity behaves random over time. At $Re = 2071$ there are still some clear peaks visible in the spectrum, which indicates that some transition takes places. However, at $Re = 2485$ the noise is homogeneously distributed, no clear pattern is visible and almost no significant peaks in velocity are present, which indicates that the flow is turbulent.

5 Conclusions

5.1 Honeycomb 3

Driessen performed measurements on Honeycomb 3 starting around $Re \approx 1160$, so here it was chosen to extend this research by performing measurements for Reynolds numbers ranging from $Re = 580$ up to $Re = 1160$. The results regarding the turbulence intensity for $Re = 1160$ are identical to Driessen's result. Lowering the Reynolds number leads to a decrease of the turbulence intensity peak, while simultaneously shifting away from the honeycomb. The decay characteristics determined by applying the decay power law, show some interesting results: the virtual origin x_0/D_h increases for decreasing Reynolds numbers and the decay coefficient A reaches a maximum for $Re = 928$ followed by a decrease for lower Reynolds numbers. The noise as a function of the Reynolds number has relatively large uncertainties. It is believed that this is due a combination of the low number of points fitted and the fact that these were the very first measurements which required adjustment of the setup during the measurements, leading to possible fluctuations. Investigation of the velocity profile shows that the velocity profile is fully developed for $Re = 580$, $Re = 696$ and $Re = 812$ and not fully developed for $Re = 928$ and $Re = 1160$, which is in accordance with expectations based on the Reynolds number and hydrodynamic entrance length. The ratio $U_{measured}/U_{\text{average HC}}$ turns out the be consistently too high for all Reynolds numbers. It is believed that this is due to the inhomogeneity of the flow caused by the length of the honeycomb, as was investigated by Driessen. Finally, the turning point for the occurrence of a turbulence intensity peak for this honeycomb turns out to be instant and takes place at $Re \approx 679 \pm 6$.

5.2 Honeycomb 2 and 4

Dellaert found some odd behaviour of the turbulence intensity of Honeycomb 4; a second peak arises for some Reynolds numbers. It is found in this research that this second peak in turbulence intensity is due to the low porosity of the honeycomb, resulting in a misalignment of average flow velocity between the honeycomb part and side channels. For $Re = 849$, $Re = 1591$, $Re = 2334$ and $Re = 3076$, it is found that equalizing the initial top and bottom velocity with the average flow velocity inside the honeycomb, results in a disappearance of the second turbulence peak. Furthermore, the height of the first turbulence peak decreases, while the position of the peak behind the honeycomb does not change. More extensive research on $Re = 1591$ shows that the disappearance of the second peak and general decrease of turbulence, is gradually for initial top and bottom velocities approaching the average flow velocity inside the honeycomb. Cross sectional measurements confirm that equalizing the initial top and bottom velocity with the average flow velocity inside the honeycomb, results in the least amount of turbulence at any arbitrary point inside the wind tunnel; initial top and bottom velocities below or above the equalized velocity always result in more turbulence at certain positions in the tunnel. Applying the decay power law shows that the virtual origin x_0/D_h reaches its maximum distance behind the honeycomb, around equalized top/bottom velocities. Both increasing or decreasing the initial top and bottom velocity with respect to the equalized case, results in shifting of the virtual origin towards the honeycomb. The noise N and decay coefficient A both linearly decrease for initial top and bottom velocities above the equalized velocity and linearly increase for initial top and bottom velocities below the equalized velocity.

Honeycomb 2 has a lower porosity compared to Honeycomb 4. For Honeycomb 2 is also investigated whether creating the same difference in top/bottom flow velocity and center velocity, as induced by the porosity of Honeycomb 4, results in a second turbulence peak. It is found that such a peak indeed occurs for an absolute difference of 2.92 m/s and a relative difference of 79.6 % between the top/bottom flow velocity and center velocity, where the top/bottom velocity was lower than the center velocity. So the similarity for assymmetric injection and the manifestation of a second turbulence peak is proved clearly. It can be concluded that the difference in flow velocity is the reason for the second turbulence peak; it induces Kelvin-Helmholtz instabilities which results in a turbulent flow.

5.3 Honeycomb 1

Research on two different variants of Honeycomb 1, where the difference is the length of the honeycomb, shows that the turbulence intensity for the short honeycomb is generally lower compared to the longer variant for Reynolds numbers in the laminar regime. The turbulence peak arises due to mixing of the individual flow profiles behind the honeycomb. For the short honeycomb, the flow is far from developed, resulting in smaller differences in velocity across the flow, which results in less turbulence when these individual profiles mix compared to fully developed profiles for the longer honeycomb. For turbulent Reynolds numbers, the hydrodynamic entrance length is shorter which means that there is almost no difference in turbulence intensity, decay characteristics and velocity profiles leaving the cells of the honeycomb, between the short and long version of Honeycomb 1. Therefore, the length of Honeycomb 1 only plays a significant role for Reynolds numbers in the laminar regime.

Furthermore, an interesting phenomenon at $Re = 1726$ is found for the long variant of Honeycomb 1. The turbulence intensity right behind the honeycomb is higher than expected and a fluctuating pattern in streamwise velocity over time is found behind the center cell of the honeycomb. It is believed that this pattern appears due to an interaction between separate honeycomb cells which continuously alter from laminar to turbulent or vice versa. The measured velocity in the center of a cell is different for laminar or turbulent flow, such that altering between laminar and turbulent over time results in a pattern.

6 Discussion & proposal further research

6.1 Honeycomb 3

The measurements on Honeycomb 3 were the very first measurements executed. Some adjustments during the measurements may have introduced fluctuations which influence the results. The general trend found by analyzing the measurements are in agreement with previous research and seem to be logical. To make sure the results are correct, measurements could be repeated and the number of measurement points could be increased to get a higher accuracy, especially for fitting of the turbulence decay. Furthermore, the range of Reynolds number can be extended in order to gain information, in particular Reynolds numbers below 580 are interesting.

6.2 Honeycomb 2 and 4

The hypothesis that the second peak in turbulence intensity using Honeycomb 4 is expected to arise due to a large difference in flow velocity leaving the top/bottom channel and the center channel, turned out to be correct. Measurements in the center of the honeycomb and measurements in the z-direction are performed in order to confirm this. Furthermore, a second turbulence peak is "created" using Honeycomb 2, by increasing the initial top and bottom velocity such that approximately the same difference in velocities is reached as is the case for Honeycomb 4. Therefore, it is plausible to conclude that arising of the second peak is only due to the difference in velocity. In order to confirm this, the experiment could be repeated using a different measurement method, such as Particle Image Velocimetry, to obtain a full impression of the flow. Furthermore, it can be investigated whether equalizing the initial top/bottom velocity with the average flow velocity inside the honeycomb has a positive effect on the turbulence intensity, for arbitrary honeycombs. In the center of the wind tunnel, the turbulence intensity often gradually increases in the far-field and it could be investigated whether this is due to a marginal difference in velocities leaving the different channels.

6.3 Honeycomb 1

During experiments on Honeycomb 1 and 1*, it is found that the flow shows transitional behaviour at $Re \approx 1726$. Fundamental research on this phenomenon is interesting for the future, since understanding this transition zone is necessary in order to characterize honeycombs and flow behaviour. However, currently used honeycombs often contain many individual cells which cannot be measured simultaneously. A different setup with only a few parallel channels, which can all be measured at once, is needed in order to fundamentally research what exactly happens in the transition zone.

6.4 Conveyor belt

Originally, it was planned to install a scale model of a conveyor belt inside the wind tunnel for this research. However, some interesting phenomena were found and it was chosen to investigate these in more depth. For future research, it is interesting to install a conveyor belt inside the wind tunnel, since this is also the case in the real-life MDS machine; the conveyor belt inserts the plastic particles in the machine. It is expected that such a conveyor belt has a major effect on the boundary conditions of the flow, influencing the turbulent behaviour in the wake of the laminator. At the time of writing, such a conveyor belt is installed in the setup and experiments are performed with it.

7 Acknowledgements

During my Bachelor End Project I have been supervised and supported by J.C.H. Zeegers and R.A. Dellaert. I would like to thank them for supporting me and providing a comfortable atmosphere to work in. In the beginning of my project one laser did not work properly and after a few days of struggling Dellaert managed to fix the problem. Whenever a problem occurred during a measurement, Dellaert was there to help me and often the problem was solved immediately. Zeegers kept track of me and the progress during the entire project. Results were discussed frequently and new research opportunities were communicated on weekly, if not daily, basis. The enthusiasm and commitment of Zeegers and Dellaert motivated me during my entire internship at Fluids & Flows.

References

[1] National Geographic Society / Laura Parker. A Whopping 91 Percent of Plastic Isn't Recycled, 2019.

[2] https://www.esbnyc.com/. Empire State Building Fact Sheet.

[3] Dame Ellen MacArthur. Beyond plastic waste, 2017.

[4] R. Dellaert. Reducing turbulence intensity with honeycombs. *European Journal of Mechanics - B/Fluids*, 2021.

[5] R.J.A. Driessen. Turbulence in the wake of a honeycomb. *Bachelor End Project, Technical University Eindhoven*, 2021.

[6] L. S. Vervoort. Turbulence decay in honeycomb wakes measured with Laser Doppler Velocimetry . *BSc Thesis TU/e*, 2020.

[7] Engineering Toolbox. Nitrogen - Dynamic and Kinematic Viscosity.

[8] Y. Cengel and Cimbala. *Fluid Mechanics: Fundamentals and Applications, 3rd ed.* McGraw-Hill Companies, New York, 2010.

[9] V. C. Patel and M. R. Head. Some observations on skin friction and velocity profiles in fully developed pipe and channel flows. *Journal of Fluid Mechanics*, 38(1), 1969.

[10] A. G. Darbyshire and T. Mullin. Transition to turbulence in constant-mass-flux pipe flow. *Journal of Fluid Mechanics*, 289, 1995.

[11] R.K. Shah and A.L. London. Rectangular Ducts. In *Laminar Flow Forced Convection in Ducts*, pages 196–222. Elsevier, jan 1978.

[12] F.P. Incropera and T.L. Bergman. *Fundamentals of heat and mass transfer.* Wiley, January 2011.

[13] L.C. Thijs. Honeycomb wake turbulence and particle dynamics in a magnetic density separation system. *Master Thesis, Technical University Eindhoven*, 2020.

[14] S. Mohamed Mohsen and John C. Larue. The decay power law in grid-generated turbulence. *Journal of Fluid Mechanics*, 219, 1990.

[15] Yanbiao Gan, Aiguo Xu, Guangcai Zhang, and Yingjun Li. Lattice Boltzmann study on Kelvin-Helmholtz instability: Roles of velocity and density gradients. *Physical Review E - Statistical, Nonlinear, and Soft Matter Physics*, 83(5), 2011.

[16] S.H. Hollingdale. XXV. Stability and configuration of the wakes produced by solid bodies moving through fluids. *The London, Edinburgh, and Dublin Philosophical Magazine and Journal of Science*, 29(194), 1940.

[17] R. I. Loehrke and H. M. Nagib. Control of free-stream turbulence by means of honeycombs: A balance between suppression and generation. *Journal of Fluids Engineering, Transactions of the ASME*, 98(3), 1976.

[18] R. E. Roadman and R. I. Loehrke. Low reynolds number flow between interrupted flat plates. *Journal of Heat Transfer*, 105(1), 1983.

[19] F. Ahlborn. Über theoretische und natürlichen Strömungen. *Das Flugwesen*, 1930.

[20] Glenn O. Brown. The history of the Darcy-Weisbach equation for pipe flow resistance. In *Proceedings of the Environmental and Water Resources History*, 2002.

[21] L. F. Moody. Friction factors for pipe flow, 1944.

[22] TSI. Laser Doppler Velocimetry Poster.

[23] Basil E. Robbins. Water tunnel turbulence measurements behind a honeycomb. *J Hydronaut*, 12(3), 1978.

Appendices

A Honeycomb 3

Table A.1: The near-field decay constants of the power law for a range of Reynolds numbers (HC3).

Re	**region**	**p**	**A**	$\mathbf{x_0/D_h}$	**N**
696	near-field	-2	2.10 ± 1.21	12.57 ± 2.06	0.055 ± 0.036
812	near-field	-2	2.35 ± 1.12	9.89 ± 1.84	0.082 ± 0.012
928	near-field	-2	3.29 ± 1.33	9.34 ± 1.52	0.081 ± 0.019
1160	near-field	-2	0.96 ± 0.33	7.97 ± 1.15	0.085 ± 0.005

Table A.2: The extrapolated values of $U_{measured}$ at $x = 0$ and the calculated ratio $U_{measured}/U_{average\ HC}$ for different Reynolds numbers (HC3).

Re (-)	**Extrapolated U_{measured} at x = 0 (m/s)**	$U_{\text{measured}}/U_{\text{average HC}}$ **(-)**
580	1.37	2.44
696	1.64	2.44
812	1.88	2.40
928	1.91	2.13
1160	2.49	2.22

B Honeycomb 2+4

Table B.1: The extrapolated values of $U_{measured}$ at $x = 0$ and the calculated ratio $U_{measured}/U_{average\ HC}$ for different Reynolds numbers (HC4).

Re (-)	**Extrapolated U_{measured} at x = 0 (m/s)**	$U_{\text{measured}}/U_{\text{average HC}}$ **(-)**
849	4.27	2.05
1591	7.35	1.88
2334	8.09	1.41
3076	10.53	1.39
849 (top+bottom 2.08m/s (equalized))	4.49	2.16
1591 (top+bottom 3.85m/s (equalized))	7.79	1.99
2334 (top+bottom 5.73m/s (equalized))	8.42	1.47
3076 (top+bottom 7.55m/s (equalized))	9.99	1.32

Table B.2: The extrapolated values of $U_{measured}$ at $x = 0$ and the calculated ratio $U_{measured}/U_{average\ HC}$ for low Reynolds numbers (HC4).

Re (-)	**Extrapolated $U_{measured}$ at x = 0 (m/s)**	**$U_{measured}/U_{average\ HC}$ (-)**
106 (top+bottom 0.26m/s (equalized))	0.59	2.27
159 (top+bottom 0.39m/s (equalized))	0.86	2.22
212 (top+bottom 0.52m/s (equalized))	1.15	2.22
318 (top+bottom 0.78m/s (equalized))	1.74	2.25
424 (top+bottom 1.04m/s (equalized))	2.22	2.15

Table B.3: The near- and far-field decay constants obtained using the power law for a range of Reynolds numbers (HC2 + HC4).

Re	**HC**	**region**	**p**	**A**	**x_0/D_h**	**N**
849 (top+bottom 2.08m/s (equalized))	4	near-field	-1.4	1.90 ± 0.29	7.62 ± 0.50	0.070 ± 0.048
1008	2	near-field	-2	1.29 ± 0.47	15.56 ± 1.25	0.022 ± 0.021
1008	2	far-field	-0.73	0.032	15.56	0.022
1513	2	near-field	-2	0.80 ± 0.22	11.19 ± 0.72	0.024 ± 0.017
1513	2	far-field	-0.25	0.004	11.19	0.024
1591 (top+bottom 3.85m/s (equalized))	4	near-field	-2	1.40 ± 0.47	9.22 ± 0.57	0.076 ± 0.015
2334 (top+bottom 5.73m/s (equalized))	4	near-field	-2	0.83 ± 0.13	3.82 ± 0.37	0.042 ± 0.006
3076 (top+bottom 7.55m/s (equalized))	4	near-field	-2	0.99 ± 0.23	3.06 ± 0.65	0.021 ± 0.017

Table B.4: The near-field decay constants obtained using the power law for a range of Reynolds numbers (HC4).

Re	**region**	**p**	**A**	**x_0/D_h**	**N**
1591 (top/bottom 3.00 m/s)	near-field	-2	2.35 ± 0.34	8.68 ± 0.56	0.098 ± 0.004
1591 (top/bottom 3.22 m/s)	near-field	-2	1.63 ± 0.12	9.09 ± 0.16	0.099 ± 0.001
1591 (top/bottom 3.43 m/s)	near-field	-2	1.59 ± 0.18	9.44 ± 0.22	0.084 ± 0.003
1591 (top/bottom 3.85 m/s)	near-field	-2	1.40 ± 0.47	9.22 ± 0.57	0.076 ± 0.015
1591 (top/bottom 4.28 m/s)	near-field	-2	1.14 ± 0.26	8.43 ± 0.41	0.071 ± 0.005
1591 (top/bottom 4.71 m/s)	near-field	-2	0.98 ± 0.15	8.23 ± 0.39	0.068 ± 0.003
1591 (top/bottom 5.78 m/s)	near-field	-2	0.52 ± 0.03	8.02 ± 0.20	0.067 ± 0
1591 (top/bottom 6.74 m/s)	near-field	-2	0.47 ± 0.17	7.61 ± 0.53	0.060 ± 0.008

C Honeycomb 1

Table C.1: The near-field decay constants obtained using the power law for a range of Reynolds numbers (HC1 + HC1).*

Re	HC	region	p	A	x_0/D_h	N
1035	1	near-field	-2	2.66 ± 0.65	-0.66 ± 1.60	0.051 ± 0.004
1726	1	near-field	-2	1.27 ± 0.21	-0.97 ± 0.93	0.042 ± 0.002
3037	1	near-field	-2	0.62 ± 0.14	-0.05 ± -1.21	0.033 ± 0.002
1035	1*	near-field	-2	1.13 ± 0.45	10.67 ± 1.29	0.092 ± 0.007
1726	1*	near-field	-2	0.78 ± 0.10	4.08 ± 0.41	0.050 ± 0.002
3037	1*	near-field	-2	0.95 ± 0.11	-3.24 ± -0.73	0.025 ± 0.002